REGION OF INTEREST BASED LOSSLESS COMPRESSION OF MRI AND ULTRASOUND MEDICAL IMAGES

A THESIS

Submitted by

LIDIYA LILLY THAMPI

(Reg. No: 4862)

for the award of the degree of

DOCTOR OF PHILOSOPHY

DIVISION OF INFORMATION TECHNOLOGY

SCHOOL OF ENGINEERING

COCHIN UNIVERSITY OF SCIENCE & TECHNOLOGY, KOCHI

AUGUST 2019

CERTIFICATE

This is to certify that the thesis entitled **REGION OF INTEREST BASED LOSSLESS COMPRESSION OF MRI AND ULTRASOUND MEDICAL IMAGES** submitted by **Lidiya Lilly Thampi (Reg. No: 4862)** to the Cochin University of Science & Technology, Kochi for the award of the degree of Doctor of Philosophy is a bonafide record of research work carried out by her under my supervision and guidance at the Division of Computer Science and Engineering, School of Engineering, Cochin University of Science and Technology. The content of this thesis, in full or in parts, have not been submitted to any other University or Institute for the award of any degree or diploma.

I further certify that the corrections and modifications suggested by the audience during the pre-synopsis seminar and recommended by the Doctoral Committee of **Ms. Lidiya Lilly Thampi** are incorporated in the thesis.

Kochi – 682 022
Date: 24.08.2019

Dr. Varghese Paul (Research Guide)
Professor (Retd.)
Division of Information Technology
School of Engineering
Cochin University of Science and Technology

DECLARATION

I hereby declare that the work presented in the thesis titled **REGION OF INTEREST BASED LOSSLESS COMPRESSION OF MRI AND ULTRASOUND MEDICAL IMAGES** is based on the original research work carried out by me under the supervision and guidance of Dr. Varghese Paul., Professor, School of Engineering, for the award of the degree of Doctor of Philosophy with Cochin University of Science and Technology. I further declare that the contents of this thesis in full or in parts have not been submitted for the award of any degree, diploma, associate ship, or any other title or recognition from any other University/ Institution.

Kochi – 682 022 **Lidiya Lilly Thampi**

Date: : 24.08.2019 Research Scholar

This thesis is dedicated to the memory of my father……….

ACKNOWLEDGEMENTS

'Knowledge is power'

All praise and thanks to God Almighty for all the blessings showered on me from time to time.

First and foremost, I owe my profound sense of reverence to my supervisor and guide, **Dr. Varghese Paul,** for his patience, enthusiasm, invaluable guidance, stimulating encouragement, immense knowledge and motivating nature and endless support, which paved the way for the successful completion of my doctoral dissertation.

I would like to express my sincere thanks to the Doctoral Committee members **Dr. Philip Samuel** and **Dr. Sudheep Elayidom M**, for their valuable suggestions and constant support rendered to me.

I am much grateful to **Prof. (Dr.) George Mathew**, Principal, for the whole hearted support and constant encouragement. I would like to express my sincere thanks to **Prof. Dr. G. Madhu** and **Dr. Radhakrishna Panicker** former Principal, School of Engineering, CUSAT for providing adequate help and fruitful suggestions.

I am extremely thankful to **Dr. Renumol V G,** Head, Division of Information Technology for providing me the facility, support and encouragement to pursue the PhD work in the department. I also extend my sincere thanks to **Dr. Shelbi Joseph and Dr. Philip Samuel**, former Heads, Division of IT. I gratefully acknowledge all the teaching and nonteaching staff of Division of Information Technology who has been very forthcoming to offer advice and help in their respective roles.

I would like to extend my sincere and immense gratitude to **Dr. Amel Antony**, Radiologist, Head of the Department, **LIRRIS** (Lisie Institute of Radiology and

Imaging Sciences) for his guidance and support throughout by providing the real data set which played a major part in the successful completion of my research work. I am so thankful to **Sruthy K S**, the Technician in LIRRIS also played a major role in getting the data collected.

A word of mention is deserved by **Dr. Limce Thampi,** my loving sister and **Ms. Sreekala M**, my fellow researcher who has been a constant support and encouragement throughout my research period.

I fondly remember the friendship I had with the research scholars in our IT Division especially Sandya N, Nisha S Raj, Uma Narayan, Sreeja Unnikrishnan, Jeevamol Joy, Smitha John, Sreelakshmi and Jeseena K. U.

I dearly dedicate my thesis to the memory of my father, who first wished to see my work finished. Your absence still and will always hurt me, but your memories will stay in my heart forever. I am deeply indebted to my mother Lilly Thampi and my sibling sisters Dr. Limce Thampi and Timce Thampi along with my in-law family members, who have been always a great and inseparable source of inspiration, offering a helping hand with reassuring support in all situations.

Finally and most importantly, words are too short to express my deep sense of gratitude towards my beloved husband Mr. Rijo Baby Thomas and our loving child Enric Rijo Thomas for their support, understanding, encouragement, patience and unwavering love. I vouch that this journey would not have been possible without their priceless and perpetual support, invaluable help and inspiration.

Lidiya Lilly Thampi

ABSTRACT

KEYWORDS: Region of Interest (ROI); lossless compression; lossy compression; female pelvic magnetic resonance imaging; female pelvic ultrasound imaging; Segmentation;

Medical imaging techniques in hospitals and medical centers have widened from X-rays and now boosted to different imaging modalities like ultrasound, MRI, CT etc. These imaging modalities are generating large amounts of image data which can be used for different purposes like surgical and diagnostic plans. The medical images in raw format will take huge storage space, so compression is inevitable for handling this huge image repository. Depends upon the area of application certain important measures should be considered while performing compression. The medical field always demanding a high quality of images and therefore lossless type of compression techniques are mostly preferred. Direct application of lossy or lossless is not recommended, because of their reconstruction and quality problem. However, a combination of lossy and lossless type of compression will be of great interest and that is called as Region of Interest (ROIs) based medical image compression.

The main motive of our work is to develop an ROI based medical image compression for female pelvic Ultrasound and MRI imaging modalities. Before applying the compression technique an automatic detection method is developed to segment ROI from MRI and Ultrasound imaging modalities. Then the entire input medical image is segmented into two parts: ROI regions and non-ROI regions. A preprocessing step is initialized before doing the segmentation step. An SRAD based filtering approach is

used in female PUS imaging modality whereas a median type of filtering was performed in MRI imaging modality

The algorithm for two imaging modality works in the following way: initially a filtering approach is carried out as a preprocessing stage, and the region of interest is separated from the female pelvic ultrasound images. Then the texture and shape features are extracted from the segmented ROI component. The results of shape similarity indices between manual and automated segmentations are also illustrated. The comparison result gives an average similarity index of 82.65% and JSI of 76.5% and a DSC of 83.8%. An average total time taken for segmenting the Ultrasound image is 1.825s and that of MRI is 1.25s.

An improved medical image compression based on region of interest on different imaging modalities was performed. The compression ratio is validated with compression standards defined by a group of radiologists. In this research work, the image processing and GUI interface was carried out in MATLAB environment. The enhancement, segmentation and compression techniques developed are also evaluated separately. The algorithms developed for segmenting the ROI from both MRI and ultrasound have been tested and evaluated using real image datasets and also compared against gold standards.

The limitations and scope for future work are also discussed

TABLE OF CONTENTS

LIST OF TABLES

LIST OF FIGURES

ABBREVIATIONS

AMBTC	Absolute Moment Block Truncation Coding
AWMF	Adaptive Weighted Median Filter
BCFCM	Bias Corrected Fuzzy C-Means
BTC	Block Truncation Coding
BUS	Breast Ultrasound
CAD	Computer-aided detection or diagnosis
CALIC	Context Based Adaptive Lossless Image Compression Standard
CAR	Canadian Association of Radiologists
CMYK	Cyan Magenta Yellow Black
COC	Coefficient of Correlation
CT	Computed Tomography
DCT	Discrete Cosine Transform
DPCM	Differential Pulse Code Modulation Coder
DRG	German Rontgen Society
DRLSF	Distance Regularized Level Set Function
DSC	Dice Similarity Index
DWT	Discrete Wavelet Transform
EM	Expectation maximization
EZW	Embedded Zero tree Wavelet
FCM	Fuzzy C-Means
FN	False Negative
FNR	False Positive Rate
FP	False Positive
FPR	False Positive Rate

FSVM	Fuzzy Support Vector Machine
GAC	Geodesic Active Contour
GAP	Gradient Adjusted Predictor
GED	Gradient Edge Detection
GLCM	Grey level Co-occurrence Matrix
GUI	Graphical User Interface
HIS	Gray-Level Histogram
HOG	Histogram of original gradient
HPV	Human Papillomavirus
HSV	Hue Saturation Value
ISOM	Incremental Self Organizing Maps
IWT	Integer Wavelet Transform
JPEG	Joint Photographic Experts Group
JPEG2K	Joint Photographic Experts Group 2000
JPEG-LS	Lossless JPEG
JSI	Jaccard Similarity Index
LSF	Level Set evolution Function
MATLAB	Matrix Laboratory
MED	Median Edge Detection
MMA-SOM	Merging Moving Average Self Organising Maps
MMCWS	Morphological Marker Controlled Watershed Segmentation
MMSE	Minimum Mean Square Error
MRI	Magnetic Resonance Imaging
MSE	Mean Square Error
OMP	Orthogonal Matching Pursuit
PACS	Picture Archival communication systems
PCA	Principal Component Analysis

PDE	Partial Differential Equation
PMRI	Pelvic Magnetic Resonance Imaging
PSNR	Peak Signal to Noise Ratio
PUS	Pelvic Ultrasound
RCR	Royal College of Radiologists
RGB	Red (R), Green (G), Blue (B) Color space
RGB	Robust Graph Based segmentation
ROI	Region of interest
RSF	Region Scalable Fitting
SeLIC	Selective Medical Image Compression
SI	Similarity Index
SPIHT	Set Partitioning in Hierarchical Trees
SRAD	Speckle Reducing Anisotropic Diffusion Filter
SVD	Singular Value Decomposition
SWT	Stationary Wavelet Transform
TN	True Positive
TP	True Negative
USG	Ultrasonography
VMCWS	Variable Marker Controlled Watershed Segmentation
VQ	Vector Quantization
WA	EZW and Arithmetic Encoder
YCbCr	Luminance Chrominance Blue and Red
ZSI	Zijdenbos Similarity Index

NOTATION

English Symbols

B	the blue color channel in RGB image
Cb	the chrominance blue component in YCbCr color model
Cr	the chrominance red component in YCbCr color model
d(x)	diffusion coefficient
G	the green color channel in RGB image
I	reference image or input image
$I_1 (i, j)$	low-pass filtered image
N1, N2	the two neighbors of the pixel P_x
P_x	Pixel value
R	the red color channel in RGB image
$R_0 (i, j)$	difference image or prediction error
$S_0(i,j)$	input intensity image
T_h	threshold value
$u_{i, j}$	represents the input signal
$v_{i, j}$	represents the noise signal
$x_{i, j}$	multiplicative noise model
x_o	speckle coefficient of variation
$x_o(t)$	speckle scale function
$x(i,j;t)$	instantaneous coefficient of variation
Y	the luminance component in YCbCr color model

Greek Symbols

ρ	constant used to reduce the exponential decay rate in $x_o(t)$

∇	Gradient operator
∇^2	Laplacian operator

Miscellaneous Symbols

$\oplus$	Morphological dilation
$\ominus$	Morphological erosion
$\bullet$	Morphological closing
$\circ$	Morphological opening

Chapter -1

INTRODUCTION

Contents

1.1 OVERVIEW

The rapid advances in medical imaging technology, helps in acquiring high quality and better informative descriptions of human internal structures and functions. Due to this technological discoveries and software developments, medical image processing is now becoming a prominent branch of science, gaining wide acceptance in healthcare industry. Medical imaging is concerned with the development of various imaging devices which helps to establish a full structured database of normal and abnormal images. These datasets in hospitals help the doctors to reveal the internal abnormalities hidden by the skin and bone and aim to provide treatment for better way.

Medical imaging has developed at an astonishingly rapid speed and this will definitely encourage the researchers for superior innovations. They need a detailed study of newly discovered image features for analyzing the step by step progression of diseases. Certain products of medical imaging technologies can simplify imaging work-flows, also enhances the accuracy of diagnosis and aims to improve patient outcomes in hospital environment. Newly developed techniques will transform all the received data onto effective visual representations and this will definitely help researchers to understand the characteristics and features of data to carry out a selective study.

During the past decade certain image processing techniques has been widely used for computer aided detection (CAD) systems. These systems can improve diagnostic accuracy and also can find the missed micro calcifications where the professionals cannot. Image segmentation is the initial step carried out in most automatic pictorial pattern recognition and scene analysis problems. The method will divide the image into two sub regions based upon some grey level values.

The innovation of Picture Archival Communication Systems (PACS) upgrades the status of radiology department in several hospitals. This new imaging technology helps in transmitting the electronic images and patient records digitally and thus reduces the burden of manual labor. PACS also provides electronic image integration platform to interface other medical automation systems such as Hospital Information System (HIS), Electronic Medical Record (EMR), Practice Management Software (PMS), and Radiology Information System (RIS) to properly manage the patient exams (**Aldosari, 2017)**. A highly skilled trainer is essential for the installation and proper maintenance of PACS. Security issues, maintenance cost, possibility of breakdown is also challenging in case of PACS. An effective and consistent management is vital, for the proper growth of radiology department as it is running with this increasingly distributed environment. So the incorporation of compression in medical domain will definitely improve the flexibility in managing huge imaging datasets.

The modern-day archive of imaging techniques has widened from X-rays and now boosted to ultrasound (US), computed tomography (CT), magnetic resonance imaging and spectroscopy (MRI/MRS), and nuclear medicine (NM), positron emission tomography (PET), single positron emission tomography(SPET), photoacoustic imaging etc. These imaging modalities are generating large amounts of image data, especially from CT, MRI and PET imaging. The medical images in raw format will take huge storage space, so compression is inevitable for handling the image repository. The application of compression will reduce the dynamic range of image signal and the same time, bandwidth limiting can also be possible by reducing the bit rate of image signal.

Image compression can be performed in lossy or lossless manner. Depends upon the area of application certain important measures should be considered while performing compression. In the domain of medical images, compression research is still at its peak point position. The medical field always demanding a high quality images and therefore lossless type of compression techniques are mostly preferred. Direct application of lossy or lossless is not recommended, because of their reconstruction and quality problem. A combination of lossy and lossless type of compression will be of great interest and that is called as Regions of Interest (ROIs) based medical image compression (**Doukas, 2007**). Thus preserving the quality in diagnostically important regions while allows lossy encoding in other regions of image.

1.2 ROLE OF COMPRESSION IN MEDICAL IMAGES

Diagnostic centers and hospitals are generating tremendous amount of digital medical images every day and medical imaging grows to an unavoidable part of the biomedical sciences for diagnosis and now increasingly for treatment. It is the responsibility of every hospital authorities to properly manage these image datasets for better storage and future needs. There comes the role of digital image compression which aims at reducing the number of bits needed to represent an image by utilizing the redundancies in an image data.

A digital image is basically listed into three type of redundancy: Interpixel redundancy, coding redundancy and psychovisual redundancy (**Zuo, 2015**). Interpixel redundancy is due to the correlation between adjacent pixels in an image. If the pixels are highly correlated then the value of any given pixel can be predicted from its neighbours. This type of redundancy can be achieved through the difference of neighbouring pixels. Coding redundancy is associated with grey level information in an image. A set of events or information is represented in the form of codes. If the grey levels in an image use more code symbols than it is needed to represent each grey level, then that image contains coding redundancy. Instead of using natural binary code, exploitation of variable length code and nonunifrom histograms can reduce coding redundancy. Psychovisual redundancy is associated with visual information in an image. Human perception is less sensitive to luminance value in the image. Removal of such type of redundancy will cause loss in image quality, which is commonly referred to as quantisation. This irreversible operation is preferred only in lossy type of compression.

The removal of three types of redundancy depends upon the type of image compression. The data compression algorithms are broadly classified into lossy and lossless. In irreversible lossy compression scheme, reconstructed image is obtained with acceptable degree of deterioration with a very high compression ratio such as in JPEG (**Wallace, 1992)**, JPEG2K 9/7 (**Skodras, 2001)**. The lossless compression techniques are usually applicable to data where high qualities of reconstructed images are required. An example of such type includes medical imaging, satellite imaging etc.

Lossless image compression guarantees for image quality at the same time provides slight compromise in compression ratio LOCO-I (**Weinberger, 2000)**, CALIC (**Wu, 1997**), JPEG2000 5/3 (**Wu, 2005)**.

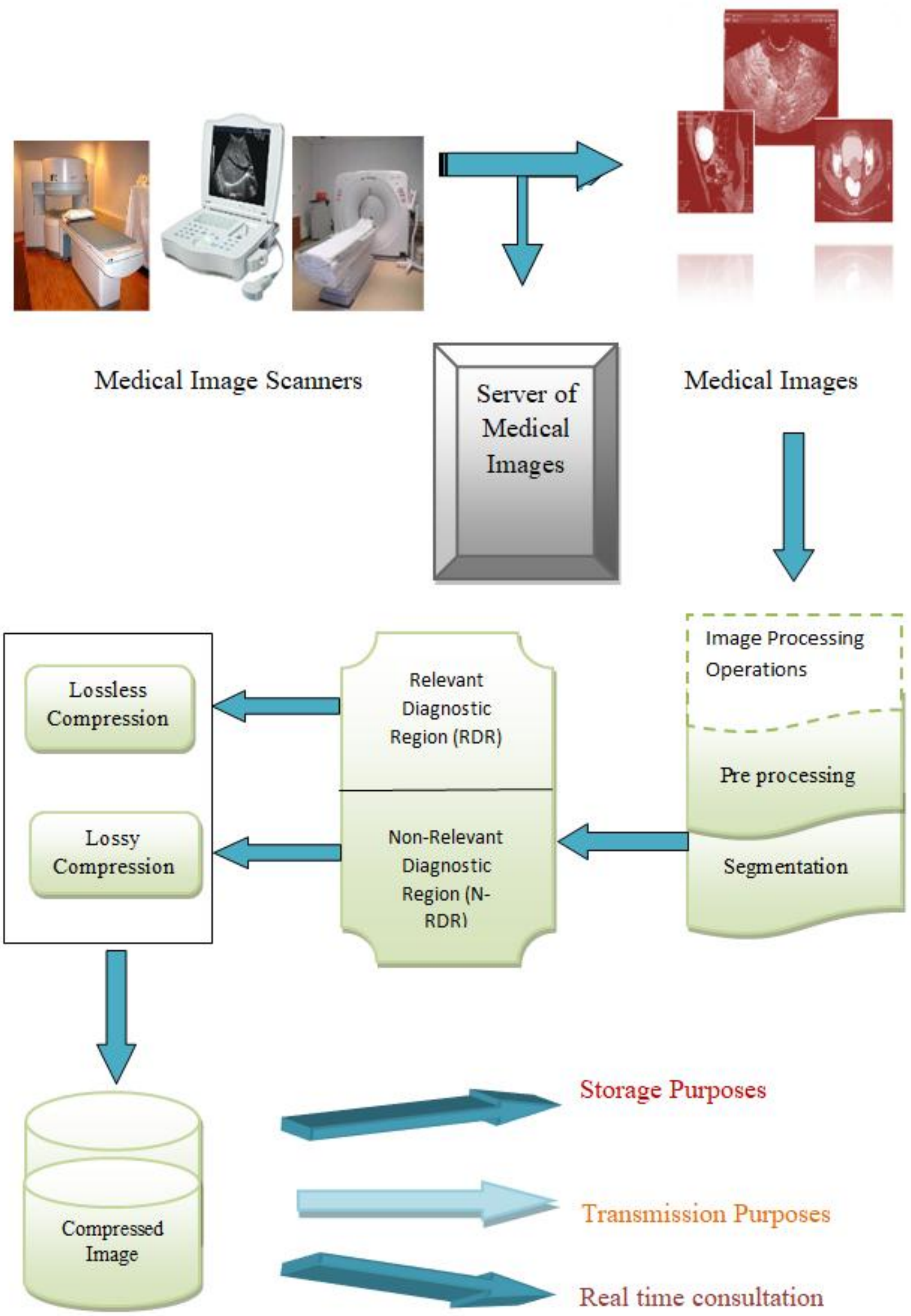

Fig. 1.1: Schematic representation of compression procedure for medical images.

India, the second most populous country in the world is geographically large with towns and villages. A shortage of senior radiologists around this developing nation is causing delay for patients and other medical problems. Arrival of telemedicine finds a solution to this problem which helps to provide an efficient patient care in limited time. Different kinds of data like text, images, audio, and video are used in entire telemedicine process. To handle the large volume of data without losing the important diagnostic information, faithful compression methods are recommended. In the compression of medical images certain parameters like bandwidth, transmission rate, quality and volume of the medical images need to be considered.

The role of image compression in telemedicine is discussed in (**Sapkal, 2011)**. Telemedicine is working with mass volume of data approximately in the range of 100's Mb **(Sapkal, 2011).** Transferring of these huge volumes of data through the network is time consuming, so there is no easy solution other than image compression to handle this problem. The schematic representation of compression procedure is shown in Figure 1.1

1.3 MOTIVATION

According to a new Lancet study, India and China are two countries with the largest number of women diagnosed with breast and cervical cancer. India is the second most populous country in the world, with 1.34 billion populations. Out of that, 432.2 million women aged 15 years and older are at risk of developing cancer. Cervical cancer has a major impact on woman's lives worldwide and one in every five women suffering from cervical cancer belongs to India. When considering the low and middle income countries (LMICs), number of women diagnosed with cervical cancer is expected to rise by at least 25 per cent to over 7, 00,000 by the year of 2030

[**Sreedevi, 2015**]. With the population growth rate at 1.2%, India is predicted to have more than 1.53 billion people by the end of 2030. Every year in India, 122,844 women are diagnosed with cervical cancer and 67,477 die from the disease (**Bruni, 2017**) but where a woman lives will largely determine her chance of survival.

In South Asia, India ranks the highest age standardized incidence of cervical cancer, when compared with Bangladesh, Sri Lanka, and Iran (**Sreedevi, 2015)**. Therefore, it is vital to understand the epidemiology of cervical cancer in India. It is the second most common cancer in women aged 15–44 years. The lack of data collection on the extent and nature of cancer is an enormous challenge to understanding the true burden of cancer in LMICs and needs to be improved. The number of new cases (Cancer incidence) and the number of cancer deaths (Cancer mortality) at different age group is shown in Figure.1.2 and Figure 1.3. It can be observed that the age-specific rates of cancer increases substantially after the age group of 40 years, in that the peak rate of cancer cases occur in age group of 55-59. An estimate in the year of 2012 (**Bruni, 2017**) and 2018 **(Bruni, 2014)** for cervical cancer incidence and mortality in India is shown in Figure 1.4 and 1.5.

If a centralized database is available in hospitals then it will be easy for the doctors for quick reference of medical images to obtain a correct diagnostic. But in today's scenario the volume of digital imagery produced by hospitals and their new filmless radiology departments has been increasing even faster. This bulk images can't be stored for a long time due to storage constraints. This increasing demand widened the area of image compression. Since the problem is particular to medical imaging field, care must be taken as distortion of information in medical images may lead to inaccurate diagnosis.

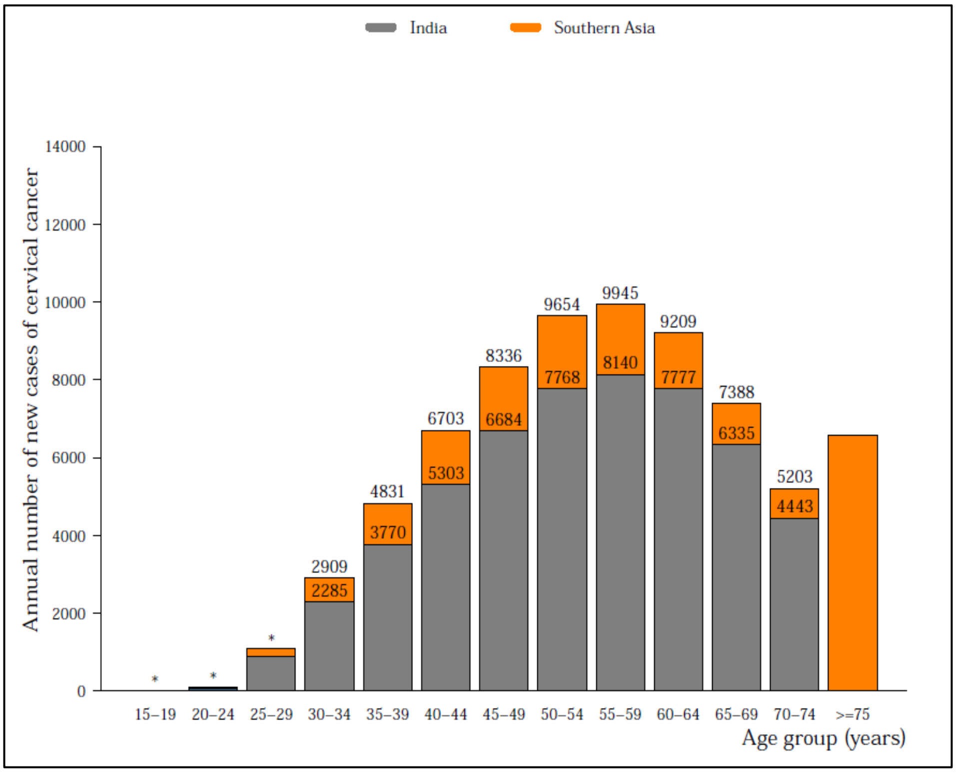

Fig. 1.2. Annual Number of New Cases of Cervical Cancer by Age Group in India (estimates for 2018) Adapted from Bruni et.al (2018).

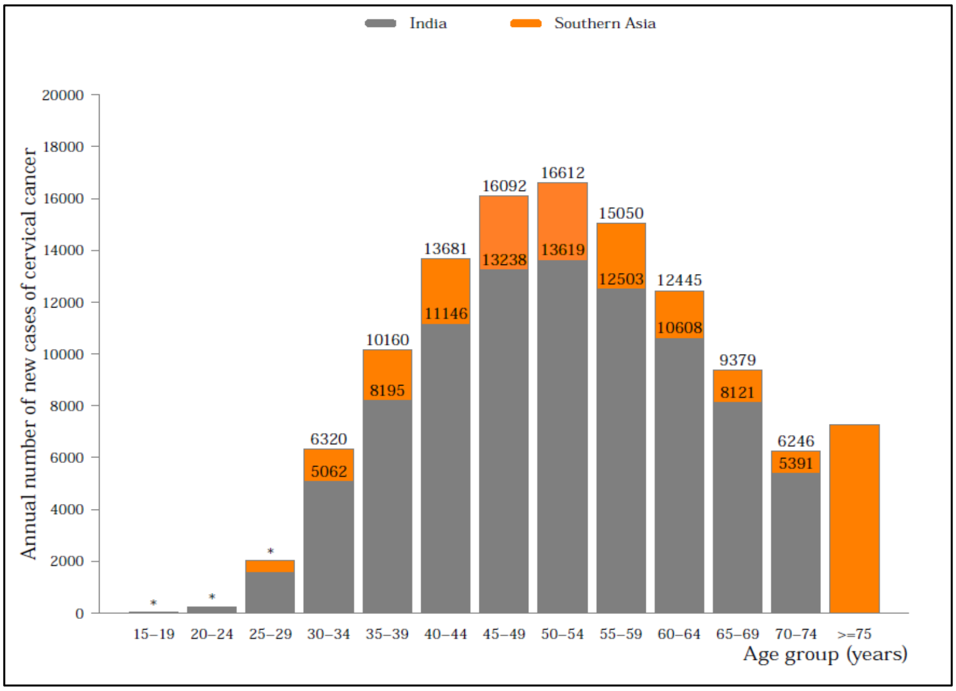

Fig. 1.3. Annual Deaths Number of Cervical Cancer by Age Group in India (estimates for 2018) Adapted from Bruni et.al (2018)

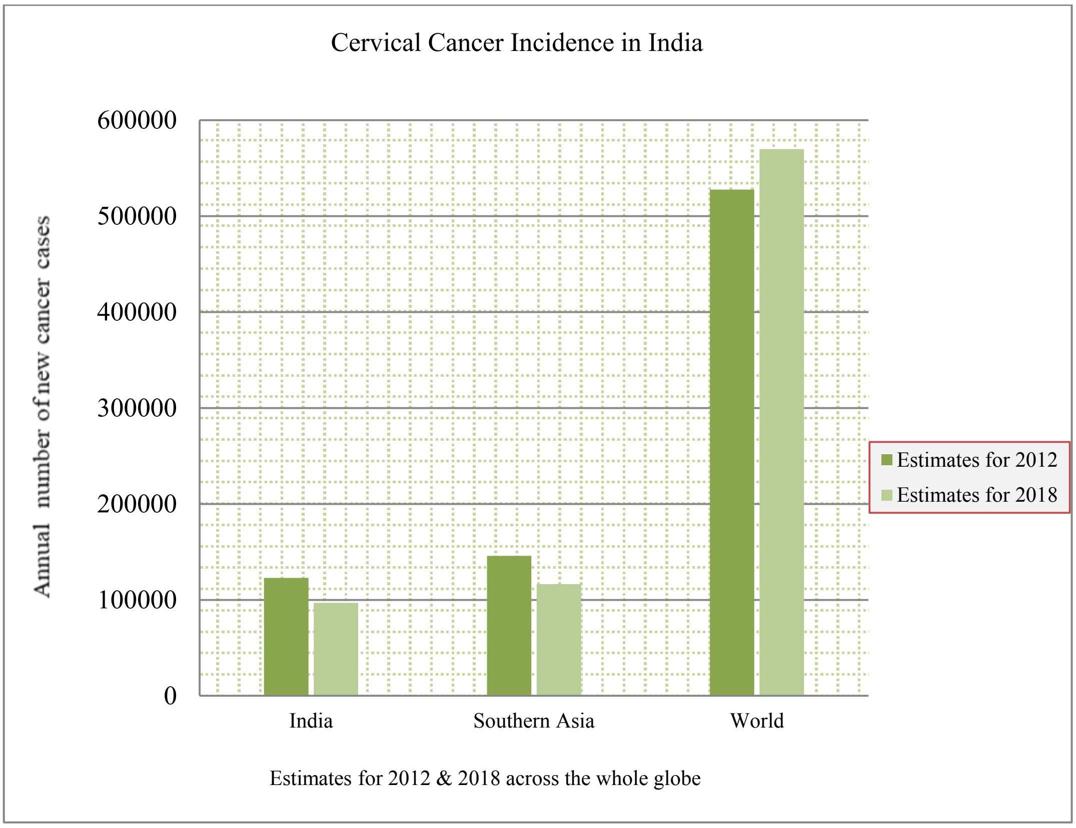

Fig. 1.4. Cervical Cancer Incidence in India Estimates for 2012 and 2018.

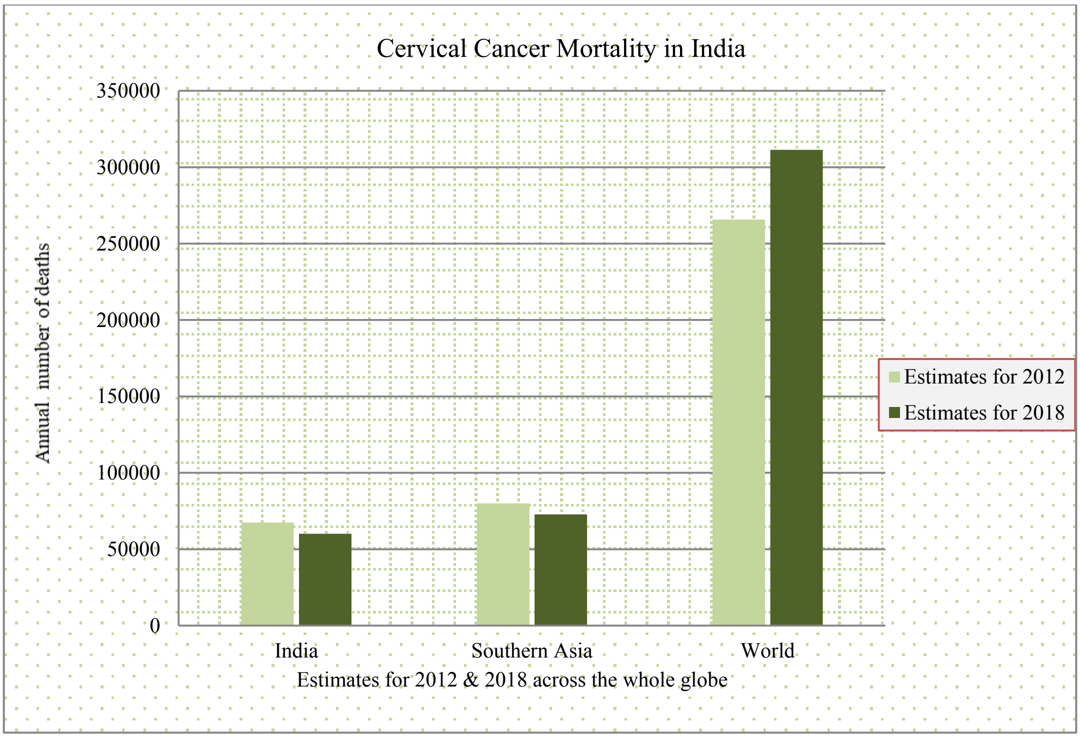

Fig. 1.5. Cervical Cancer Mortality in India Estimates for 2012 and 2018.

Nowadays many hospitals make use of teleradiology applications in which the radiographers or a technician can control the patient without the need of an expert radiologist. They can take the X-ray or MRI or CT image and send the image through a network connection to the hospital where the diagnostic radiologist can read the image and send back a diagnosis. All these happen in a limited time otherwise the patient have to wait in imaging apparatus till the remotely located diagnosing radiologist gets a good image from which he can deduce. If a good quality compressed image reaches the other side radiologists, a solution to this problem can be achieved at the same time, the waiting time of patients can also be reduced.

Better bandwidth utilisation can reduce the transmission time which can provide a quick medication to patients in limited time. Segmentation and reliable extraction of important features from the female pelvic images should be properly taken and should be compressed in a lossless manner. An attempt is made in this work to develop a novel algorithm for the extraction of important diagnostic region from the female pelvic images and also proposed an improved compression method for better storage and transmission.

1.4 OBJECTIVE OF THIS WORK

The digital technology based imaging modalities like MRI, Ultrasound, CT scan, Digital mammograms etc. producing a hundreds or thousands of images per day in hospitals. These rapid changes in radiology workflow have resulted in virtual explosion in the amount of image data. The medical images in raw format will take huge storage space, and many hospitals haven't much storage facility to manage this bulk image data. Small size of the image is advantageous in case of medical image transmission in terms of bandwidth conservation.

The main objectives of this research work are:

1. To develop a lossless image compression technique based on region of interest.

2. To develop an automatic segmentation method to detect the important diagnostic region in female pelvic Ultrasound and MRI imaging. The method should preserves the true diagnostic information, at the same time reduce storage and transmission costs.

3. Testing and validating the algorithms using real image datasets.

My contributions to this work is

1. To develop novel and efficient segmentation method for the extraction of
   (i) Ovarian Cyst in female PMRI imaging
   (ii) Endometrial Carcinoma in female PUS imaging

2. The algorithms developed for female pelvic imaging modalities are simulated using MATLAB environment.

1.5 LAYOUT OF THE THESIS

The thesis is organized into the following 7 chapters. A brief review of medical image compression is given in chapter 1. The objective of the work, motivation and outline of the thesis are elaborated in this chapter.

Chapter 2 sketches the structure of female pelvic system, its important parts and the details of current imaging modalities used for female pelvic examination Further the abnormalities in both uterus and ovary are briefly described towards the end of the chapter.

The work done in this research can be partitioned as enhancement, segmentation of important diagnostic part and region of interest based compression. The literature reviews on the three modules are discussed in Chapter 3. The literature survey is done separately for female Pelvic Ultrasound (PUS) imaging and female pelvic MRI (PMRI) imaging in case of enhancement and segmentation. At the end of the chapter details about the compression standards for different medical imaging modalities defined by a group of radiologist's are discussed.

Chapter 4 begins with the pre-processing operations for female Pelvic Ultrasound (PUS) imaging. Then the chapter proceeds with the segmentation of region of interest in PUS imaging. Later it discusses the enhancement and segmentation algorithms for female pelvic MRI (PMRI) imaging. The details about the colour plane, filtering methods are also discussed. Finally at the end of the chapter information about the datasets are given.

Chapter 5 describing the different compression techniques and how the region of interest based medical image compression is achieved in both modalities, without losing the important diagnostic information.

Chapter 6 discusses the experimental results of both segmentation and compression methods. A number of tables and graphs are used to compare the performance of different algorithms. Compression ratio and psnr values are used for measuring the quality of reconstructed images. They are also compared with the compression standards defined by radiologist's society. A GUI or graphical user interface was created for user interface.

Chapter 7 summarizes the observations and inferences brought out in the previous chapters. The suggestions for future advancement of this work are also given in this Chapter.

Chapter -2

IMAGING OF FEMALE PELVIS

Contents

2.1 INTRODUCTION

The Pelvis is a hard ring of bone seen in the lower part of trunk, located between the abdomen and the legs. This region supports and protects the pelvic organs and the contents of abdominal cavity. The female pelvic is structurally formed with pelvic bones, muscles, pelvic organs and pelvic ligaments. Female pelvis is adapted for child bearing and it is more delicate than, wider than and not as high as the male pelvis. The female pelvis develops and reaches its full width around the age of 25-30 years.

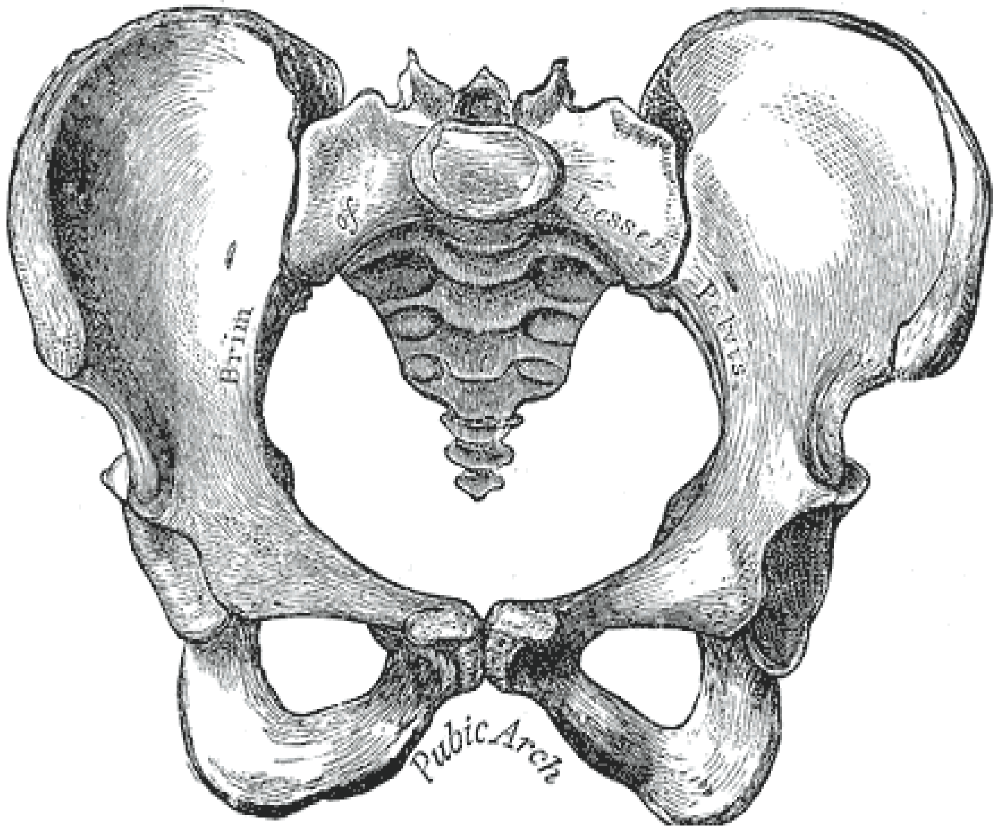

Fig. 2.1. Female Type Pelvis

2.2 UTERUS ANATOMY

The female pelvic organs include the ovaries, uterine tubes or fallopian tubes, uterus, cervix, urinary bladder, ureters, vagina, and rectum. The uterus is a powerful muscle located in woman's lower abdomen between the bladder and the rectum. It is also called womb, a major female hormone-responsive reproductive sex organ of most mammals including humans. Ovary is a ductless reproductive gland situated on either side of the uterus. These pair of ovaries produces eggs and secretes the sex hormones such as estrogen and progesterone which regulates menstruation and control the development of sex organs. One of the main functions of the uterus and ovaries is cardiovascular protection. The anatomy of the uterus consists of 3 layers which together forms the uterine wall (**Behra, 2015)**. From innermost to outermost these layers are endometrium, myometrium and perimetrium. The fallopian tubes or uterine tubes connect each ovary to the uterus. The uterus has three parts:

Top: The top (fundus) of uterus is shaped like a dome. From the top of the uterus, the fallopian tubes extend to the ovaries.

Middle: The middle part of uterus is the body (corpus). This is where a baby grows.

Bottom: The narrow, lower part of the uterus is the cervix. The cervix is a passageway to the vagina

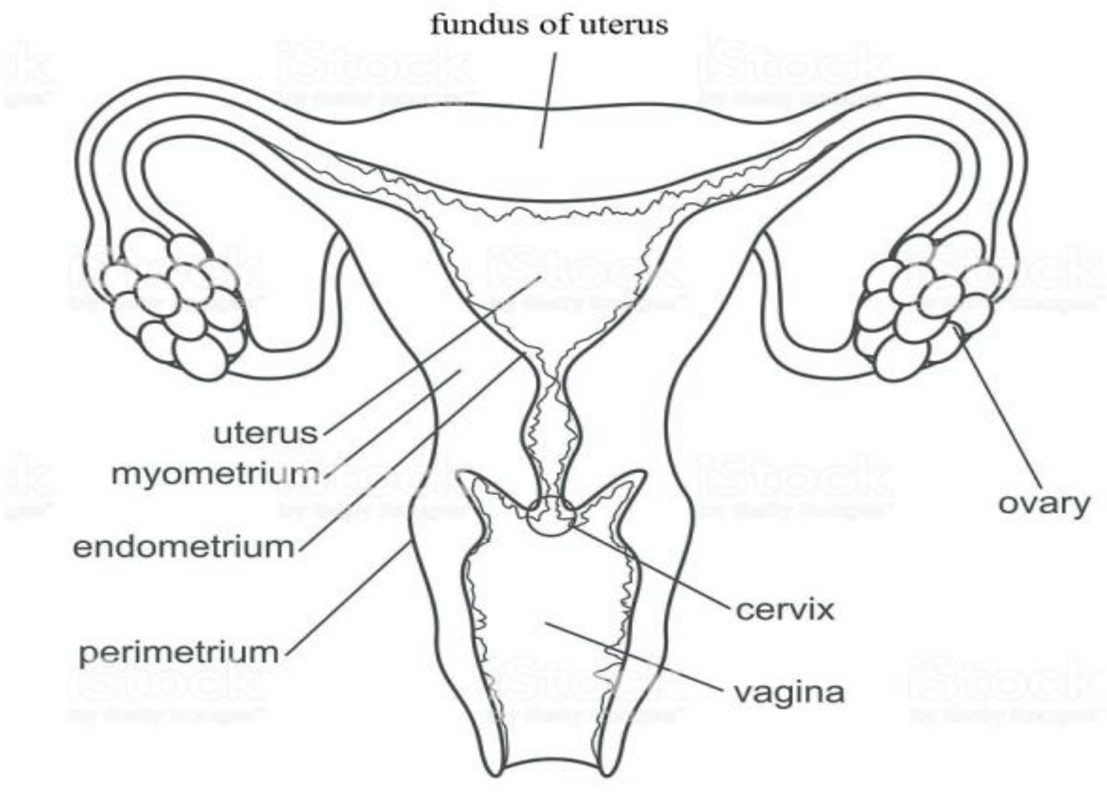

Fig. 2.2. Schematic Diagram of Uterus

2.3 FEMALE PELVIC EXAMINATION

The diagnosis of gynecology related symptoms are normally performed through periodic pelvic examinations by an expert radiologist. The doctors suggest additional diagnostic treatment or testing as part of this pelvic examination. Experts and gynecologists recommend a routine pelvic examination for all women unless any medical problem, preferably after 21 years. A routine pelvic exam can definitely help to find the possible signs of ovarian cysts, sexually transmitted infections, uterine fibroids or early-stage cancer.

However this clinical or physical examination overestimates or underestimates the actual extent of disease and getting troubled with wrong decision (**LaPolla, 1986**). For this reason, several imaging modalities like transvaginal ultrasonography (TVUS), computed tomography (CT), and magnetic resonance imaging (MRI) have been used as a diagnostic tool for the pre-treatment work-up of cervical cancer all over the world (**Faria, 2015**).

In developing countries like India, there is a lack of effective screening programs for cervical cancer, so that there is no reduction in the incidence of cancer nowadays (**Sankaranarayanan, 2009**). There are a number of different types of screening methods available. A large scale cytological testing for women is recommended in developed countries regardless of their age and sexual history (**Sankaranarayanan, 2009**). Papanicolaou-stained (Pap) smear or Pap test are important tests, is a part of well woman exam or pelvic exam, and helps to identify the small changes in cervical cells. If the results of Pap test are abnormal, then the doctors take a sample of the tissue of the respective part and send it to the laboratory for analysis. The tissue sample is taken in different ways. Punch biopsy and endocervical curettage is performed to examine the cervix. Dilation and curettage (D&C) or endometrial biopsy is selected for uterine cancer. The doctors follow different diagnostic procedure for treating different part of the uterus.

Cytology deals with the study of individual cells whereas cytopathology details about the study of individual cells in disease. Sampled fluid/ tissue from a patient are smeared onto a glass slide of about 25 x 50 mm. The cells are stained, fixated, and then visually examined under a microscope by the anatomical pathologist to look at the number of cells, and how the stage of cells are grouped together with respect to their shape, size, texture, ratio of nucleus and cytoplasm etc. This information is useful in determining the signs of malignancy on a specimen.

2.3.1 Female Pelvic Ultrasound (Pus) Imaging

Ultrasound or Ultrasonography uses high frequency sound waves to create pictures of the internal organs. This less invasive, less expensive imaging modality is considered as the first imaging modality used in women with pelvic symptoms (**Benacerraf, 2015**). A small device called ultrasound probe which is a type of transducer produce high frequency sound waves. These sound waves bounce off to different parts of the body and that backscattered echoes are picked up by these device and turned into a moving image. Figure 2.3 shows the different ultrasound scanning machines. Figure 2.3 (a) is a trolley based and Figure 2.3 (b) is a portable one.

Alcazar et al. (**Alcázar, 2014)** described that the role of ultrasound imaging was increased for assessing the cervical cancer. If the ultrasound cancer detection provides greater accuracy, then unnecessary surgical biopsies can be avoided (**Cheng, 2010)**.

Therefore, ultrasound imaging is preferable in large-scale screening programmes because of its cost effectiveness and lesser radiation effect.

Fenster et.al (**Fenster, 2011)** had point out some advantages of three dimensional ultrasound images over conventional two dimensional images. 3D ultrasound imaging provides accurate results in estimating the tumor volume (**Fenster, 2011; Chou, 1997**). Since 2D ultrasound imaging transducers are controlled manually, it is difficult to relocate the exact location when imaging a patient. Interventional procedures also take the advantage of arbitrary selection, which is not possible in conventional ones for optimal viewing of image planes.

(a) (b)

Fig. 2.3. Ultrasound Scanning Machines.

(a) Philip IU622 trolley ultrasound system

(b) DP-1100 Plus portable ultrasound machine

2.3.2 Female Pelvic Magnetic Resonance (PMRI) Imaging

Magnetic Resonance Imaging or nuclear magnetic resonance imaging uses strong magnetic field and radio waves to create detailed images of the internal organs and tissues. The scanner is a large tube containing powerful magnets. During scanning the patient will be asked to lie on a movable table (in the middle) to scan the specific portion of the body. The strong magnetic field (range 0.2 to 3 tesla) from this scanner aligns the hydrogen atoms within the body. The radio waves are turned on and off in a series of quick pulses which causes the hydrogen atoms to change its alignment. This process emits different amount of energy from the type of body tissue they are in. The coils in the MRI scanner will capture this energy to create detailed cross sectional images of the scanned tissue. This non-invasive method does not use any ionizing radiations.

The technicians control the scanner using a computer which is kept outside the scanning room, away from the magnetic environment. Through two-way intercom facility, the technologist can easily communicate with the patients. To enhance the visibility of particular tissue, a contrast material will be used in MR exam. Technologist will insert an IV (intravenous) line or intravenous catheter into the vein of patient’s hand. A saline solution or gadolinium may be injected through IV. Additional series of scans may be taken during or following the IV injection as per the doctor’s instruction.

Brocker et.al **(Brocker, 2011)** was reviewed for methods used to diagnose the abnormalities in female pelvis with special emphasize on the role of MRI as the best imaging method. MRI has complemented other existing diagnostic techniques like CT (computed tomography) and or sonography in monitoring anomalies in female pelvis

(Brocker, 2011; Chou, 1997). Its better tumor delineation, improved tissue contrast helps in further therapy planning. CT being the gold standard for oncology in initial staging (**Brocker, 2011)** whereas ultrasound remains the gold standard in early diagnosis (**Butler, 1984)** still facing limitations.

(a)

(b)

Fig. 2.4. MRI Scanning Machines
(a) OPTIMA MR360 1.5T
(b) OPTIMA MR450w 1.5T

MRI provides superior soft tissue contrast than CT. It is not only limited by poor soft tissue contrast but also suffering from harmful ionizing radiation significantly decreases its value in diagnosing female pelvis. MRI is more frequently applied for pre-treatment disease staging whereas CT provides vital information about lymph nodes, peritoneal implants of the lung, liver etc. Figure 2.4 shows the pictures of different MRI scanning machines. Figure 2.5 shows the images of normal uterus. Sagittal transvaginal ultrasound of the normal uterus is shown in figure 2.5 (a), whereas in (b) sagittal plane of MRI is given.

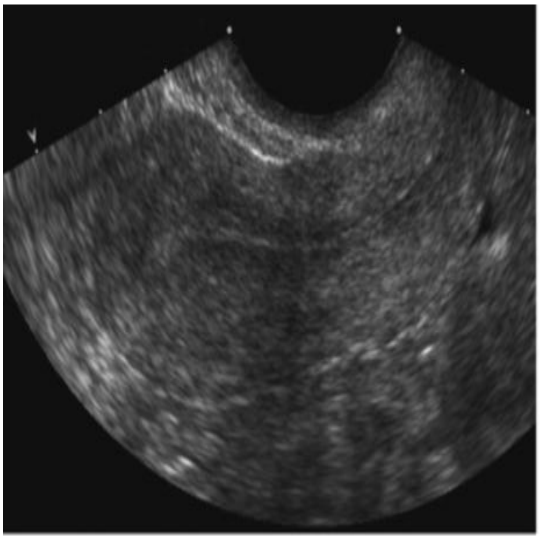

(a) (b)

Fig. 2.5. Ultrasound and MRI images of normal uterus.

2.4 ABNORMALITIES IN FEMALE PELVIS

Abnormalities in female pelvis are associated with benign and malignant neoplasms of the uterus, ovaries, fallopian tubes, and cervix. Abnormalities in the pelvis can prevent the egg from attaching to the lining of the uterus and can block the fallopian tubes which may cause birth defects and growth of fibroids inside the uterus. A pelvic abnormality can be detected during a routine gynaecologic examination.

A pelvic mass may be cancerous or non-cancerous and type of mass is varying by age group **(Barad, 2018)**. Non-cancerous or benign tumors remain similar to the tissue of their origin and won't invade nearby tissues or spread to other areas of the body causing metastasis (**Fayed, 2019)**. Benign tumors need to be removed to prevent them becoming malignant or cancerous. Once these tumors are removed it won't occur again periodically and if that happened, it will occur in same place (**Fayed, 2019)**.

Malignant tumors are made of cancerous cells and it can invade surrounding tissues. Cancerous cells break away from the parent tumor and advance through the body via bloodstream or lymph nodes, where they can spread to other tissues within the body and form new tumors (**Fayed, 2019)**. The cell growth is faster when compared with benign one. Malignant tumors recur after removal, sometimes in areas other than the previous place. The most common gynecological cancers affecting women worldwide and in India are ovarian and cervical cancer (**Maheshwari, 2016)**.

2.4.1 Abnormalities in Uterus

Abnormality of the uterus or Uterine abnormality is female medical condition in which woman's uterus cause some change from the normal one in terms of structure rather than position.

2.4.1.1 Cervix Cancer

Cervical cancer is the type of the cancer that occurs in the lower part of the uterus (cervix). In India Cervical cancer is the second most common gynecological cancer among women (**Maheshwari, 2016)** and is common among young agers also. Abnormal growth of cervical cells results from the human papillomavirus (HPV) infection, transmitted during sexual intercourse. Cervical cancer may not produce any symptoms or signs in the early stage. It starts showing the signs only when it moves to metastasis stage. The symptoms include abnormal vaginal bleeding, foul smelling discharge and pain in the pelvic area. Routine pap tests and other imaging techniques like MRI, CT can detect predict the stages of cancer. Accurate pap tests can detect the symptoms in early stage and can steer treatment to improve the cure rate. Without proper treatment, cancer cells grow and multiply out of control and invade to other parts of the body and cause death.

2.4.1.2 Uterine Sarcomas

Uterine Sarcomas are highly malignant type of cancers developing from the uterine corpus (middle part of the uterus). It is different from the cancer of the endometrium, as in this type malignant cells are form in the muscles of the uterus rather than lining of the uterus. Uterine sarcomas are uncommon and are faster in growing. Symptoms include pain in the abdomen, a lump or growth in the vagina, feeling of fullness in abdomen etc.

2.4.1.3 Endometrial Cancer

Endometrial Cancer is a type of cancer that develops in the lining of the uterus. It is also called as uterine cancer or cancer of the uterus. Uterine cancer is a malignant type of gynecology cancer commonly seen in developed countries. In India the incidence rate of this type of cancer cases are very low, the highest being observed in Bangalore (4.2) and in Delhi (4.3) (**Balasubramaniam, 2013)**. Type I and type II are the two types of endometrium cancers. Former is estrogen dependent and latter is estrogen independent (**Setiawan, 2013).** Type I are generally slow growing and not very aggressive in nature. Types II is more aggressive and tend to occur in older women. Type II is more likely to spread than Type I.

2.4.1.4 Uterine Fibroids

Uterine Fibroids are benign tumors of the uterus composed of muscles and fibrous tissues. Fibroids may be microscopic or grow into bulky masses and mostly never develop into cancer. They can distort and enlarge uterus and can cause pain, abnormal vaginal bleeding, and repeated miscarriages. Hormone level can stimulate fibroids growth, it become larger during pregnancy and tends to shrink at the time of decrease in hormone levels (**David, 2014**).

Based upon their position within the uterus, fibroids are divided into intramural (in the wall), submucosal (in the lining) and subserosal (in the outer surface) (**David, 2014**). Doctors can diagnose the fibroids during pelvic examination or by an ultrasound. The different abnormalities in uterus are shown in Figure 2.6 and Figure 2.7. First column shows the abnormalities like fibroid, endometrium cancer and cervical cancer. In the second column ground truth images are given. Datasets are provided by LIRRIS (Lisie Institute of Radiology Research and Imaging Sciences).

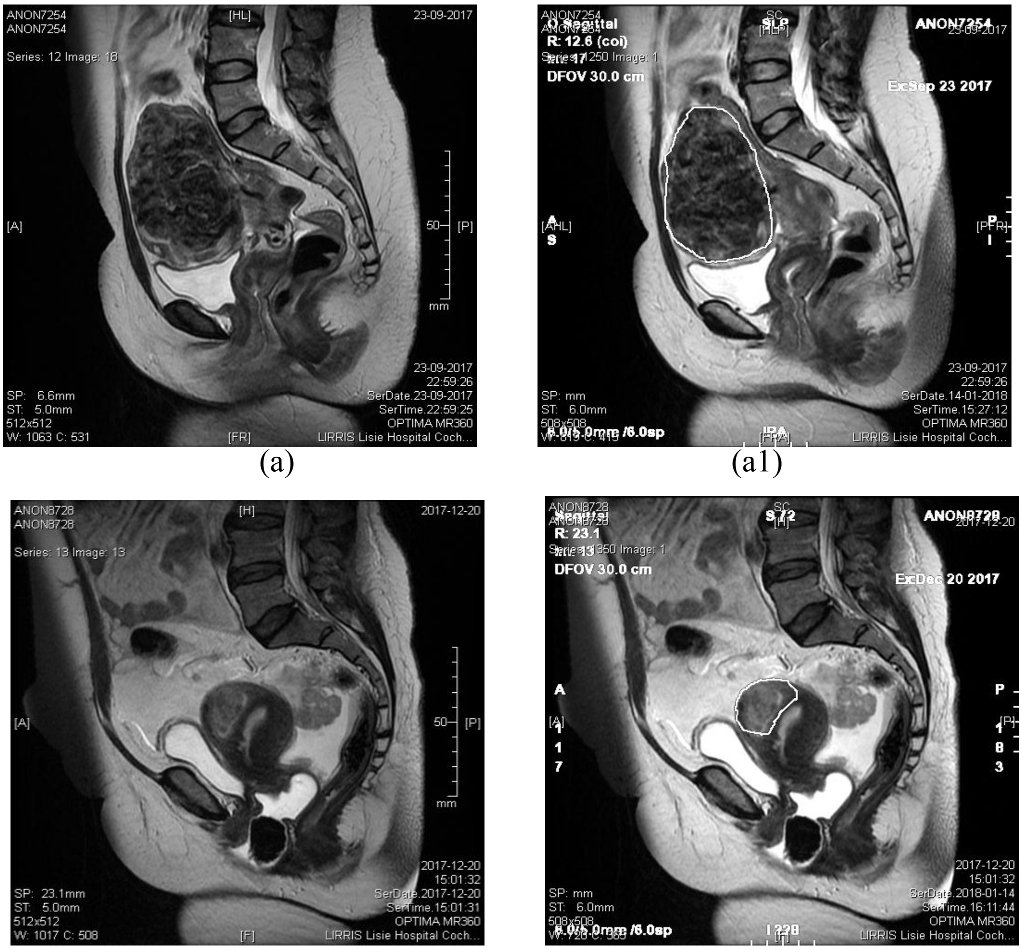

(a) (a1)

(b) (b1)

Fig. 2.6. Abnormalities in Uterus. (a) Fibroid, (b) Endometrium Cancer. (a1, b1) Corresponding ground truth images marked by radiologists.

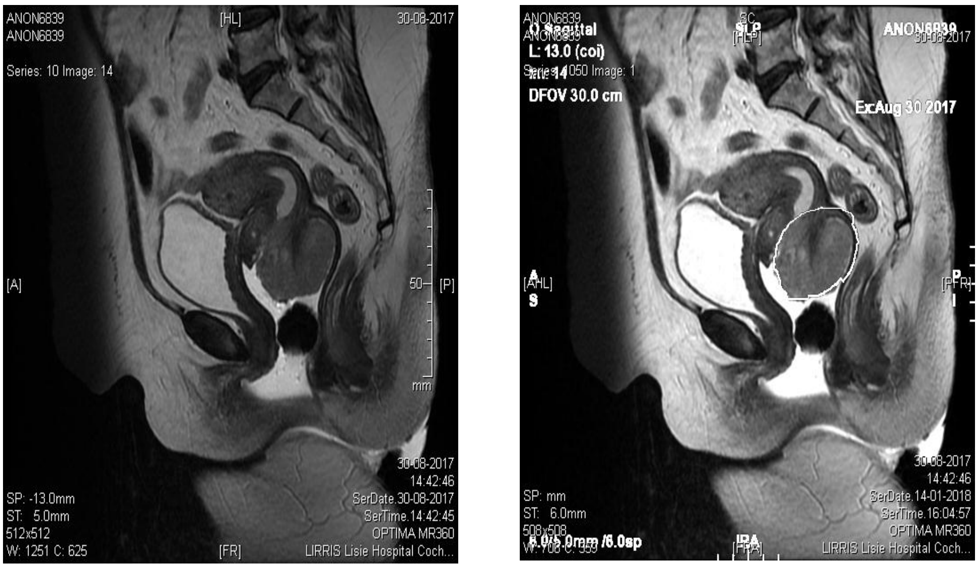

(a) (a1)

Fig. 2.7. Abnormalities in Uterus. (a) Cervix Cancer (a1) Corresponding ground truth images marked by radiologists.

2.5.1 Abnormalities in Ovary

Women have two ovaries, one on each side of the womb. Some of the abnormalities in ovary include ovarian cancer, polycystic ovarian syndrome, ovarian cysts, ovarian torsion etc.

2.5.1.1 Ovarian Cysts

Ovarian cysts are fluid filled sacs within the ovary or on its surface. Most of them are asymptomatic and harmless.it can be benign, can be borderline (low malignant potential) or malignant and usually form during ovulation. Benign ovarian cysts include functional cysts and tumors. Follicle cysts and corpus luteum cysts are the two types of functional cysts. Other type of cysts includes ovarian cystadenomas, ovarian dermoid cysts and ovarian endometriomas. Usually these types of cysts behave as benign, but occasionally they can be malignant.

(a) (a1)

Fig. 2.8. Abnormalities in Ovary (a) Ovarian cyst (a1) Corresponding ground truth images marked by radiologists.

2.5.1.2 Ovarian Cancer

Ovarian cancer is type of cancer that develops in the ovary. It is one of the common malignancy effecting women in India and shows an increasing incidence rate (**Maheshwari,2016)**. It is very difficult to treat the ovarian cancer in the late stage detection. Many women have no symptoms until the cancer is advanced to metastasis stage. Obese women have a higher risk of getting ovarian cancer than non-obese women. It is more common in women ages 50-60 years.

The different abnormalities in ovary are shown in figure 2.8 and Figure 2.9. First column shows the images of ovarian cyst and granulosa cell tumor (malignant stage of ovarian cancer). In the second column ground truth images are given. Datasets are provides by LIRRIS (Lisie Institute of Radiology Research and Imaging Sciences).

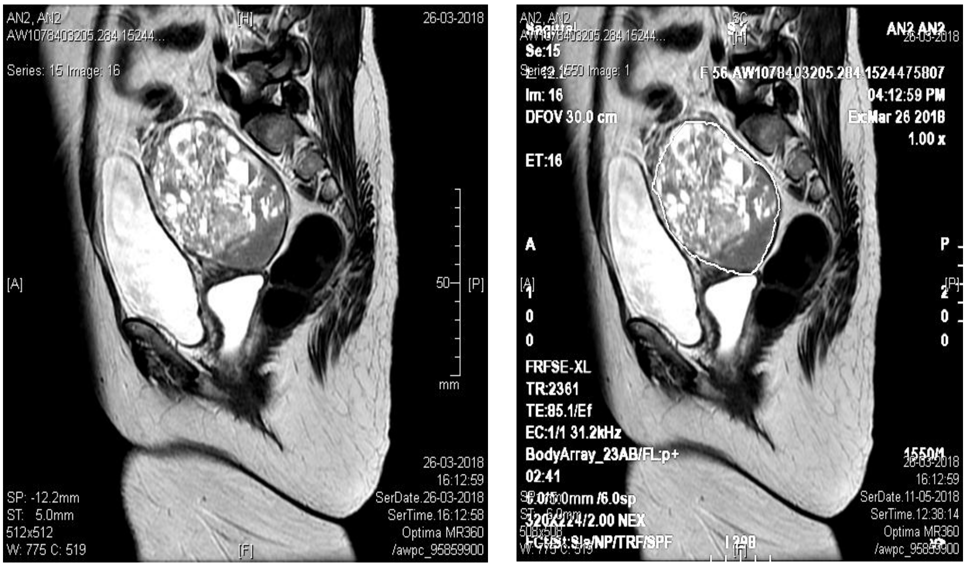

(a) (a1)

Fig. 2.9. Abnormalities in Ovary (a) Granulosa cell tumor (a1) Corresponding ground truth images marked by radiologists.

2.6 SUMMARY

This chapter gives the brief idea about female pelvic organs and imaging in female pelvis. Female pelvic ultrasound imaging and female pelvic MRI imaging was discussed in detail. This chapter also highlights the different type of abnormalities in uterus and ovary with sufficient images.

Chapter -3

REVIEW OF LITERATURE

Contents

3.1. INTRODUCTION

Literature review, an important section of report deals with the study of existing methodologies and published results, helps in the evolution of new algorithms and gives an exact direction in the area of research. This chapter introduces various work grouped under the headings of image enhancement, segmentation and region of interest based medical image compression techniques. The initial two sections of this Chapter presents the previous works related to image enhancement and segmentation in both Ultrasound and MRI modalities. The final section introduces the relevant foregoing works on compression techniques, used in medical image processing and thereby discovering the scope for this research.

3.2 IMAGE FILTERING AND ENHANCEMENT

Image Enhancement is a sort of image editing to improve the information in images which helps the human, a better visualization and can easily identify the key features in images. It includes filtering, contrast adjustment, image brightening, edge or boundary sharpening to provide a better input to coming image processing techniques. This section covers the literature review on both ultrasound and MRI imaging modalities.

3.2.1. Enhancement In Ultrasound Imaging Modality

Speckle is a form of multiplicative noise commonly seen in medical ultrasound images effects the image edges and makes the diagnostic interpretation difficult. So it's important to remove speckle from the input images without destroying the important image features (edges, boundaries). Speckle reduction techniques are mainly classified into three groups (1) filtering techniques, (2) Wavelet domain techniques, and (3) Compound approaches. The area of our research is more focusing on linear and non-linear types of filtering techniques. Linear type of filtering includes mean and adaptive mean filters. **(Calóope, 2004)** gives a comparison of filters for ultrasound images. The results shows that mean filters are not much effective in ultrasonic imaging as stated; speckle is a multiplicative model with non-Gaussian noise. Adaptive filters on the other hand outperforms the mean filters, selectively removes the speckle from different parts of the image. Lee **(Lee, 1980),** Kuan **(Kuan, 1985)** and Frost **(Frost, 1982)** proposed some commonly used adaptive mean filters. For preserving the important edges and features, local statistics like mean, variance, and spatial correlation have been used.

Median filters, a type of non-linear filtering maintains edge sharpening and having less blurring effect than mean filters (**Calóope, 2004**). Loupas (**Loupas,1986)** developed an adaptive weighted median filter (AWMF) based on weighted median coefficients. With the adjustment of these weighted coefficients, the filter can able to suppress the speckle noise and at the same time important image features can be preserved. The algorithm can easily detect small and precise image variations but it is failed in enhancing other image features such as, line segments. Although the existing despeckle filters have the advantage of edge preserving, but they are subjected to some major limitations.

It was Perona and Malik (**Perona, 1990)** who first proposed the idea of anisotropic diffusion which served as a useful tool for multiscale image segmentation, edge detection and enhancement. The proposed conventional anisotropic diffusion performs well with additive Gaussian noise, but failed in the presence of multiplicative noise.

Speckle Reducing Anisotropic Diffusion filter is provided by Yu and Acton (2002) **(Yu, 2002)**, a diffusion method specially tailored for ultrasonic and radar imaging applications. This Partial Differential Equation (PDE) based approach is adaptive and not using any hard thresholds (one used in enhanced version of Lee and Frost Filters) to alter the performance of homogeneous regions. In order to maintain the useful information in imagery, the algorithm directly processes the data without using any log compression (**Cheng, 2010**).

Wang et.al (**Wang, 2007**) introduced a hybrid method for speckle suppression and edge enhancement for ultrasound images. The method is purely based on anisotropic diffusion utilizing the denoising properties of median, isotropic diffusion and improved anisotropic diffusion filtering. The threshold values are chosen by experiments and their results shown that the method can markedly improve processing speed, and can enhance edges and therefore considerable to 3D ultrasound imaging. Q. Huang et.al (**Huang, 2015)** filtered 2D ultrasound breast image using a total variation model. The method was adapted from Rudin et.al (**Rudin, 1992)**. This nonlinear noise removal method is based on an energy minimization problem yields sharp edges of images.

3.2.2. Enhancement In MRI Imaging Modality

MRI imaging, as with any other imaging modality, has its share of artifacts. It is important to recognize these artifacts and certain necessary steps should be taken to eliminate the root of its origin or at least minimize them. Since the noise reduction is vital and necessary, the reduction methods are carried out either in acquisition mode or in the post-acquisition mode. The literature mainly targeting on the filtering based approach rather than transform and statistical based approaches of denoising methods. J. Mohan **(Mohan, 2014)** presented a survey based on MRI denoising methods. The survey is mainly focusing on post-acquisition image denoising methods. Using the available quantitative performance metrics, they compared existing methods with one another and their limitations and advantages are discussed. Their results show that none of the single method is superior to others in terms of their output characteristics in noise reduction, computation cost and edge preservation.

A new method was proposed by (**Manjón, 2012**) for spatially varying Rician noise in MRI images. Here the denoising strength of the filter depends upon the local noise information of images. This information is extracted using a new local estimation method. Again the same author J. Manjon (**Manjón, 2010**)presented two approaches for 3-Dimensional (3D) denoising of MRI images. The proposed two methods are particularly for typical type of Rician noise in MRI images.

Some of them presented a combination of earliest methods; one among them is a combination of both median and mean filter. Nobi et.al **(Yousuf, 2011)** proposed this simple and efficient method, for removing noise from MRI medical images. This new added method is compared with smoothing, median and midpoint filter and their results shows the proposed method is better in terms of structure details. Suhas and Venugopal **(Suhas, 2017)** proposed a technique that combines both linear and non-linear filters.

A new precise value for the pixel is calculated from old median and mean filter values. MRI brain images and spinal cord images are used as test images for the above proposed method. M. Gupta **(Gupta, 2018)** conducted the analysis of three different filters by adding three types of noises like Gaussian noise, salt and pepper noise and speckle noise to the input MRI images. For their experimentation they selected Gabor Filter, Arithmetic Mean Filter and Order Filter and their results proved that the last two filters are good in denoising the above mentioned noises.

In **(El-Dahshan, 2014)** El. Dahshan presented a survey of studies done on MRI brain segmentation methods. According to his study, median filter is the appropriate denoising method that can be used for MRI images. Joseph et.al (**Joseph, 2014)** also used the median filter to preserve the edges of MRI brain images. Mohammed (**Mohamed, 1999)** added Gaussian noise with diverse signal to noise ratio and monitored their results on synthetic images. They choose values in a range of 5, 10, and 20. Traditional FCM algorithm, hybrid median filter and a modified fuzzy is employed for comparison. The results of modified FCM algorithm shows superiority over FCM algorithm as it can recover the image from noisy environment without effecting the edges.

3.3 REGION OF INTEREST BASED SEGMENTATION

The earliest systems have mostly relied upon the traditional methods of image segmentation which is confined to the basic edge based and region based segmentation techniques. This section focuses on the literature on segmentation techniques, in both ultrasound and MRI imaging modalities.

3.3.1. Segmentation in Ultrasound Imaging Modality

The segmentation of ultrasound images is not very easy task because of its low contrast characteristics. The edge detection is very sensitive to noise and artefacts and it badly affects the edge detector for proper boundary extraction. It was Kass (**Kass, 1988)** who initially proposed the widely used edge segmentation method called active contour model or snakes. So many algorithms are developed from this basic platform of segmentation methods.

Selvathi have made an attempt to extract the local properties such as phase, energy and amplitude from the grey scale ultrasound kidney images using the property of monogenic signals (**Selvathi, 2017**). The concept was based on regularized level set evolution which is an active contour based segmentation. (**Belaid, 2010**) Ahror Belaid used an approach called Phase based level set, to extract the left ventricle boundaries of ultrasound images. They integrated the use of novel speed term based on local phase and local orientation derived from the monogenic signal. B-mode echocardiography images are used to test the performance of algorithm. Both the authors used the Cauchy functions, instead of the traditional Log Gabor functions for the purpose of feature extraction.

(**Antunes, 2011)** proposed an active contour model, based on phase symmetry and level set evolution for the segmentation of speckle noise effected echocardiography images. Here a new logarithmic based stopping function is used to extract all heart cavities in fully automatic way. The method can able to segment four hear chambers and shows 4% superiority than other existing methods. **(Li, 2011)** tested the performance of algorithms coming under basic segmentation algorithms like edge based, texture based, region based and active and contour based techniques using kidney cyst images and phantom kidney images. The study shows that algorithms are effective only for homogeneous image features rather than heterogeneous lesions. For segmenting this kind of divergent area lesions they suggested the techniques rely on image intensity discontinuities.

(Chang, 2003) introduced a 3D ultrasound segmentation method to identify tumor shape and size equally. Here 3D breast tumor images are considered. Initially histogram equalisation is performed for contrast enhancement. Then a 3D stick method is performed to obtain detailed shape information of the tumor. To separate the tumor from background they used threshold method, since the tumor regions are always dark (black) in color when compared with the other regions. Thus they got the binary image with tumor in black and background in white color. The used automatic threshold determination method was adapted from Ramesh (**Ramesh, 1995**). He found out the threshold value, by minimizing the sum-of-square errors SSE (t) between the grey values and the mean values in the two regions.

(**Huang, 2015)** Applied robust graph based (RGB) segmentation method for the breast ultrasound images (BUS). A large number of sub-regions are obtained using this RGB method. Then a pattern recognition is developed to identify the lesion from the normal tissues ie, region of interest. This object recognition is carried out in three steps, feature extraction, feature selection and classification. The authors considered five categories of BUS image features which includes the gray-level histogram (HIS), the gray level co-occurrence matrix (GLCM), the histogram of original gradient (HOG) and finally the shape and location. Ultimately they validated the tumor region using an SVM classifier.

Using a fuzzy support vector machine (FSVM) classifier **(Shi, 2010)** made an attempt to classify the masses in BUS images. A total of 151 features are derived from the dataset of 87 breast ultrasound images. A fully automatic classification method for BUS is presented (**Shi, 2010**). The method focused on finding a credible ROI, instead of pointing a precise tumor location. Also the method can able to classify tumors without human intervention. (**Liu, 2010**) proposed a new structure based on neural network for segmenting medical images. The method was named as merging moving average self-organising maps (MMA-SOM). In the initial segmentation phase a modified self-organising maps are used for segmenting the image. Then a merging process is carried out to connect the segmented objects. After that 2D discrete wavelet transform is used to put up the input feature space of network. For performance evaluation they tested the proposed method on breast ultrasound images, MRI head images and computerized tomography (CT) head images.

A hybrid segmentation approach is proposed by Gupta et.al (**Gupta, 2017)**. Here the automatic segmentation algorithm is formulated using Kernel fuzzy C-means clustering and edge based active contour method. The result of clustering is exploited to complete the distance regularized level set function (DRLS). Real ultrasound and synthetic images were taken for conducting experiments. For assessing the effectiveness of this hybrid method, the authors compared with other methods like the Geodesic active contour method (GAC), region scalable fitting method (RSF), level set evolution function (LSF). With the inclusion of this DRLS, processing time can be reduced and at the same time manual requirement can be avoided accordingly.

3.3.2. Segmentation in MRI Imaging Modality

A different method of conventional FCM algorithm was presented (**Chuang, 2006**). Here the spatial information is incorporated into the membership function for clustering (sFCM). To carry out the study, the authors considered one T1 weighted image and one T2 weighted MRI image of the same patient. Six clusters are formed from these images. The cluster includes gray matter (GM), cerebrospinal fluid, white matter (WM), fat, bone and air. The authors point out some advantages of sFCM, showing the superiority over conventional FCM method.

In 2002 **Ahmed (Ahmed, 2002)** presented a novel algorithm for fuzzy segmentation in MRI image data. The algorithm is named as BCFCM ie, Bias Corrected Fuzzy C-means objective function. Here the objective function of standard FCM is modified to compensate for MRI intensity in homogeneities. The labelling of a pixel is influenced by the neighbourhood pixel, which is not considered in case of standard FCM. The method is compared with Expectation maximization algorithm (EM) and FCM algorithm. The effect of neighbour term is controlled by a regularization parameter. This method gives better result in images corrupted with salt and pepper noise.

(**Parvati, 2008)** proposed a method for color gray scale MRI medical images. Edge detection is performed using marker controlled watershed segmentation. So the method called as morphological marker controlled watershed segmentation (MMCW). They considered MR medical images, aerial images and high resolution satellite images as test images. In 2012 Allaoui (**El Allaoui, 2012)** tested the same method in a set of medical images.

Rajyalakshmi (**Rajyalakshmi, 2017**) presented integrated variable marker controlled watershed segmentation (VMCWM). Breast cancer biopsy images are taken for testing the proposed method. (**Wang, 2014**) Proposed a method based on morphological structuring element map modification and MCW (marker controlled watershed) segmentation. From the morphological gradient image, sum of variance of specific regions is computed. Then a structuring element map is constructed with these details. The authors prove that this type of image modification will eliminate noise and can remove small objects gradually. The method purely focuses on large object contours rather than small ones.

In (**Li, 2011)** a novel region based method for MRI image segmentation is proposed. The method demands it can able to work with intensity inhomogeneity images. The method begins with a local intensity clustering criterion in each point of neighbourhood pixel. Later this property is integrated to center neighbourhood pixel to form a global criterion of image segmentation. By minimizing this energy function, (global criterion) the method can bring out good results in intensity inhomogeneity images. The developed method has been validated on synthetic images and real images of various modalities like ultrasound, MRI and X-ray imaging.

A multi-resolution edge detection and region selection method of MRI brain image segmentation is presented (**Tang, 2000**). The method mainly focuses on extracting the white matter structure in brain image. The process put together image filtering, region growing and automatic intensity threshold methods to delineate white matter, gray matter and CSF (cerebral spinal fluid) flow in MRI brain images.

Dahshan (**El-Dahshan, 2014)** reviewed the current studies of diverse segmentation, feature extraction and classification algorithms done in MRI brain tumor between the years 2006 and 2012. The authors put forward a new hybrid technique for CAD (computer aided detection) system for processing the brain tumor through magnetic resonance images. The system starts with a feedback pulse coupled neural network to identify the ROI part. Then the DWT is utilized to bring out the features from ROI and principal component analysis is performed to reduce the dimensionality of wavelet coefficients. Then the optimized feature set is selected and send back to the feed forward back propagation network to classify the lesion into normal and abnormal. The system is validated with 101 MRI test images and yields a classification accuracy of 99%. In **(Joseph, 2014)** a computer aided diagnostic system to separate tumor from MRI brain images is proposed. K means clustering is used to identify the tumor location. In order to avoid the misclustered regions, morphological filtering is done after clustering.

3.4. REVIEW OF DIFFERENT IMAGE COMPRESSION METHODS

Image Compression has been a widely researched field for decades, which was also showing an exponential growth in applications like medical imaging, satellite imaging and telemedicine.

Image compression is mainly classified into lossless and lossy. The selection of lossless (original data can be recovered totally) or lossy type (original data cannot be fully recovered) of compression technique is dependent upon the area of application. The most popular entropy coding techniques are Huffman coding (Huffman, 1952 (**Huffman, 1952**) and Arithmetic coding (**Witten, 1987)**, Rissanen (**Rissanen, 1979**). Former assigns a set of prefix codes to symbols based upon their probabilities. Huffman coding shows some inefficiency in coding when the alphabet size is small. But the latter is more efficient when the alphabet size is small or the symbol probabilities are highly skewed.

Block truncation coding or BTC **(Delp, 1979)** is a lossy compression method, divides the image into number of blocks, then apply quantization on these blocks of pixels to reduce the number of grey level values in each block whilst maintaining the same mean and standard deviation. Another variation is Absolute moment block truncation coding (AMBTC) algorithm **(Lema, 1984)** which is computationally simple and results in low MSE values. Instead of using the standard deviation, the first absolute moment is preserved along with the mean.

Klema and Laub **(Klema, 1980)** had outlined the potential application of singular value decomposition in linear algebra and linear systems. Two applications in the domain of image processing based on SVD are demonstrated in **(Chen, 2018).** Main focus is on image compression and image recovery. Since the portions of image having diverse level of complexity and smoothness, direct application of SVD to images will be very time consuming. So the large images are divided into multiple sectors and then applying SVD with different k (rank) values. Optimum k value should be selected such that there is no damage to image quality and at the same time storage space occupied by image is reduced.

The lossy type of compression techniques has attained more attention due to its ability to achieve high CR values. Wallace (**Wallace, 1992**) introduced DCT based JPEG standard and Skodras (**Skodras, 2011**) presented a DWT based JPEG2K, both these irreversible method yields higher compression ratios. The latter presents a superior compression performance and also provides additional features like ROI based coding, lossy (9/7 orthogonal type filters) to lossless coding etc. A high performance reversible method is given by Wu and Lin (**Wu, 1997; Wu, 2005**) which uses 5/3 orthogonal type filters. Since these transform based methods are unable to capture the directional information, conventional DCT's are replaced by a set of trained dictionaries. These elements are trained using an Orthogonal Matching Pursuit (OMP) algorithm (**Pati, 2015**).

Said and Pearlman **(Said, 1996)** had presented an algorithm called Set Partitioning in Hierarchical Trees (SPIHT), which was completely based on embedded coding. The algorithm was an extension of EZW **(Shapiro, 1993).** The algorithm is nearly lossless method ie, the compression may not be reversible as the transform coefficients are truncated while precision. For getting a reversible lossless compression, integer multi resolution transform such as S+P transform can be used. The incorporation of adaptivity in low complexity framework is possible through FELICS **(Howard, 1993)**.

An excellent compression standard is presented by Weinberger (**Weinberger, 2000)** LOCO-I (LOw COmplexity LOssless Compression for Images). It outperforms other compression schemes with similar complexity which includes FELICS, PNG, and JPEG-Huffman and it attains compression ratios similar or superior to those of higher complexity schemes based on arithmetic coding (e.g.,JPEG-Arithm, CALIC **(Wu,1997)**.

An adaptive block truncation coding for satellite/aerial color images was introduced in **(Balakrishnan, 2018)**. Input RGB color image is converted to HSV plane. Here the features like texture, structure and edge based features need to be handled in different manner for performing quantisation. The quantisation in H and S planes is done by quad clustering and V plane is encoded using BTC based bi or tri clustering. Since it is processing with aerial image, minimal distortion in reconstruction side is acceptable. The method cannot applicable for medical images as the information content need to be preserved.

3.4.1. Methods Based on Medical Image Compression

Medical image compression techniques are mainly based on lossless type of methods. Loucas **(Lucas, 2017)** had described a highly efficient method for lossless compression of medical images using 3D predictor. The method was compared with standard JPEG-LS, JPEG2K and CALIC algorithms and achieves gains above 15% and 12% for 8 bit and 16 bit depth images respectively. The method was based on minimum rate predictors and this was particularly for MRI and CT scanning technologies. Avramovi **(Avramović, 2011)** proposed a new predictor which evolves from the standard median predictor (MED) and gradient based predictor (GAP). The new Gradient Edge Detection (GED) is based upon a single threshold value rather than multiple threshold values in GAP. This novel prediction algorithm shows satisfactory result for CT and MRI medical images.

Lossless compression for 3D MRI brain images using Stationary wavelet transform is described in **(Anusuya, 2014)**. The 3D input images are divided into 2D slices and then applied 2D SWT. The decimated coefficients are compressed in parallel using EBCOT algorithm. Using inverse SWT bit streams are decoded and reconstructed image is formed. An idea of incorporating parallel computing to compress different medical imaging modalities is also point out for future applications.

A delimiter based lossless medical image compression is given in **(Reddy, 2014)**. Here the input medical image is converted into binary image matrix and then to row matrix. Number of occurrences is noted and removes the repeated elements and stored in new vector. Finally merge these vectors and then apply quantisation to get the compressed image. The method was tested on X-Ray, CT, Ultrasound and MRI medical images. But the direct conversion of input color image to binary may cause loss in information. Akkala **(Akkala, 2014)** studied various global and local compression techniques and tested the results using kidney ultrasound images. To conduct the study they used log compression, Gamma compression and Wavelet compression. Gamma compression yields best results in terms of image quality, but its statistical properties may lose during expansion. Since these statistical properties are important for doctors to carry out diagnosis. So this problem can be avoided by using wavelet based compression techniques.

3.4.2. ROI Based Medical Image Compression Methods

Zuo **(Zuo, 2015)** proposed an improved medical image compression technique in which a region based active contour model have been applied for segmenting the image into ROI and non-ROI part. JPEG-LS algorithm is then applied to marked area of ROI and the wavelet based lossy compression algorithm is utilized in blurred non-ROI region. ROI mask is accurately transmitted to the decoder in order to achieve good compression ratio.

Cyriac M **(Cyriac, 2016)** introduced an object based lossless compression using differential pulse code modulation coder (DPCM). Here MRI (head) and CT (brain, elbow, coronary) images are considered as input images. Input test images should be classified based on their object content. Using a sobel edge operator, boundaries of the objects are identified. Instead of creating a ROI mask for the object, here the object itself is surrounded with a bounding box. Apply DPCM to both object region and background region. Then a Huffman encoder is applied to object region and background vectors (background region is converted to 1D vector) and finally the size information is transmitted along with the encoded region. Results shows that the proposed coder outperforms the direct coders, object based wavelet coders and JPEG-LS coders in terms bit per pixel values.

A new scheme based on integer wavelet transform (IWT) was developed in **(Moorthi, 2015)**. The IWT transformed ROI and Non-ROI are subjected to arithmetic (lossless) coding and EZW (lossy) coding which is then combined and transmitted. The area of interest (ROI) is selected using seed point which is selected by extracting run length features. The proposed method is combined with three existing methods for proving the effectiveness of method. The real MRI brain images (number not specified) from patients are considered for testing the proposed algorithm.

In 2016 Chaabouni **(Chaabouni, 2016)** proposed new technique based on region of interest (ROI) and incremental self-organizing maps (ISOM). It is an incremental neural network having an unsupervised learning approach. For getting a better compression rate, here DWT is combined with ISOM. Manual method is selected for separating ROI region from the background region. Thyroid ultrasound images having a size of 512* 512 are considered as input images. The proposed method is compared with JPEG and SPIHT using psnr, mse and bpp for performance evaluation.

Kaur **(Chaabouni, 2016)** implemented a context tree prediction algorithm for ROI part and a fractal compression for N-ROI part. The preprocessed input image is divided into ROI, Non-ROI and background based upon edge detection and texture analysis. The proposed strategies attained a good quality image in contrast with the past methods. A hybrid model of medical image compression technique for colon CT images is given **(Gokturk, 2001)**. They had chosen colon wall as region of interest and segmented out the region using 3D morphological operations. Then a hybrid lossless compression scheme is used in the region of interest and a motion compensated lossy is applied in other regions. Their result suggests that motion compensated coding is better than DCT, PCA, block wise Vector Quantisation (VQ) for the compression of colon CT abdomen images.

Bruckmann **(Bruckmann, 2000)** have introduced and compared different techniques in SeLIC (Selective medical image compression) for telemedical and archival applications. They developed a graphical user interface which allows an interactive marking of arbitrarily shaped ROI's from input image. Strom and Cosman **(Ström, 1997)** presented and compared several new algorithms for lossless medical image compression. One is purely based on lossless and the other is two is a combination of lossy with either spatial domain or transform domain. Thus the three approaches include S algorithm, WA algorithm (embedded zero tree wavelet and arithmetic encoder in spatial domain), and WSP (embedded zero tree wavelet and lossless s+ p in transform domain). Region of interest were selected manually by hand. The performance of these algorithms is depends upon the size of ROI's. The WA algorithm performs well for small sized ROI's. The S algorithm does well for large size ROI's and showing poor performance in small sized ones. The WSP algorithm is superior to other algorithms when the ROI area was increased sufficiently. The algorithms were tested on MRI brain, MRI chest, CT chest and mammograms.

3.4.3. Medical Image Compression Standards

Since the imaging department in hospitals are generating a large volume of image data, necessary steps need to be taken for the proper management of imaging environment. A group of radiologists in different regions of the world provide some guidelines for the safe use of image compression in the clinical environment **(The Royal College of Radiologists 2008; Canadian Association of Radiologists 2011; Loose, 2009).** Some of them include The Royal College of Radiologists (RCR) , Canadian Association of Radiologists (CAR), German Rontgen Society (DRG) .

The wide use of multislice computed tomography scanners and magnetic resonance scanners in hospitals suggests the safe use of irreversible compression techniques to reduce the cost of storage and transmission **(The Royal College of Radiologists 2008; Canadian Association of Radiologists 2011; Loose, 2009).** The DRG, RCR, and CAR guidelines recommend compression ratios up to 7:1, 25:1, and 24:1, respectively, for MRI imaging modality. The radiologists in hospitals should follow the recommendations of RCR, CAR, or DRG for patient care and safety. The recommended compression factors for individual imaging modalities by different group of radiologists are given in Table 3.1.

Table 3.1. Medical image compression standards

Imaging Modality	RCR	CAR	DRG
MRI	25:1	24:1	7:1
Ultrasound	9:1	12:1	-
CT	4:1 to 20:1	12:1	8:1
CR/DR	-	30:1	10:1
Nuclear Medicine	-	11:1	-

3.5 SUMMARY

This chapter helps to understand the works done currently in the areas of enhancement, segmentation and compression in ultrasound and MRI imaging modalities. The literature review on segmentation of ultrasound and MRI imaging modality has separately done. Rare works are seen in the detection and compression of important diagnostic part for female pelvic ultrasound and MRI imaging. The role of compression in medical images was also highlighted. Certain medical image compression standards using by different hospitals was also discussed. The main aim is to improve the compression rate and quality, so as to achieve less computational time for medical image compression and decompression.

Chapter -4

SEGMENTATION OF ROI FROM FEMALE PELVIC ULTRASOUND AND MRI IMAGING MODALITIES

Contents

4.1 INTRODUCTION

In this chapter, an overview of various enhancement and segmentation techniques used for different medical imaging modalities are discussed. Next, in this chapter, a novel segmentation method for the extraction of important diagnostic region from the female pelvic ultrasound imaging and female pelvic MRI imaging was detailed. The simulation result analysis was carried in MATLAB.

4.2 BACKGROUND

The main motive of our work is to develop an ROI based medical image compression for female pelvic Ultrasound and MRI imaging modalities. Medical images are always deteriorated due to noise from various sources of interference, which makes the diagnosis difficult. So the input medical image should be preprocessed in an efficient manner for better ROI separation. The separation or extraction of the important diagnostic region is done through the process of segmentation. Segmentation plays a key role in the computational processing of medical images. Since the medical images are highly corrupted with noise, a fully segmented algorithm is indispensable to visualize the relative position and shapes of internal tissue.

4.2.1 Image Preprocessing Techniques

Preprocessing is the step taken before the major image-processing task. Medical image preprocessing consists of detection of poor image quality, color channel separation or color normalization, contrast enhancement and edge or boundary sharpening. The main aim of any image denoising algorithms is to remove noise without losing the important diagnostic features. Different imaging modalities concern with the different type of noises or artifacts. Each type of noise requires a different method of removal. Therefore, a proper preprocessing procedure should be decided for better segmentation results.

Speckle is a form of multiplicative noise commonly seen in B-mode ultrasound images appears as *small snakes or dense granular* like structures leading to low imaging quality. Speckles are formed when random values get multiplied with individual pixel values of an image. On the other side Gaussian noise is formed when random values added to pixel and both appear superficially similar. These types of noises can be cleaned using spatial filtering techniques.

Many adaptive and Non-adaptive filters have been used earlier, in that the most widely cited applied filters include Lee **(Lee, 1980),** Kuan **(Kuan, 1985)** Frost and Median filters **(Loupas, 1989).** Median filters are nonlinear spatial filters whereas Lee, Kuan, and Frost are adaptive mean (linear) filters. In Lee filters, the output image is formed by the linear combination of center pixel value inside the filter window with the average pixel intensity of the window. In this, filter achieves a balance between average and identity filter, where average points for homogeneous regions and identity filter for edges and point features. Their experiment result shows that a 7x7 window size is better suited for processing the noise effected images (**Lee, 1981)**. In the frost filter, the balance is achieved by a low and high value of the coefficient of variation. In case of high coefficient of variation, the filter is more identity-like (edges and points in images), and in cases of low coefficient of variation, the filter attempts to preserve homogeneous regions.

Although the existing despeckle filter preserves important edges and features in images, they are also facing some major limitations. Selection of filter window size and shape according to an image is one among them. Another limitation is, they only preventing smoothing near edges and at the same time, they are not magnifying the edges in images. These despeckle filters are non-directional i.e., inhibition of smoothing is different for parallel and perpendicular directions of the edges. These filters use hard thresholds to change the act of homogeneous regions or regions near the edges.

These limitations can be overcome by a PDE based filter approach called SRAD, which was proposed by Yu and Acton **(Yu, 2002).** This adaptive SRAD filter is independent of using hard thresholds to alter the performance of edges. It intensifies the edges and at the same time inhibits diffusion from one side to another side of the boundary of images. The diffusion technique used here is an extension of Lee and Kuan which is based on a MMSE (minimum mean square error) design approach. A multiplicative noise model can be written as

$$x_{i,j} = u_{i,j} v_{i,j} \quad (4.\ 1)$$

where $u_{i,j}$ is the input signal is $v_{i,j}$ represents the noise signal also $u_{i,j}$ is independent of $v_{i,j}$. Mean and variance of this input signal is given by

$$\text{Mean of } x_{i,j}\ ,\ \bar{x} = \bar{u}\,\bar{v} \quad (4.\ 2)$$

$$\text{Variance of } x_{i,j} = E[(uv - \bar{u}\,\bar{v})^2] \quad (4.\ 3)$$

$$= E[u]^2 E[v]^2 - \bar{u}^2 \bar{v}^2 \quad (4.\ 4)$$

Like other imaging techniques MRI also having its share of artifacts. Radiofrequency related artifacts, external magnetic field artifacts, magnetic susceptibility artifacts, gradient related artifacts, and patient-related artifacts are some of the common artifacts occur during magnetic resonance imaging. Some artifacts will affect the diagnostic quality, while others confused with pathology.

The presence of artifacts causes alternate white and dark bands that may be mistaken as lesions which tend radiologists to take the wrong decision. The non-linear filtering type median filtering is commonly used. The size of the mask or window should be properly chosen, as the output value is the median of the values in the mask. Median filtering replaces the noisy value with one closer to its surroundings.

4.2.2 Color Space Transformation

A Color space is a useful tool for understanding the important information in an image. A set of numbers are used to represent these colors and these color models create different color from the basic primary colors. RGB color space contains larger part of the visible spectrum than other color models. There are other color models besides RGB which also represent colors numerically namely, HSV, YCbCr, YIQ, CMYK etc.

An RGB color image consists of three color channels, viz red (R), green (G), blue (B) and has been used for object recognition in different fields of application. All these three primary colours (R, G and B) are combined to form white and their absence makes black color. RGB color space is convenient one because it resembles the working of human visual system. RGB and CMYK (Cyan/Magenta/Yellow/Black) are the commonly used color systems, where the former is an additive one and the latter is a subtractive color model.

In HSV (Hue/Saturation/Value) model hue represents color and has a scale of 0 to 360 includes almost all colors. The range of grey is indicated by saturation. It ranges from 0 to 100. The degree of brightness is given by value. Value also ranges between 0 and 100. A dark color has low intensity and when the value is increasing, color space brightens up and shows high intensity colors.

In YCbCr color model, Y represents the luminance, Cb and Cr represents the blue and red components of chrominance. Luminance contains the most important gray-scale information of the original image. Cr is strong in places of occurrence of reddish colors and Cb in blue colors. Both are weak in case of a color like green. Luminance is represented in an 8-bit range of 16 to 235 and chrominance has scaled to a range of 16 to 240.

Female pelvic MRI image and its YCbCr color model representation is shown in Figure 4.1 (a) shows the original color image, Figure 4.1 (b) shows the YCbCr image, Figure 4.1 (c), shows the luminance component and Figure 4.1 (d) chrominance (blue) component. From the figure it is understood that luminance component gives the information of original image than other components.

This research work considers RGB and YCbCr color space models to extract the image features. Below shows the equation for converting RGB to YCbCr color space,

$$Y = (77/256)R+(150/256)G+(29/256)B \tag{4.5}$$

$$Cb = -(44/256)R-(87/256)G+(131/256)B+128 \tag{4.6}$$

$$Cr = (131/256)R - (110/256)G -(21/256)B + 128 \tag{4. 7}$$

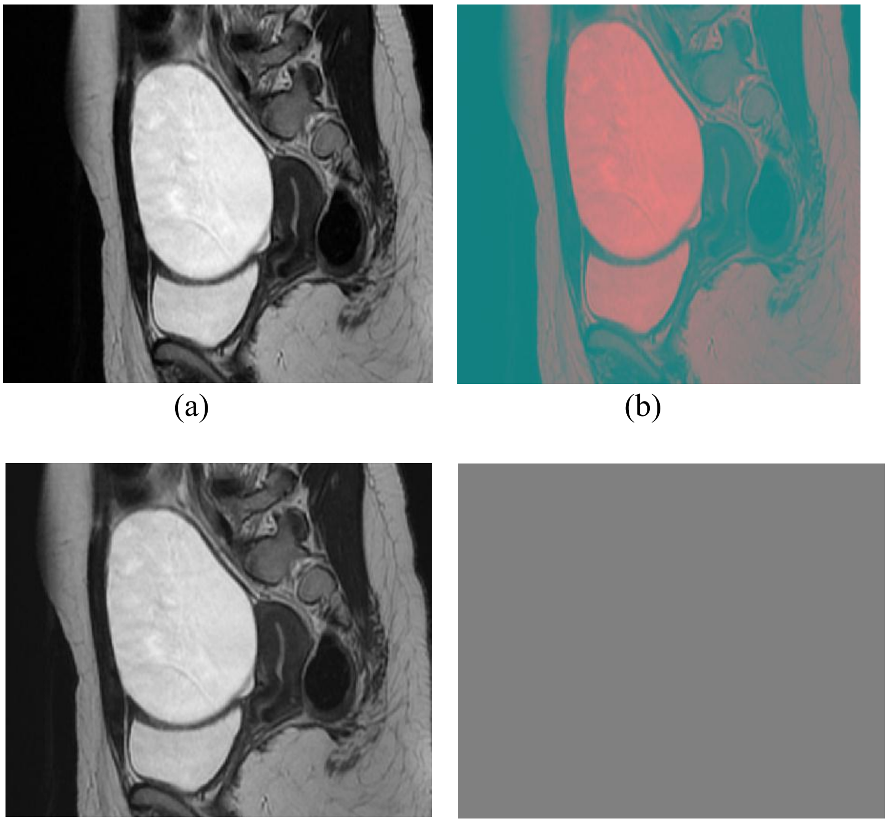

(a) (b)

(c) (d)

Fig. 4.1. YCbCr Image and its Components

(a) Orginal color input image
(b) YCbCr image
(c) Luminance Component of YCbCr image
(d) Chrominance (blue) Component of YCbCr image

4.2.3 Image Segmentation

Image segmentation divides the image into different objects. In our work we concentrated on thresholding and edge based segmentation methods. Thresholding can be achieved through single, double or adaptive Thresholding. The input grey scale image is converted into a binary image i.e., either black or white by choosing a grey level value T_h. A pixel becomes

$$P_x = \begin{cases} 1, \text{ if gray value} > T_h \\ 0, \text{ if gray value} < T_h \end{cases} \tag{4.8}$$

Thresholding helps to bring out hidden details. It also plays a good role when we want to remove unnecessary detail from an image to stick on essentials. It also isolates objects from the background of image. All these things depend upon the selection of appropriate threshold value. An automatic method for choosing an optimal threshold value is first developed by **(Otsu, 1979)**. A histogram based threshold method was used to separate the tumor region from the background image **(Chang, 2013)**. The method was adapted from **(Ramesh, 1995).** He found out the threshold value by minimizing the sum-of-square errors SSE (t) between the gray values and the mean values in the two regions.

Edge based segmentation methods can able to identify the local discontinuity in the pixel value. An edge is an observable difference in pixel values. Edge finding operators can easily classify the objects by isolating them from background. The operators are based on first derivatives, second derivatives of an image. Prewitt, roberts, sobel are edge detection filters based on first derivatives. Second order derivatives having the advantage of rotation invariant over first order and laplacian, LoG or laplacian of gaussian are some of the second order derivative filters. Another type of edge detection that uses multi stage algorithm to detect all type of edges is canny edge detector. This having low error rate detection, but it is more complex when compared to other edge detectors.

4.2.4 Mathematical Morphology

Mathematical morphology or morphology is the branch of image processing that is particularly useful for analysing shapes and structures in images. It was initially developed for binary images and was later extended for grayscale images. Dilation and erosion are the elementary operations of morphology and all other operations are built from these basic operations.

Mathematical morphology deals with the non-linear process which can be applied to an image to remove details smaller than a certain reference shape, usually called as kernel or structuring element. A structuring element is a matrix used to probe the given input image with simple, predefined shape.

Dilation is an expansion operation that grows an image. It is used for expanding an element *I* by using a structuring element *B.* This operator increases the boundaries of the region, while the small holes present in the image become smaller. The process assigns the value 0 or 1 to the overlapping pixels under the centre position of the kernel.

If I is the reference image and B is the structuring element, then the dilation of *I* by *B* is denoted as,

$$I \oplus B = \bigcup_{x \in b} I_x \tag{4.9}$$

The operation $I \oplus B$ is obtained by replacing every point (x,y) in *I* with a copy of *B* placing the centre (0,0) point of *B* at (x,y).

Erosion is a shrinking operation which removes structures of certain shapes and size given by structuring element. It makes the object smaller by removing the outer layer of pixels. If *I* is the reference image and *B* is the structuring element, then the erosion of *I* by *B* is denoted as,

$$I \ominus B = \bigcap_{b \in B} I_b \tag{4.10}$$

The outcome of erosion operation will be a subset of original object. Bridging of gaps is done by dilation while erosion removes irrelevant details in an image.

Opening and closing are second set of operations formed from these basic dilation and erosion. Opening operation is an erosion operation followed by dilation operation. Given *A* and a structuring element *B*, then the opening of *A* by *B* is denoted as,

$$A \circ B = (A \ominus B) \oplus B \tag{4.11}$$

Opening operation smoothens the edges, breaks the narrow joints and thins the protrusions that are present in the image. Closing does the opposite of opening operation. Closing operation fills gaps in the contour and eliminates small holes. It is mathematically represented as

$$A \bullet B = (A \oplus B) \ominus B \tag{4.12}$$

4.3 SEGMENTATION OF ROI FROM FEMALE PELVIC ULTRASOUND IMAGING

Several algorithms have been proposed in the literature for the segmentation of important diagnostic region from ultrasound images over the past few decades. Most of the algorithms depend upon some basic assumption related to tumor intensity, shape and position. Since the image structure is different for diverse ultrasound images, algorithms based upon these primary assumptions is not enough for doing further operations. Most of them had proposed approaches for breast and kidney ultrasound images. Only limited number of attempts can be found in the literature for the localization and extraction of abnormalities in female pelvic ultrasound (PUS) images.

4.3.1 The proposed Method

The transducer attached to the scanner uses high frequency sound waves (in the range of 3–7 MHz) to create ultrasound image of the body tissues. Analysis of region of interest in noisy nature is very crucial as these real time ultrasound images can be used as a good tool for guiding other invasive procedures. If the digitized medical image meets the quality, then image enhancement or preprocessing is carried out. Preprocessing is performed using a speckle reducing anisotropic diffusion (SRAD) filter (discussed in section 4.1.1). The outputs are given in Figure 4.3 with central mass appeared as white region. The edge detection is very sensitive to noise and artefacts and it badly affects the edge detector for proper boundary extraction. The frequently used region based algorithms is a solution to this and in this work morphological marker controlled watershed algorithm is used (MMCW) to segment ROI. The detailed workflow of ROI segmentation is given in Figure 4.2.

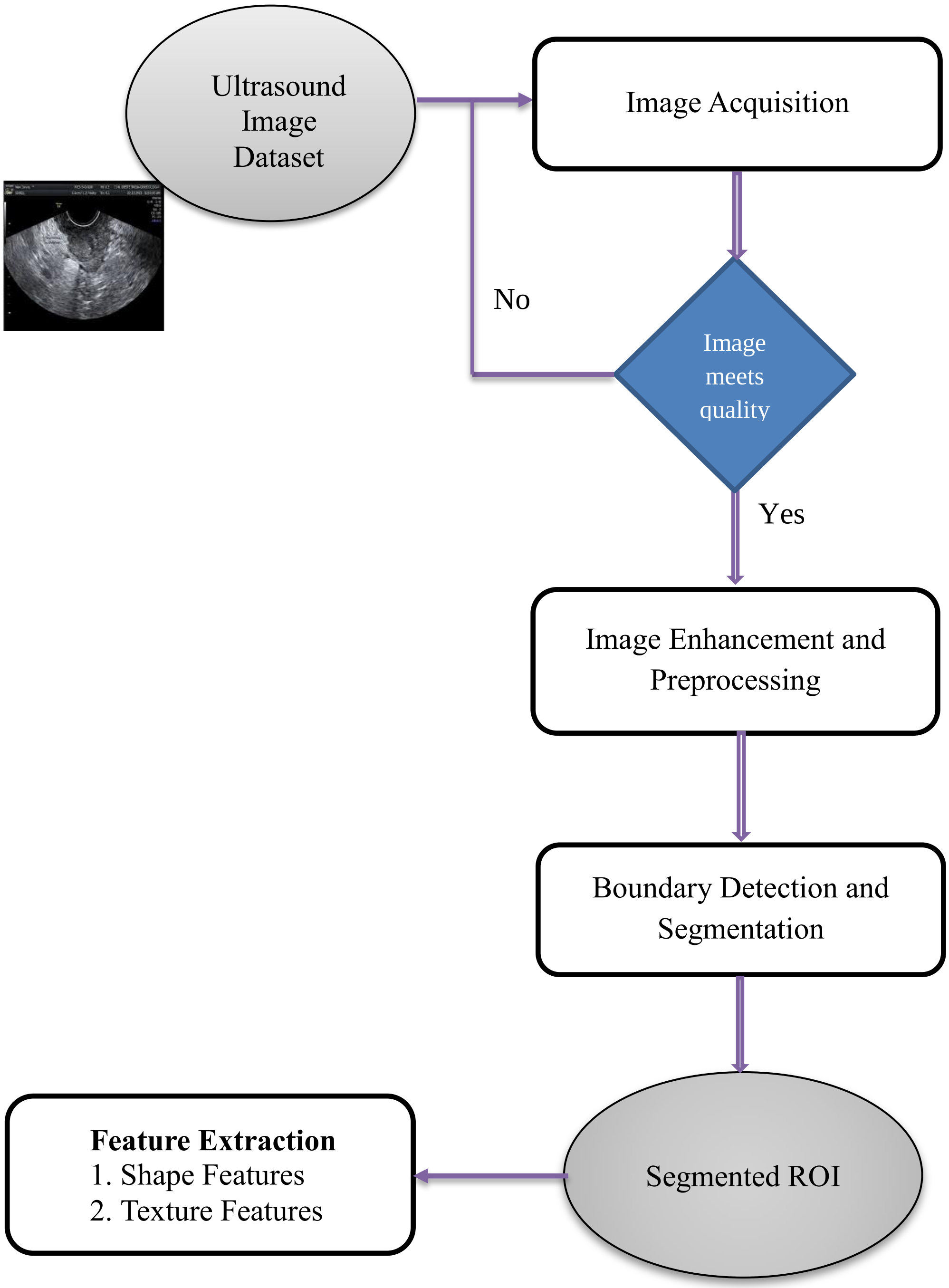

Fig. 4.2. Work flow of ROI Segmentation in Female PUS Imaging

The anisotropic diffusion method in SRAD is built from a non-linear PDE for smoothening the speckle affected image data.

$$\begin{cases} \dfrac{\partial S(i,j;t)}{\partial t} = div\left[d(x)\nabla\left(S(i,j;t)\right)\right] \\ S(t=0) \rightarrow S(i,j;0) = S_0(i,j) \end{cases} \tag{4.13}$$

S (i, j; t) is the output image obtained from the input intensity image S_0 *(i, j)* respectively.

$$d(x) = \frac{1}{1+[x^2(i,j;t)-x_0{}^2(t)]/[(x_0{}^2(t)(1+(x_0{}^2(t)]} \tag{4.14}$$

Where *d(x)* is the diffusion coefficient and *x (i, j; t)* is the instantaneous coefficient of variation. The latter is a function of local gradient magnitude and Laplacian operator to act like a good edge detector.

$$x(i,j;t) = \sqrt{\frac{(1/2)(|\nabla S|/S^2)-(1/16)(\nabla^2 S/S)^2}{[1+(1/4)(\nabla^2 S/S)]^2}} \tag{4.15}$$

$$x_0(t) \approx x_0 \exp(-t) \longrightarrow x_0(t) \approx x_0 \exp(-\rho t) \tag{4.16}$$

In order to reduce the exponential decay rate, a single constant ρ (value <1) is introduced in the speckle scale function $x_0(t)$ in the above equation. Also the speckle coefficient of variation x_0 is assumed to be 1 for ultrasound image data. The preprocessed image with time step Δt=0.02 per iteration is shown in Figure 4.3.

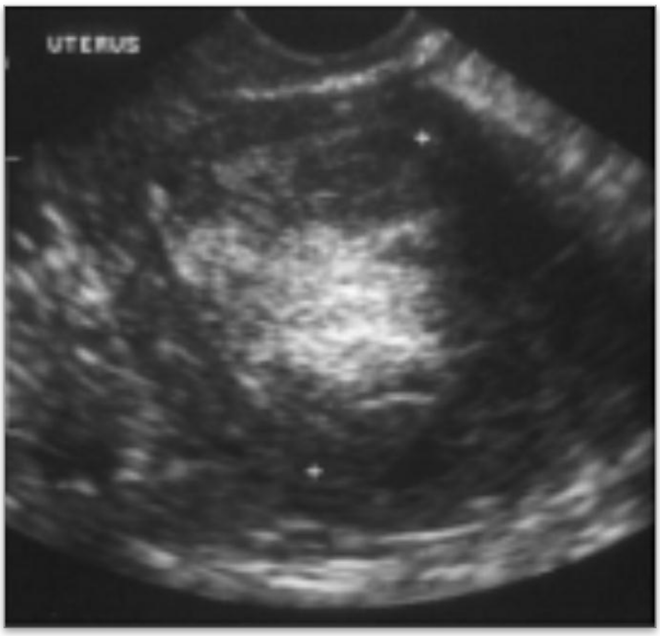

Fig. 4.3. SRAD filtered Input Image

The SRAD based filtered image is subjected to basic grey scale morphology for getting a smoothing effect. The change in intensity of each pixel can be easily measured using image gradient. The gradient is high at the boundary of the objects and showing almost low value inside of the objects. The outputs are shown in Figure 4.4 and 4.5.

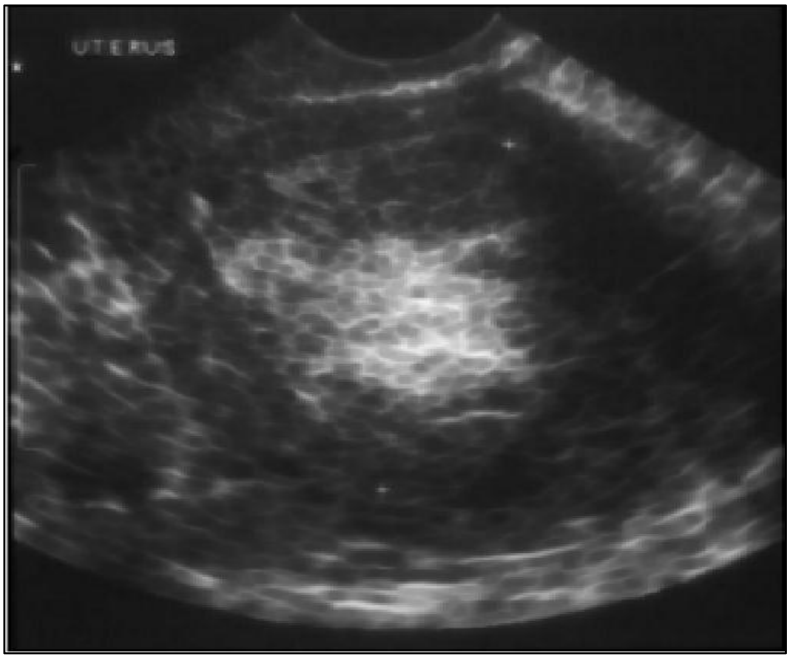

Fig. 4.4. SRAD Filtered Image After Erosion

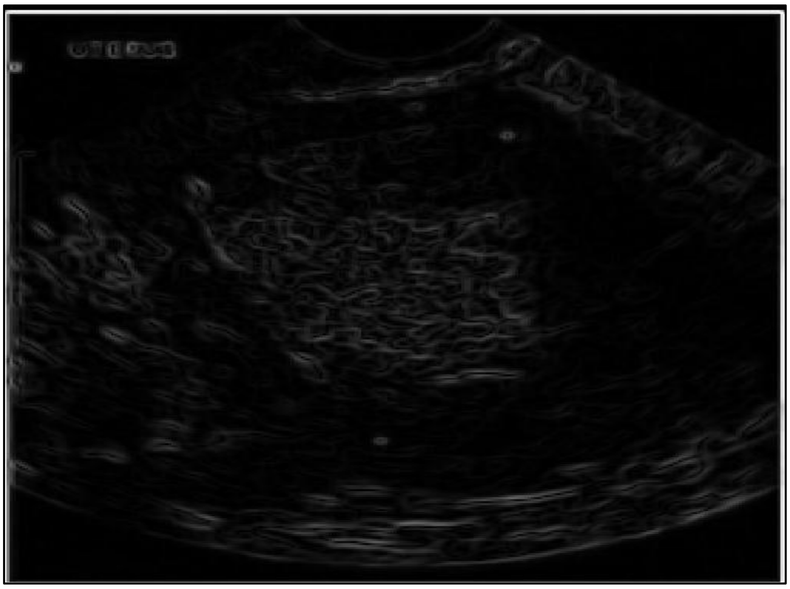

Fig. 4.5. Gradient Image

Direct application of watershed segmentation to gradient magnitude will result in over segmentation (large number segmented regions). This severe segmentation can be controlled by incorporating the concept of markers. Internal (foreground) and external (background) markers form the connected component of an image. Internal markers are associated with region of interest which is seen as blob like regions inside the foreground objects. Opening by reconstruction and closing by reconstruction morphological techniques are used for tracking the internal markers.

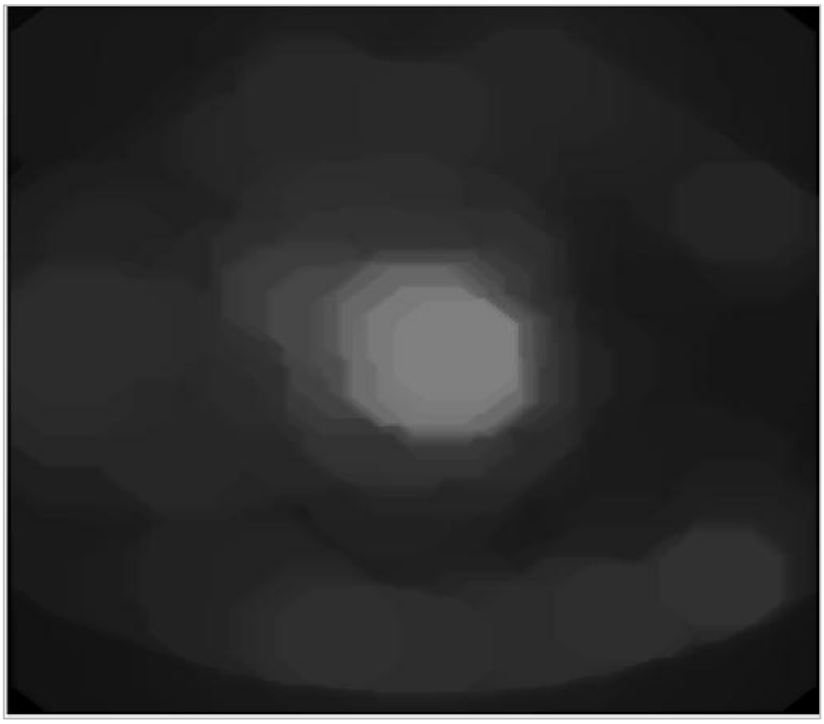

Fig. 4.6. Opening Operation

Opening operation as discussed in section 4.2.4, where opening by reconstruction is erosion followed by morphological reconstruction. Figure 4.6 to 4.9 shows the morphological operation and their corresponding reconstruction outputs.

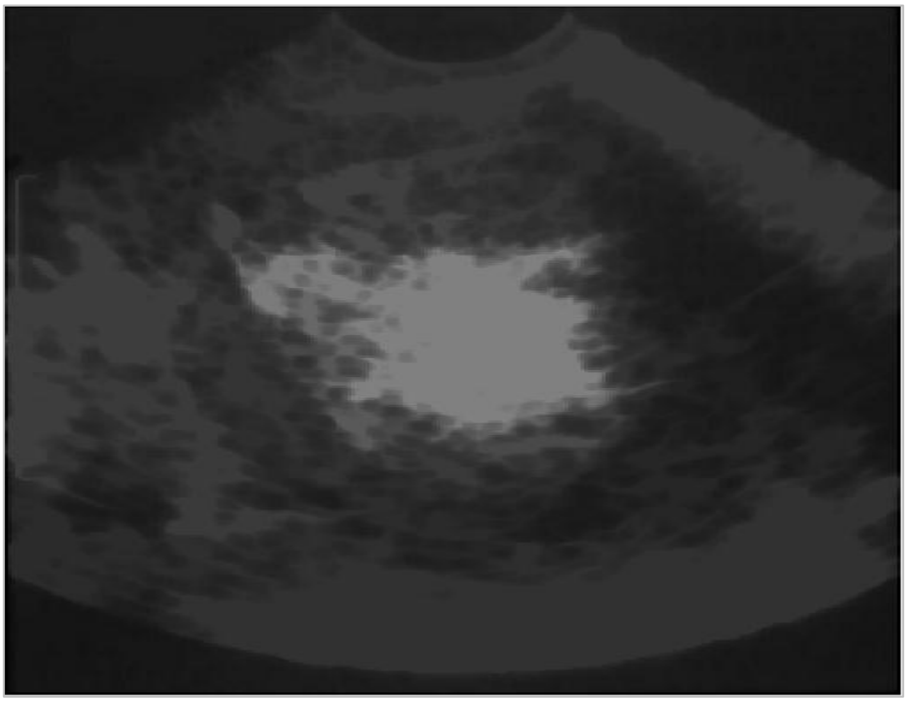

Fig. 4.7. Opening by Reconstruction

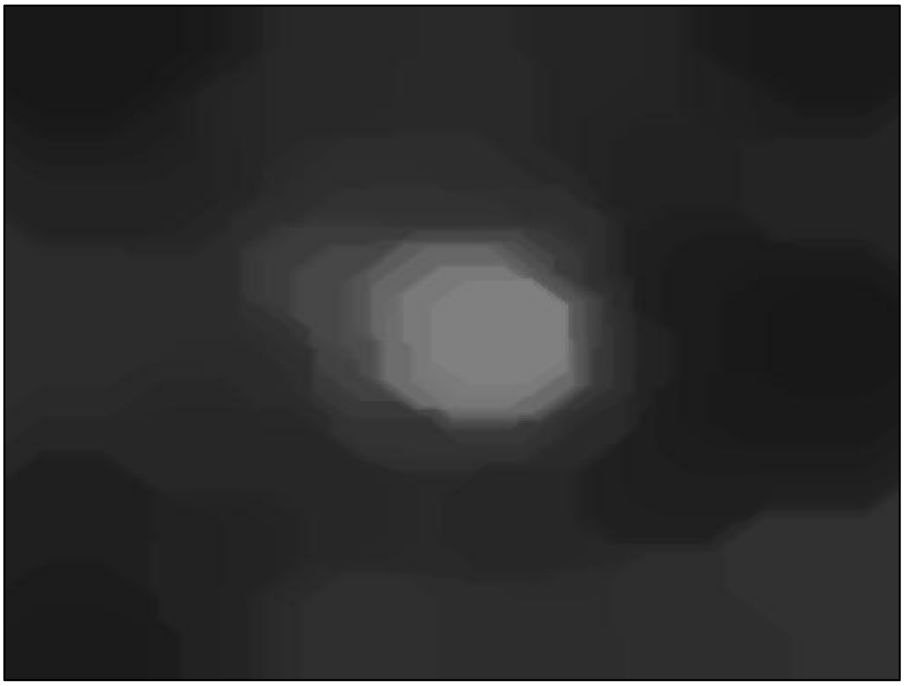

Fig. 4.8. Opening – Closing

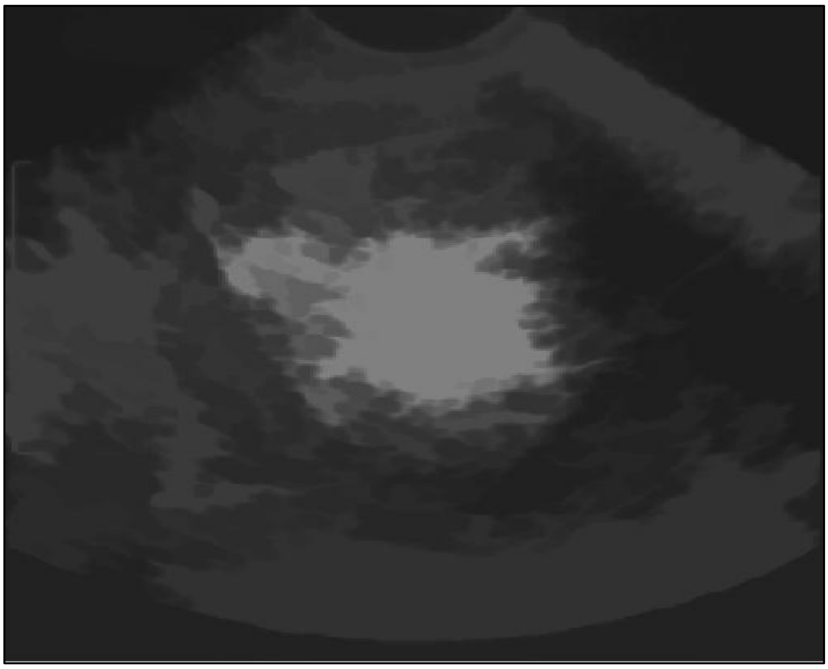

Fig. 4.9. Opening-closing by reconstruction

Regional maxima of these foreground objects is calculated for getting a smoothening edge. For a better representation of resultant image, the foreground markers are superimposed on original image.

Fig. 4.10. Regional Maxima

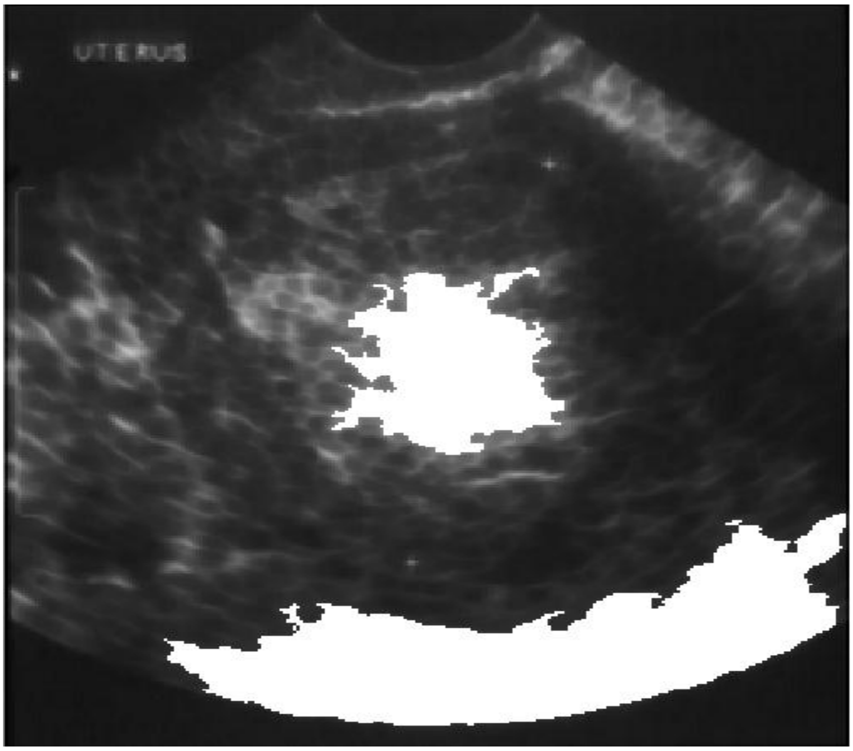

Fig. 4.11. Regional Maxima Superimposed On Original Image

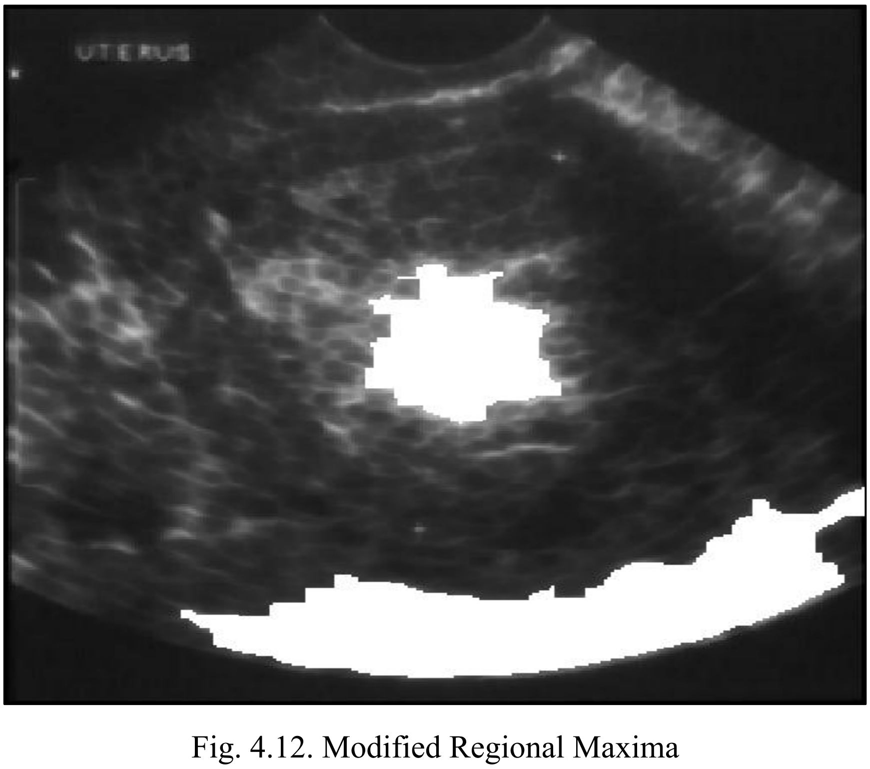

Fig. 4.12. Modified Regional Maxima

Some isolated pixels (blobs fewer than certain number of pixels) can be removed by using a Matlab function *'bwareaopen'*. That modified image is given in Figure 4.12. For computing the background markers thresholding method is initialized. The output of threshold operation is shown in Figure 4.13. The threshold value of 0.3 was selected for *'imbinarize'* function. Then for thinning the unwanted black background pixels watershed transform of the distance transform is computed.

Fig. 4.13. Thresholded Opening Closing by Reconstruction

Finally the watershed based segmentation is applied to modified gradient image to obtain the desired segmented objects.

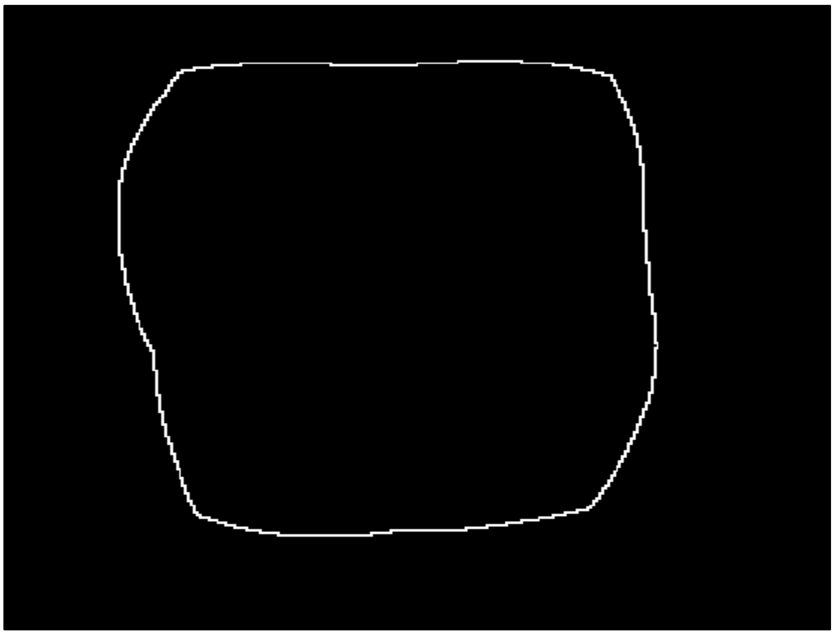

Fig. 4.14. Ridge Lines of Watershed

Figure 4.14 shows the ridge lines of watershed. Then the foreground markers, background markers, and segmented object boundaries are superimposed on the original image to obtain the final result.

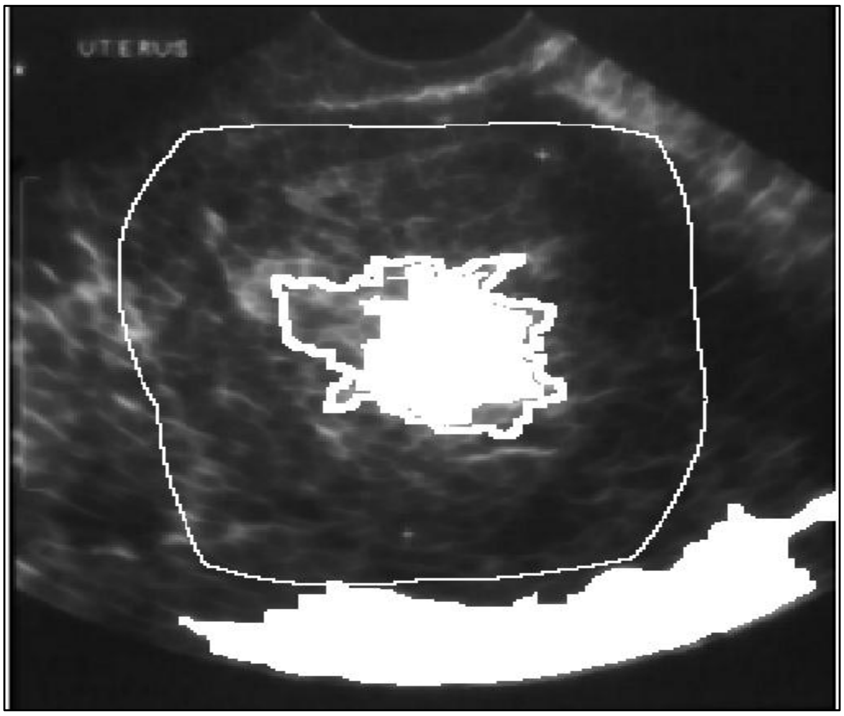

Fig. 4.15. Markers and Object Boundary of ROI

The markers and object boundaries of region of interest is show in Figure 4.15. Figure 4.16 and 4.17 shows the identified tumor (endometrial adenocarcinoma).

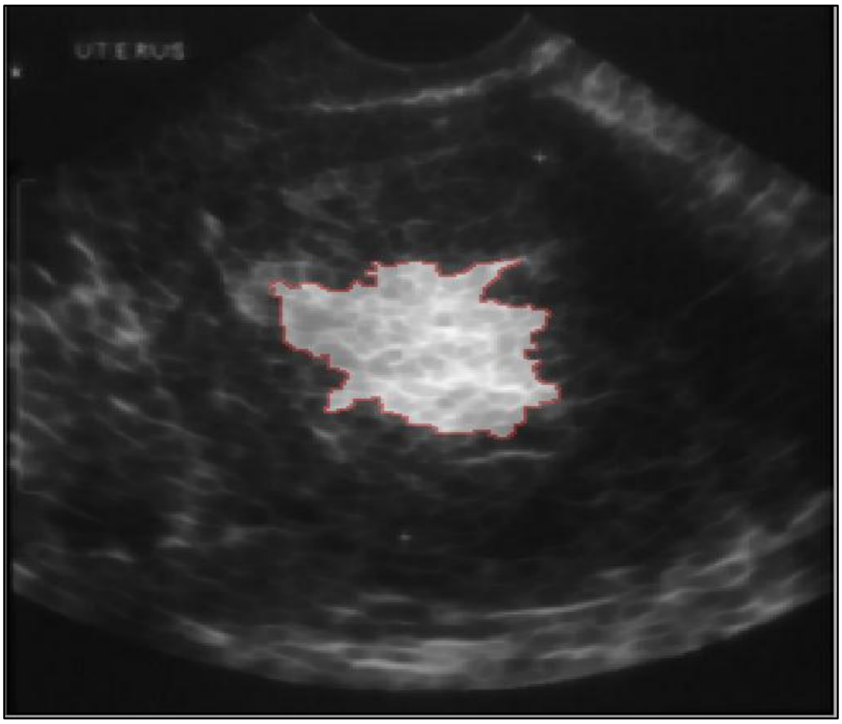

Fig. 4.16. Applying Color Label to Final Contour

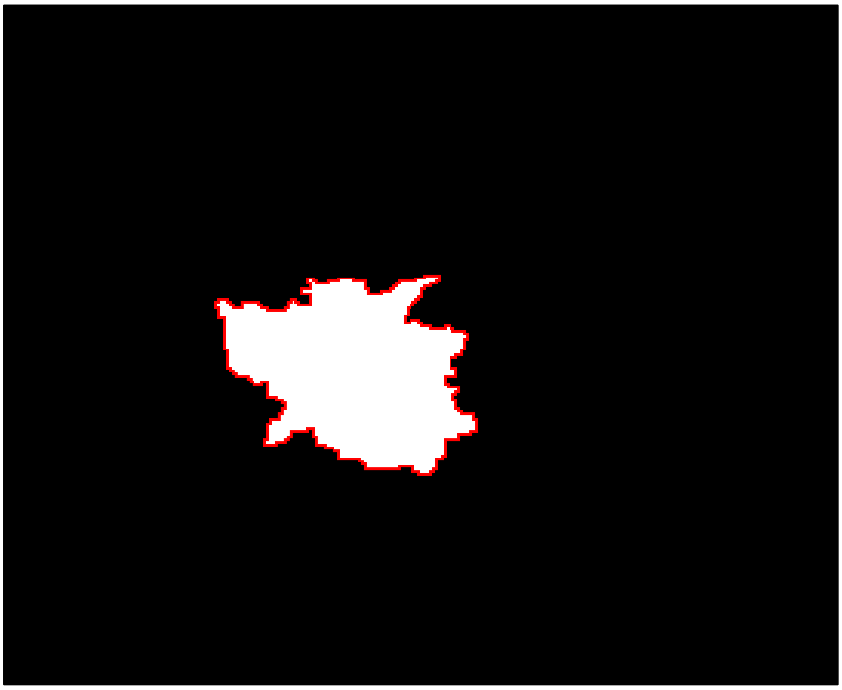

Fig. 4.17. Identified Tumor Separated

The algorithm for obtaining the final contour using morphological marker controlled watershed segmentation is shown below.

Algorithm 1: ROI Extraction from Ultrasound Imaging Modality

Initial:

1: Input RGB image is converted to gray scale image.

2: Gray scale image is filtered by using SRAD filter.

3: Erosion is done for smoothening purpose.

4: Develop the gradient image using sobel edge mask

5: Set the mask as [1 2 1
0 0 0
-1 -2 -1]

6: **Comment:** Incorporating the concept of internal and external markers.

7: Disk shaped structuring element is formed, *strel('disk', 18)*, radius=18

8: **Comment:** Marking internal or foreground markers

9: Opening operation

10: Opening by reconstruction (using *imerode* and *imreconstruct*)

11: Opening closing operation

12: Opening closing by reconstruction (using *imdilate* and *imreconstruct*)

13: Calculating regional maxima of step 11 to obtain good internal markers

14: Superimposing the modified regional maxima on the original image

15: Take the modified regional maxima

16: **Comment:** Marking external or background markers

17: Thresholding is performed on the step 11

18: Set the threshold values as 0.3.

19: Compute watershed transform.

20: Finally superimposing both internal, external markers and object boundaries on original image to get the tumor part.

end procedure

4.4 SEGMENTATION OF ROI FROM FEMALE PELVIC MRI IMAGING

Segmentation of region of interest from female pelvic MRI or PMRI imaging plays an important role in the diagnosis of diseases like cyst, fibroid, cervical cancer etc. Magnetic resonance imaging is taken in three different planes: sagittal, coronal and axial. Radiologist commonly uses sagittal plane to analyse the female pelvic abnormalities. Figure 4.19 shows the MRI image of female pelvis with cyst type abnormality oriented in sagittal plane.

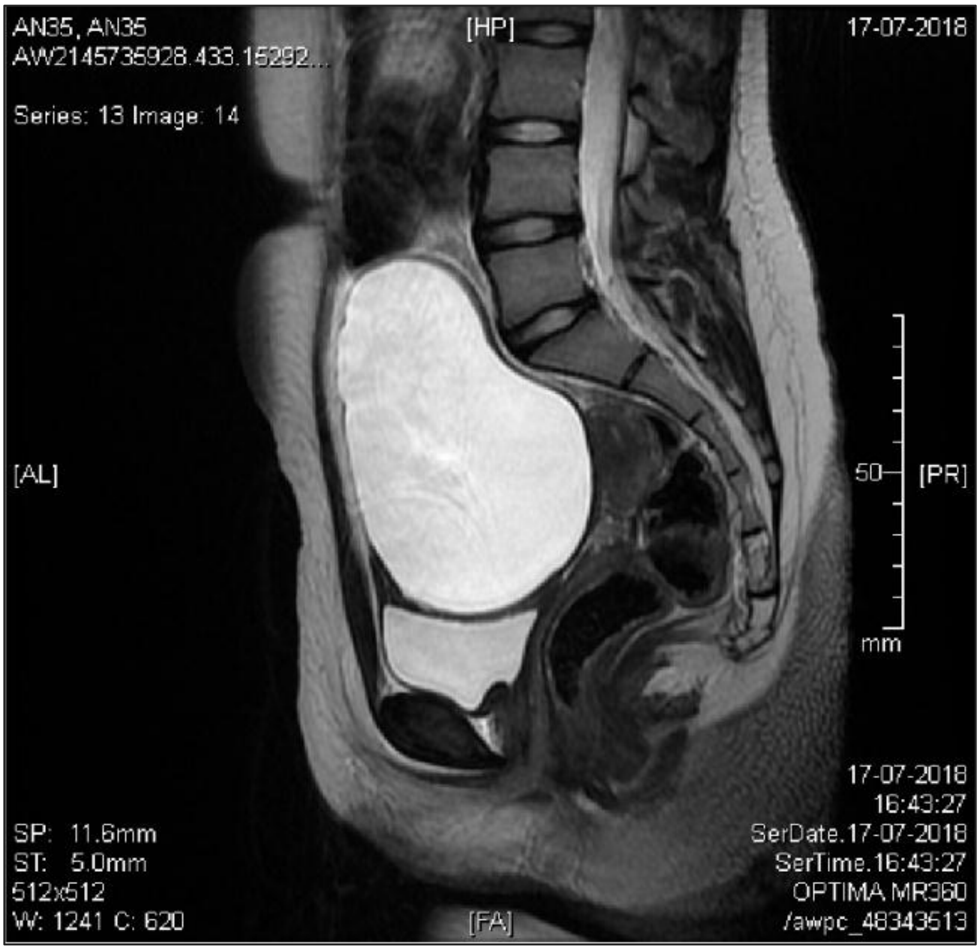

Fig. 4.18. Input MRI Image

4.4.1 The Proposed Method

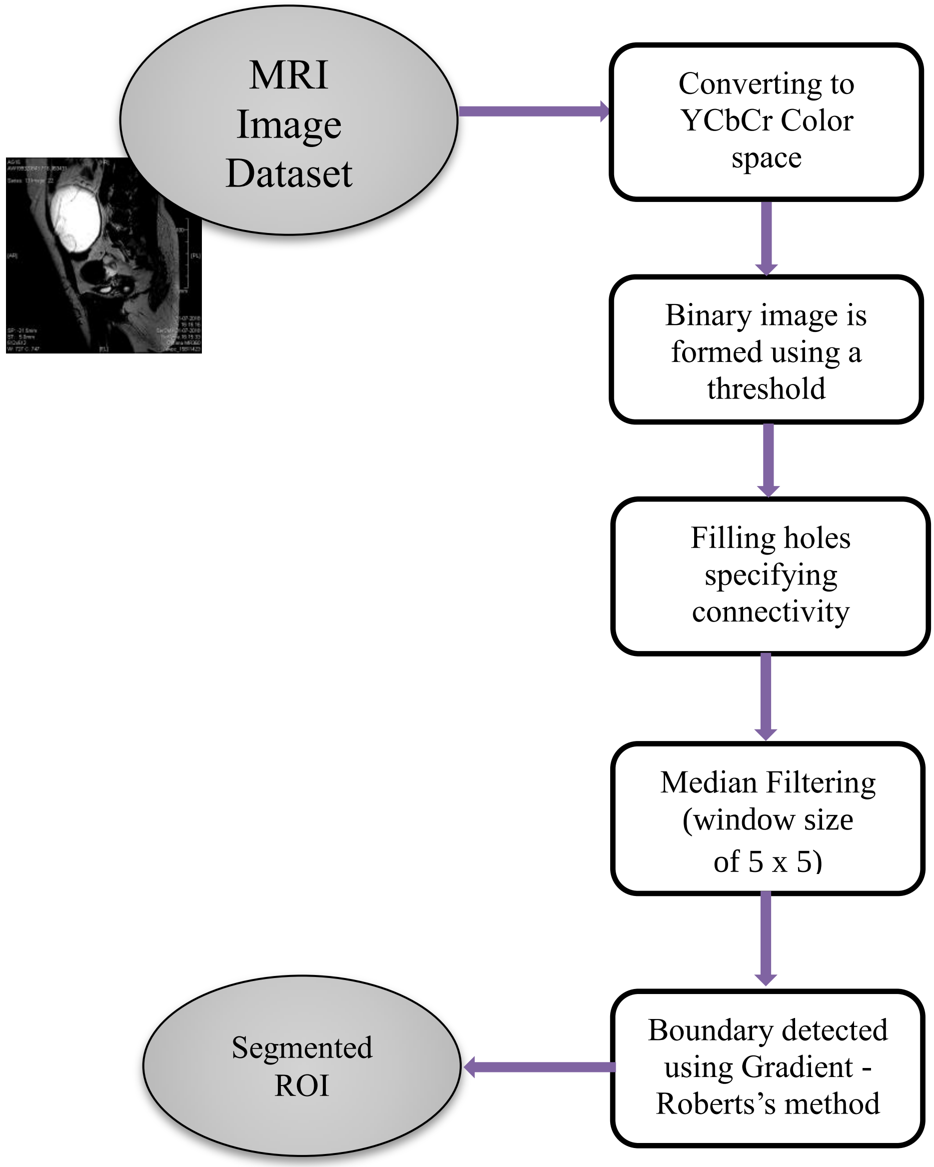

Fig. 4.19. Work Flow of ROI Segmentation in Female PMRI Imaging

The input RGB image obtained is first transformed into an YCbCr color space using a Matlab function. Then the obtained image is separated into its component images *viz*, Y (luminance), Cb (chrominance blue) and Cr (chrominance red). The values of three components for different images are noted and a mask image created from these Y, Cb and Cr values. The obtained mask image is shown in Figure 4.20.

On separating the YCbCr image into different components, the Y channel is found to exhibit a better contrast than other components. The entire workflow of female PMRI image segmentation is shown in Figure 4.18. The mask image is then multiplied with the individual Red, Green, and Blue components of original input image.

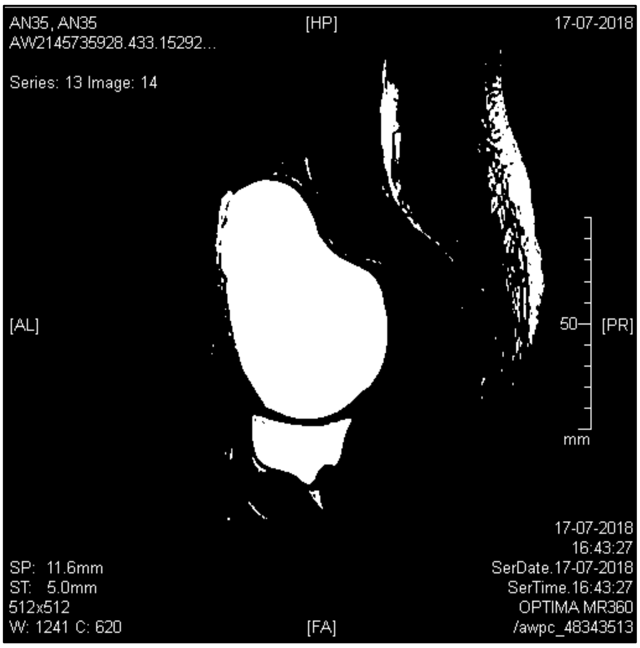

Fig. 4.20 Mask Image

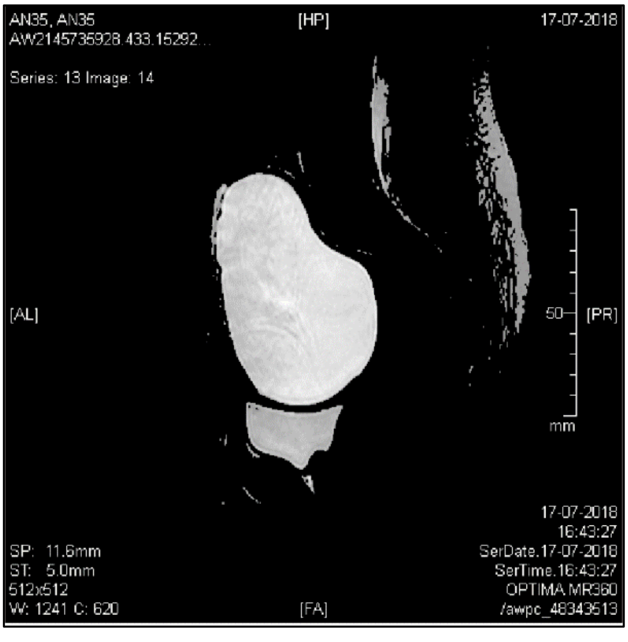

Fig. 4.21. Mask Image Multiplied in Red Plane

Then the processing is carried out in separate planes. Mask image multiplied with red plane is shown in Figure 4.21.

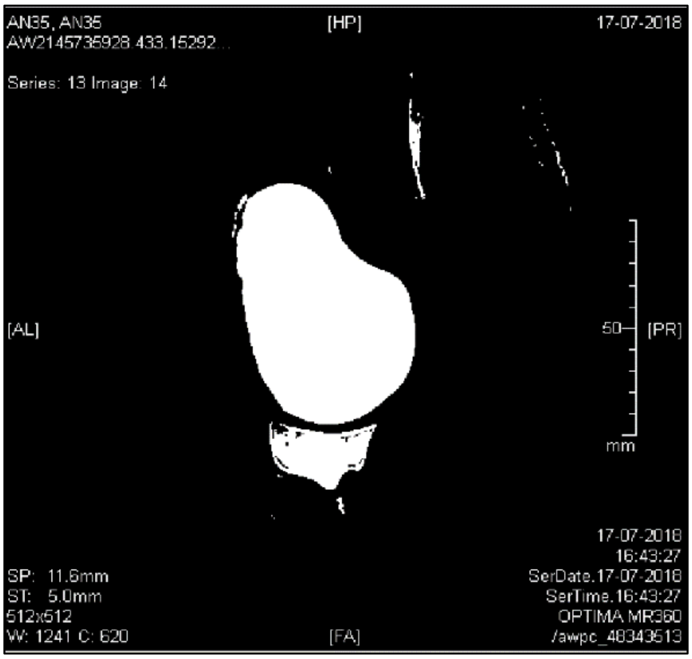

Fig. 4.22. Binary Image

A binary image is formed based on threshold value. All the imaging operations are performed in individual planes. Our experiments shows that a threshold value of 0.68 is fairly good choice. Morphological image filling operation is performed using *'imfill'* Matlab function. It fills holes in the binary image specified with a connectivity of 4.

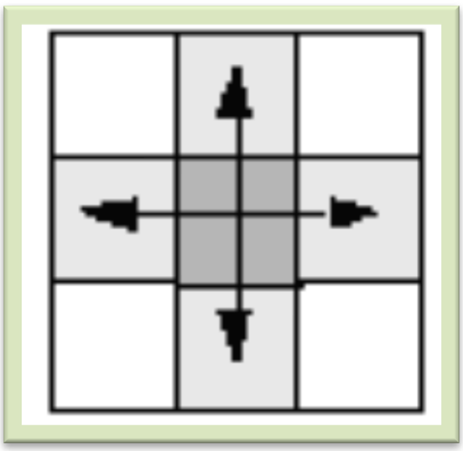

Fig. 4.23. Four Pixel Connectivity

In four pixel connectivity, the pixels are connected if their edges touch. The neighbourhood of a pixel is the adjacent pixels in horizontal and vertical direction as shown in Figure 4.22. Note that in Figure 4.23 the holes are filled, but some unwanted pixels need to be removed. For that median filtering was chosen.

Fig. 4.24. Image Filling

Figure 4.24 shows the median filtered image. Each output pixel contains the median value in a 5-by-5 neighbourhood around the corresponding pixel in the input image. Our experiments shows that 5x5 neighbourhood is fairly good choice.

Boundary of the image is detected using gradient magnitude. Median filtered image is subjected to gradient operation using a Matlab function. The results of gradient operation are given in figure 4.25 and 4.26.

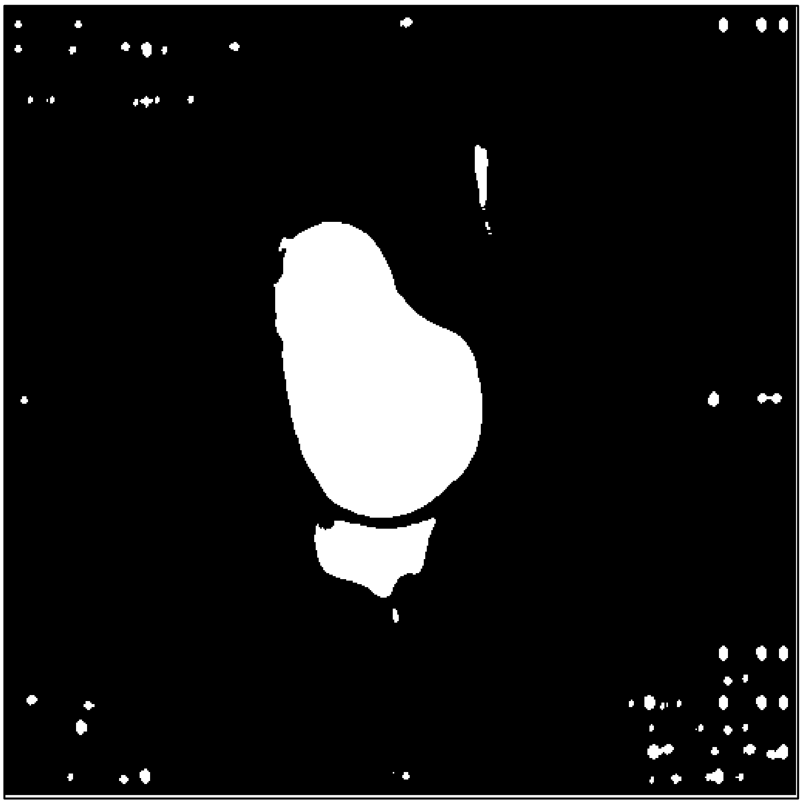

Fig. 4.25. Median Filtering

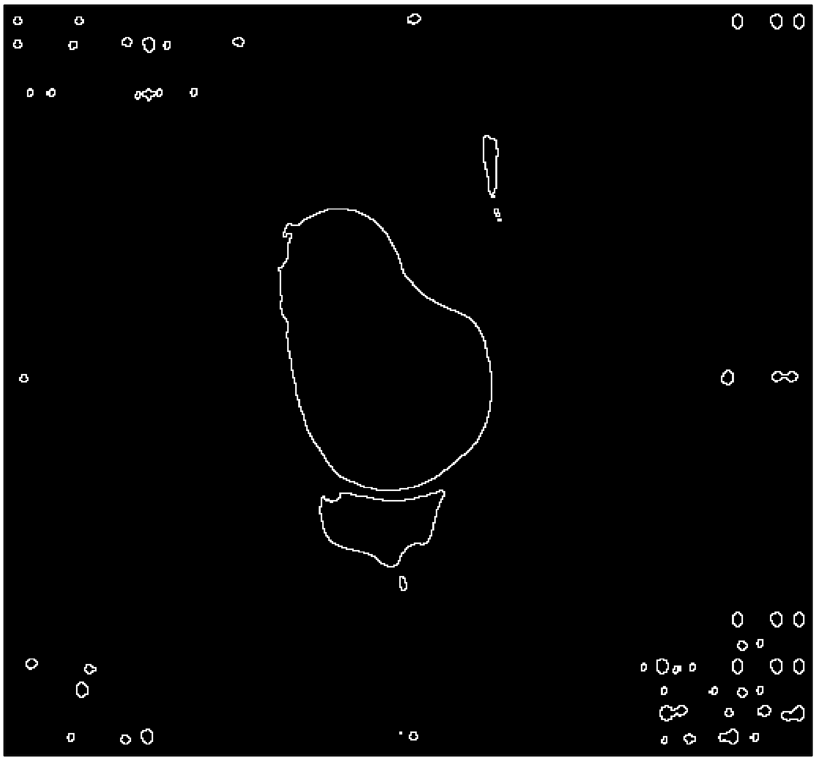

Fig. 4.26. Gradient Image

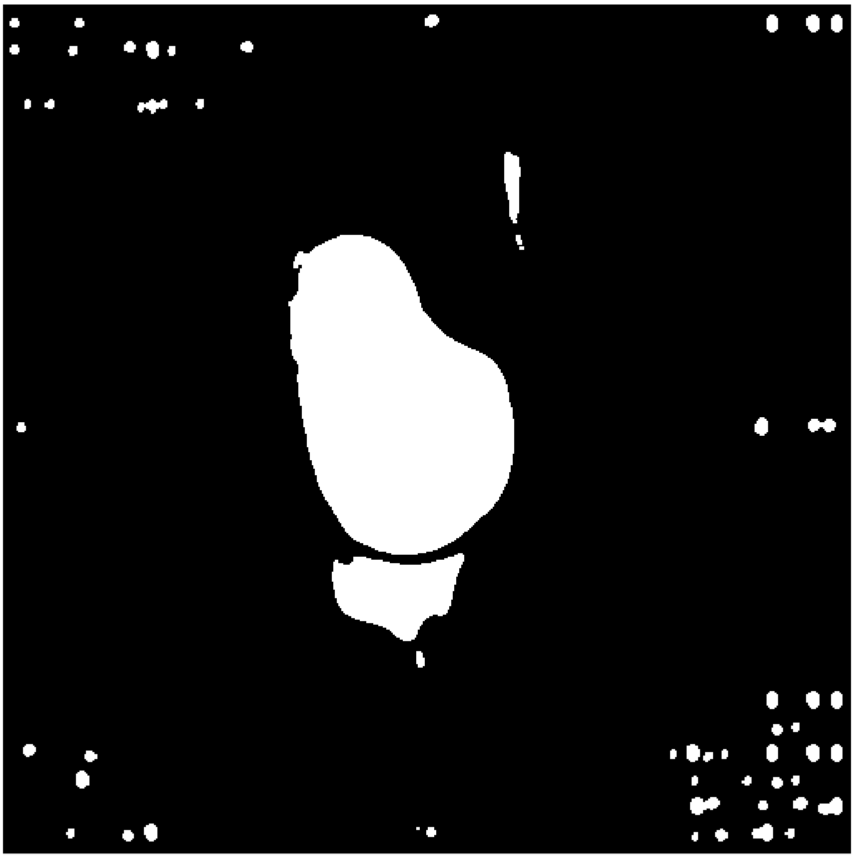

Fig. 4.27. Gradient Filling

Gradient operation is based upon different gradient operators, like prewitt, sobel, roberts, central difference, intermediate etc. Our results points to the selection of roberts type gradient operator and is valid for the whole dataset.

The Matlab function *'regionprops'* is used to obtain the bounding box values. Then the width and height (taken from the bounding box) of each image is considered to filter out the ROI. Now the important diagnostic part is segmented as shown in the Figure 4.27

The algorithm for obtaining the final contour in female pelvic MRI imaging is shown below.

Algorithm 2: ROI Extraction from MRI Imaging Modality

Initial:

1: Input RGB image is converted to YCbCr image.

2: Separating YCbCr into three planes

3: Let R, C be the size of input image, x be luminance plane, q be chrominance blue and z be the chrominance red plane

4: set i=1

5: Repeat steps 6 through 10 until i<=R

6: Set j=1

7: Repeat steps 8 through 10 until j<=C

8: *If (x(i,j)>=147 && x(i,j)<=237) && (q(i,j)==128) && (z(i,j)==128)*

9: Set final mask *roi (i,j)* =1,

10: *else*, set final mask *roi (i,j)* = 0

11: **Comment:** Binary image is formed using a threshold

12: Input RGB image is separated into red, green, blue planes

13: Each plane is multiplied with the obtained mask *roi (i,j)*

14: red* uint8 (*roi (i,j)),* do the same for other two planes

15: Set the threshold value as 0.68

16: Step 14 is converted to binary using *im2bw* function

17: Fill the holes in the obtained binary image, specifying connectivity of 4

18: Median filtering is performed. Set the window size as [5 5]

19: Gradient operation is performed using 'Roberts' operator

20: Steps 16 to 19 are separately done for three planes

21: Concatenate three planes

22: Using area and entropy the important ROI is filter out

end procedure

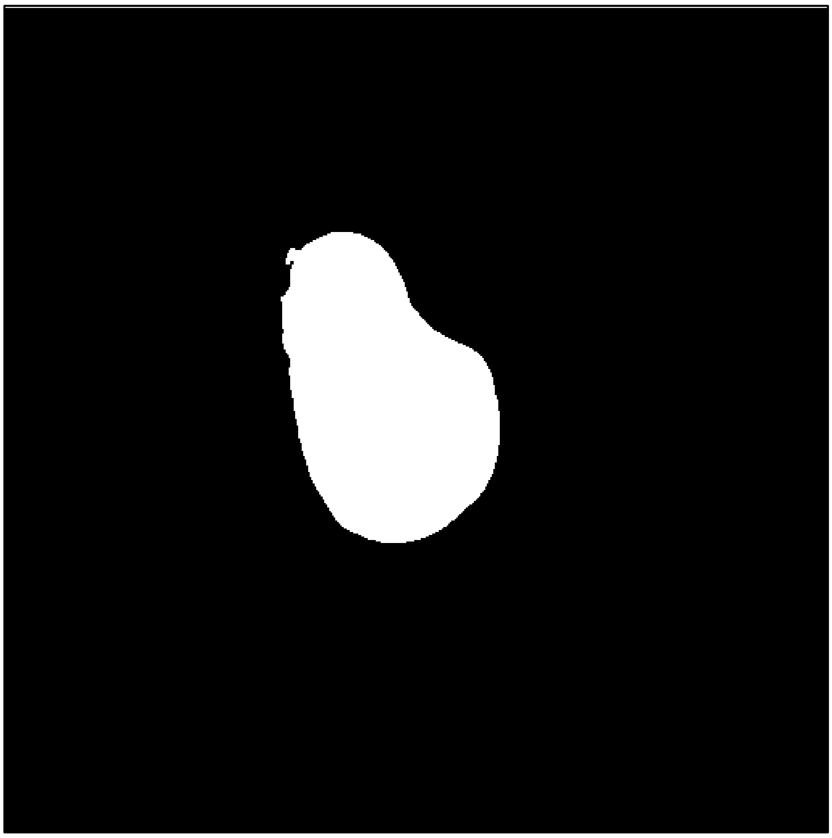

Fig. 4.28. ROI Image

4.5 SUMMARY

This chapter deals with the novel automatic segmentation of important diagnostic region from female pelvic ultrasound and MRI imaging modalities. Segmentation techniques in two imaging modalities are considered. Region of interest extraction for ultrasound imaging is different from that of MRI imaging modality. Morphological watershed based segmentation is carried out in ultrasound imaging modality whereas in MRI, a gradient based method is utilized to extract the important diagnostic part. The simulation analysis of both algorithms was implemented in MATLAB environment. The next chapter describes region of interest based compression for female pelvic images.

Chapter -5

ROI BASED IMAGE COMPRESSION

Contents

5.1. INTRODUCTION

The main objective of our research work is to develop an efficient scheme for image compression for female pelvic Ultrasound and MRI images that can preserve the true diagnostic information and reduce storage and transmission costs. The last Chapter deals with the ROI extraction inorder to do the ROI based image compression. The storage and transmission of large volume of data is challenging and image compression can definitely finds a possible solution for this problem. Care must be taken in handling medical images as the solution of compression need not effect the important diagnostic information in medical images. The simulation result analysis was carried in MATLAB 2018b.

5.2. BACKGROUND

The necessity of fast and efficient coding algorithms in medical field is increasing due to the rise of telemedicine and the wide use of digital images. Telemedicine provides healthcare services and consultations over the telecommunication infrastructure. This demand has led to the innovation of several techniques in the area of image compression.

Image compression is a key issue to be addressed in the area of transmission and storage of images which shows an exponential growth in applications like medical imaging, satellite imaging and telemedicine. Image compression is broadly classified into lossy and lossless. The selection of lossy or lossless type of compression depends upon the performance measures like storage and transmission cost.

5.2.1 Lossy Methods

Lossy type of compression methods offers a high value of compression ratio with an acceptable degree of deterioration in the reconstructed image. Lossy compression techniques are used in different field of applications. It is not necessary to transfer the whole image data in one continuous transmission especially in browsing and retrieval applications where there is a limit in bandwidth usage. In such cases the most important part of the data is decompressed first rather than the other part. In medical imaging applications the un-important part ie, the background is lossy compressed inorder to achieve a better compression ratio. Some of the lossy compression used in our method of work is discussed below.

5.2.1.1 BTC – Block Truncation Coding

Block truncation coding (BTC) algorithm is a type of lossy compression technique for digital images. It divides the original input image into number of blocks and then applies quantization inorder to reduce the number of grey levels in each block. This fast and efficient algorithm gain popularity due to its less complexity and easiness in practical implementation.

The input color image is transformed into other color space and then extracts each color plane separately. Then divide each color plane into blocks of size 4 x 4 or 8 x 8 or 16 x 16 according to the need of requirement. The mean and standard deviation for each block is calculated. The pixel values selected for each reconstructed, or new, block are chosen so that each block of the BTC compressed image will have the same mean and standard deviation as the corresponding block of the original image.

The main drawback of the conventional BTC method is the presence of blocky appearances near the edges of the reconstructed images. One of the suggestions in conventional BTC is absolute moment block truncation coding or AMBTC **(Lema, 1984),** which conserves the higher and lower mean values of each blocks and by using these values the output is quantized.

5.2.1.2 SVD – Singular Value Decomposition

The singular value decomposition or SVD for short is a matrix decomposition method widely used for applications like compression, denoising and data reduction etc [98]. Every input image is represented by pixels and these pixel values are arranged in matrix form. This matrix decomposition method will reduce this matrix to its constituent parts in order to make certain subsequent matrix calculations simpler.

Let A be the m x n input image matrix, applying SVD to this input matrix factorizes it into a product of orthogonal matrix, diagonal matrix and another orthogonal matrix.

$$A = U.S.V^T \tag{5.1}$$

Where A is an m x n matrix, U is an m x m matrix, S is an m x n matrix and V is an n x n matrix. The diagonal values in the S matrix are known as the singular values of the original matrix A. Using the input image matrix A, obtain AA^T and A^TA. Then the eigen vectors of two matrices are calculated which forms the columns of U and V matrices. So the columns of the U matrix are called the left-singular vectors of A, and the columns of V are called the right-singular vectors of A.

$$A = [u_1\ u_2\ u_3 \ldots u_m] \begin{bmatrix} s_1 & 0 & \ldots & \ldots & \ldots & 0 \\ 0 & s_2 & & & & . \\ . & & s_k & & & . \\ . & & & 0 & & . \\ 0 & \ldots & \ldots & \ldots & \ldots & 0 \end{bmatrix} \begin{bmatrix} v_1 \\ v_2 \\ . \\ . \\ v_n \end{bmatrix} \tag{5.2}$$

From the equation 5.2 it is clear that the S values in the diagonal matrix, after k terms are approximated to zero. So after the process of multiplication, the terms greater than k will be zero and the S values in the diagonal matrix is approximated to k terms. The quality of the image is proportional to the k value, but the amount of memory needed to store the image also increases. So an Optimum k value should be selected such that there is no damage to image quality.

5.2.1.3 DCT – Discrete Cosine Transform

DCT is the core of standard lossy image compression algorithm known as JPEG. The Discrete Cosine Transformation is an invertible linear transform and is widely used in many practical image compression systems and multimedia coding standards. The input image is converted into a set of blocks, normally 8 x 8 or 16 x 16 blocks are chosen. The two-dimensional DCT is computed for each block and then the DCT coefficients are quantized, coded, and transmitted.

DCT and DFT are sinusoidal transforms which uses image independent transformations. The usage of real computations in DCT transform makes the DCT hardware simpler, when compared with the complex one in DFT. Quantization and entropy coding are the two techniques used in DCT to reduce the information required to represent an image.

5.2.1.4 Image Compression based on Pyramids

Image compression based on pyramids consists of a set of low pass or band pass copies of an image and each is represented by a different scale of pattern information. We know that, the pixels in an image are highly correlated and these pixel to pixel correlations are removed by subtracting a low pass filtered copy of the image from the image itself.

Let $I_0\ (i, j)$ be the original input image, and $I_1\ (i, j)$ be the result of applying an appropriate low-pass filter to I_0. The difference image or prediction error $R_0\ (i, j)$ is then given by,

$$R_0 (i, j) = I_0 (i, j) - I_1 (i, j) \tag{5.3}$$

This process is iterated to achieve the additional data compression. The subsampled image, I_1 itself is low pass filtered to obtain I_2. The second difference image is obtained by,

$$R_1 (i, j) = I_1 (i, j) - I_2 (i, j) \tag{5.4}$$

This difference of these two functions is similar the ‘Laplacian’ operators used in enhancement of digital images [99]. The steps are repeated to generate the sequence of reduced resolution images of two dimensional arrays like R_0, R_1, R_2,…. ..., R_k. Laplacian pyramid encoding scheme requires relatively simple computations and these can be performed in parallel [100]. A new pyramid level can be build from the predecessors by using these same computations.

5.2.1.5 JPEG

JPEG stands for Joint Photographic Experts Group and it is the first international standard in image compression. This lossy compression method represents data in such a way that less memory is utilized and the data appears to be similar. But there is significant reduction in the quality of JPEG compressed images. Since the human are insensitive to colors at high frequency and the JPEG algorithm takes the advantage of this real fact and hence achieve compression.

The algorithm starts with dividing the source image samples into small non overlapping blocks having 8 x 8 dimensions. Then compute discrete cosine transform for each block. DCT transforms the information contained in each 8 x 8 block of pixels from spatial domain to frequency domain. The coefficients with zero frequency are called DC components and the rest of values are termed as AC coefficients. Then the process of quantization is performed to remove the high frequency components in an image.

Vectoring is done by applying differential pulse code modulation (DPCM) on DC components and run length encoding (RLE) on AC components. Finally the DC and Ac components are represented by a smaller number of bits and this is achieved through Huffman coding. The JPEG compression work with grayscale and color images and it fails in binary images.

5.2.2 Lossless Methods

Lossless type of compression method provides exact reconstruction of original image from its compressed form. One of the shortcomings of this method is its reduced compression ratio, approximately in the range of 5:1. This means if an input image is having the size of 100kb then its lossless compressed image having only 20kb of size. Applications in the field of medical imaging are always opting lossless type of compression methods because it is of immense importance that the image quality should be maintained and tests should be conducted to ensure that a reconstructed image has not lost diagnostically relevant information. Some of the lossless compression methods used in our work is discussed below.

5.2.2.1 JPEG-LS

JPEG-LS standard is based upon low complexity lossless compression (LOCO-I) algorithm, has excellent coding and computational efficiency and it outperforms numerous lossless image compression methods. JPEG-LS is working on three fundamental steps namely prediction, content modelling and coder. Mode of operation depends on whether the pixels are smooth or not. The encoder enters a “run” mode when a flat region is detected; otherwise the pixels are code using “regular” mode. For encoding, first the current pixel ‘x’ is predicted using the Median Edge Detector (MED) as shown in figure 5.1.

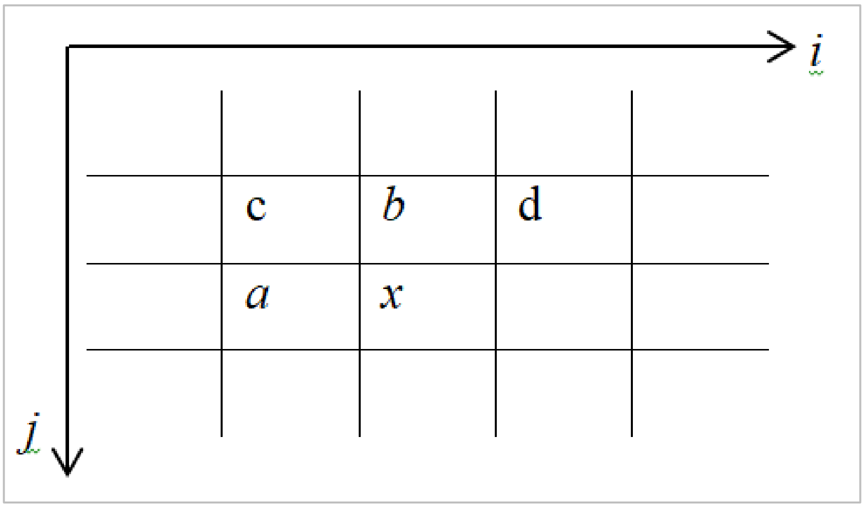

Fig. 5.1. Neighbourhood of the current pixel ‘*x*’ in JPEG-LS

$$\bar{x} = \begin{cases} \min(a,b) & \text{if } c >= \max(a,b) \\ \max(a,b) & \text{if } c <= \min(a,b) \\ a+b-c & \text{otherwise} \end{cases} \qquad (5.5)$$

MED takes the neighbour pixel values of the current pixel ‘*x*’ and computes the possibilities given above. Then, the context for pixel is based upon four pixels *a, b, c, d* and the total number of different context in JPEG-LS is 365. The local gradient is represented by the quantised differences namely *D1, D2* and *D3, where D1=d-b, D2= b-c, D3=c-a.* JPEG-LS also supports the combination of single component and multi component scans for encoding color images (three components). The results show that JPEG-LS outperforms other schemes (FELICS, JPEG-Huffman) in terms of compression ratio with similar value and superior to those of high complexity schemes (**Weinberger, 2000).**

5.2.2.2 FELICS

Felics stands for fast and efficient lossless image compression. This compression algorithm performs 5-times faster than the original lossless JPEG codec and achieves a similar compression ratio. This method uses only two nearest neighbouring pixels for both prediction and error modelling **(Howard, 1993).**

To encode a pixel 'p', the two neighbours of that pixel is noted (N1, N2). Algorithm starts with the minimum and maximum of those neighbouring pixels. The nearest neighbours and the pixel to be encoded is shown in Figure 5. 2. Let S be the min (N1, N2) and L be the max (N1, N2). Then the difference is computed, D= L-S. If the pixel value 'p' is in between these two S and L values, then a bit is used to encode which shows that the value is in range.

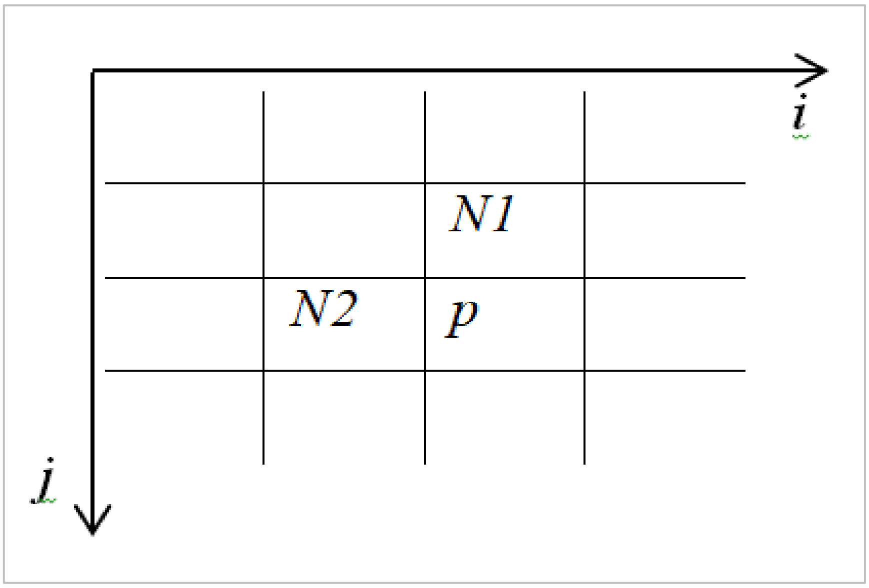

Fig. 5.2. Neighbourhood of the current pixel '*p*' in FELICS

If the pixel value *'p'* is less than the smaller value (p<S) or greater than the larger value (p>L) then two bits are used to encode. In the former case one bit is used to encode the out-of- range and the other is used to encode the below-range. In the latter case one bit is used to encode the out-of- range and the other is used to encode the above-range. In both cases a Golomb-Rice code is used to encode the non-negative integer, *p-L-1*.

5.2.2.3 CALIC

Context Based Adaptive Lossless Image Compression standard uses both context and prediction of the pixel values. The use of large number of context to process a non-linear predictor is the main feature of CALIC and also the predictor is adaptable to varying source statistics. The non-linear predictor can correct itself using an error feedback loop by learning from its past values.

CALIC is simple in arithmetic and logic operations and also added with low time and space complexities **(Khalid, 2005)**. The uniformity of time and space complexities in both encoder and decoder side also shows it's improvement in efficiency **(Wu, 1997)** The gradient adjusted predictor employed in CALICS is non-linear and more robust than traditional DPCM like linear predictors. The gradients in horizontal and vertical directions are used to detect the magnitude and orientation of edges in input image.

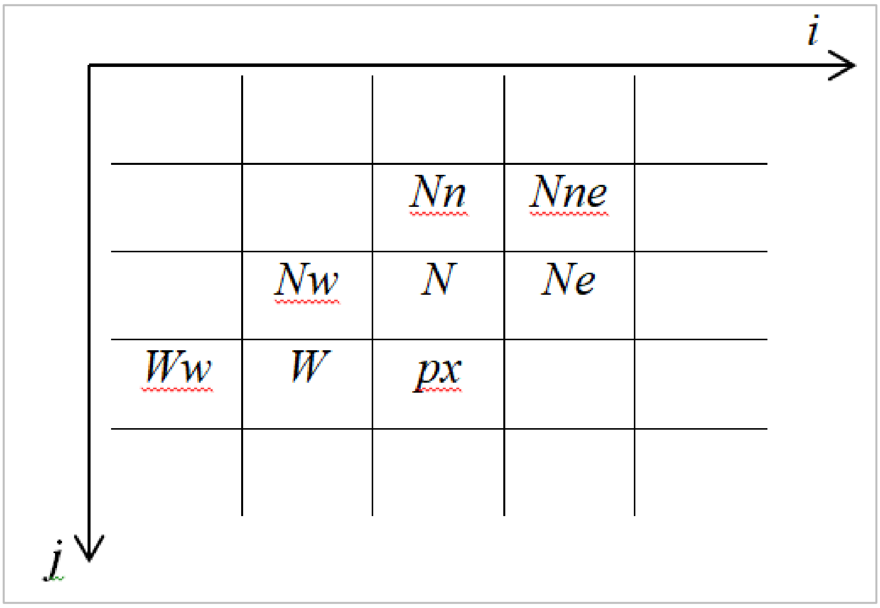

Fig. 5.3. Neighbourhood of the current pixel '*px*' in CALICS

Let d_h and d_v denotes the gradient in horizontal and vertical directions.

$$d_h = |W - Ww| + |\mathrm{N} - \mathrm{Nw}| + |N - Ne| \tag{5.6}$$
$$d_v = |W - Nw| + |\mathrm{N} - \mathrm{Nn}| + |Ne - Nne| \tag{5.7}$$

Any entropy coder can easily interface with CALIC system is its main advantage. It can be Huffman or arithmetic, static or adaptive type. CALIC is tested with 23 standard images and the results shown that it is 26% better than Huffman-coded lossless JPEG and 12% better than arithmetic-coded lossless JPEG **(Wu, 1997).**

5.3 ROI BASED MEDICAL IMAGE COMPRESSION

There is a part of the image that is more important than others, which is called Region of Interest (ROI) and in medical side it defined as the important diagnostic region (IDR). It is necessary to give importance to ROI part than the rest of the image (Non-ROI). So the important diagnostic part of the image should be coded and transmitted with better quality and less distortion than the rest of the image.

Lossy type of compression is not suggested in many of the medical imaging applications due to its quality degradation. Inorder to enhance the diagnostic value of lossy compressed images, the region of interest (ROI) coding concept is launched and it is firstly introduced by JPEG2K standard. ROI based compression methods targeted on to enhance the quality in specified regions of interest only by performing lossless compression in these regions, maintaining the high compression in non-ROI of the image.

5.3.1 The proposed Method

To improve the compression ratio, region of interest (ROI) based medical image compression is proposed here. Female PMRI and female PUS imaging are taken as input images. The image can have 3 views in MRI namely axial, coronal and sagittal. As the radiologists mostly prefer sagittal view for diagnosing the female pelvic abnormalities, individual images of each plane is considered.

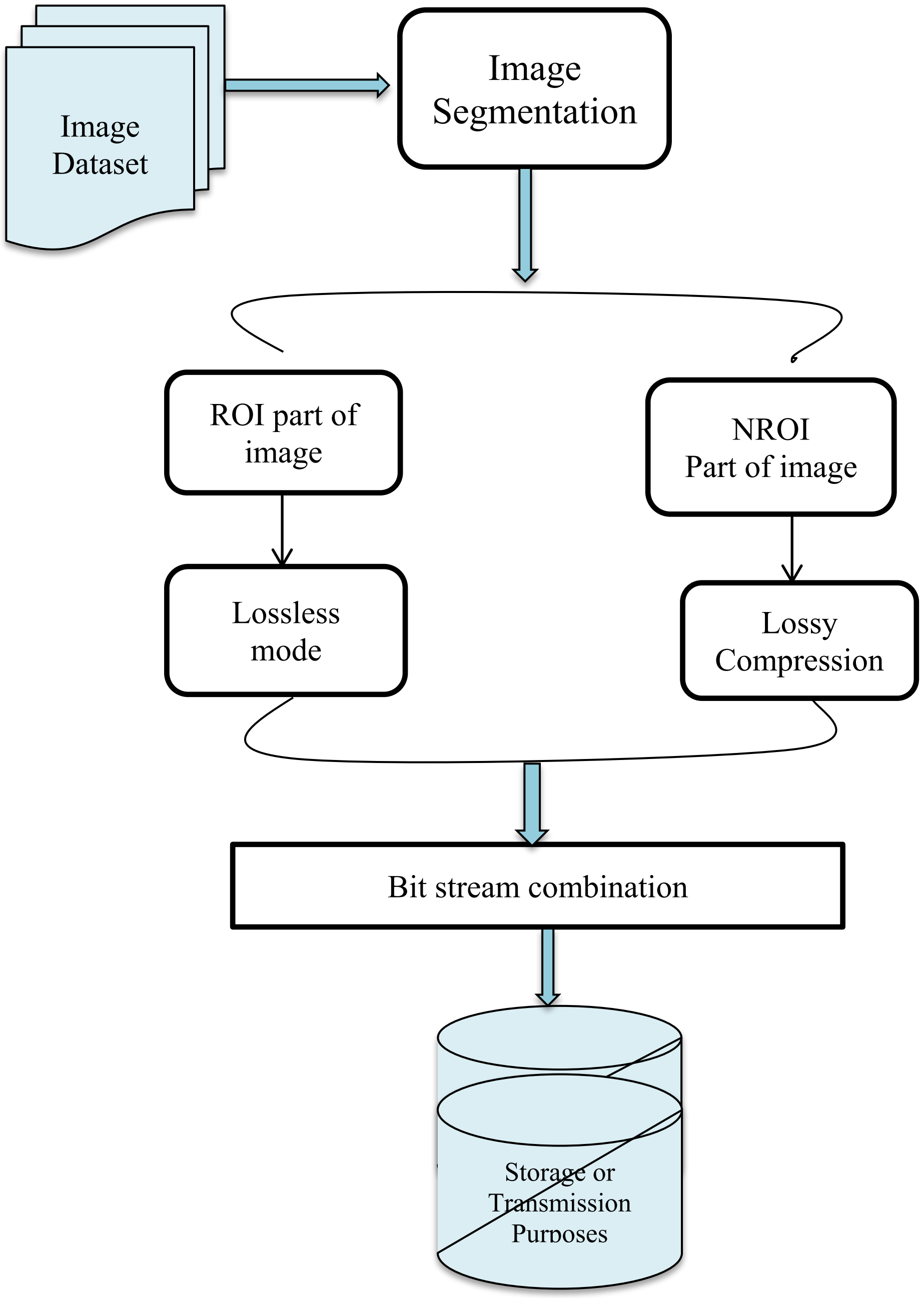

Fig. 5.4. ROI based medical image compression

Initially using the image segmentation method the whole image is divided into two parts: ROI regions and non-ROI regions. That is, the marked area of ROI is compressed using lossless compression and the other area of the image is compressed using lossy compression techniques. The image inside ROI is compressed with lower compression ratio while background area is compressed with a higher compression ratio. The detailed workflow of ROI based compression technique is shown in Figure 5.4.

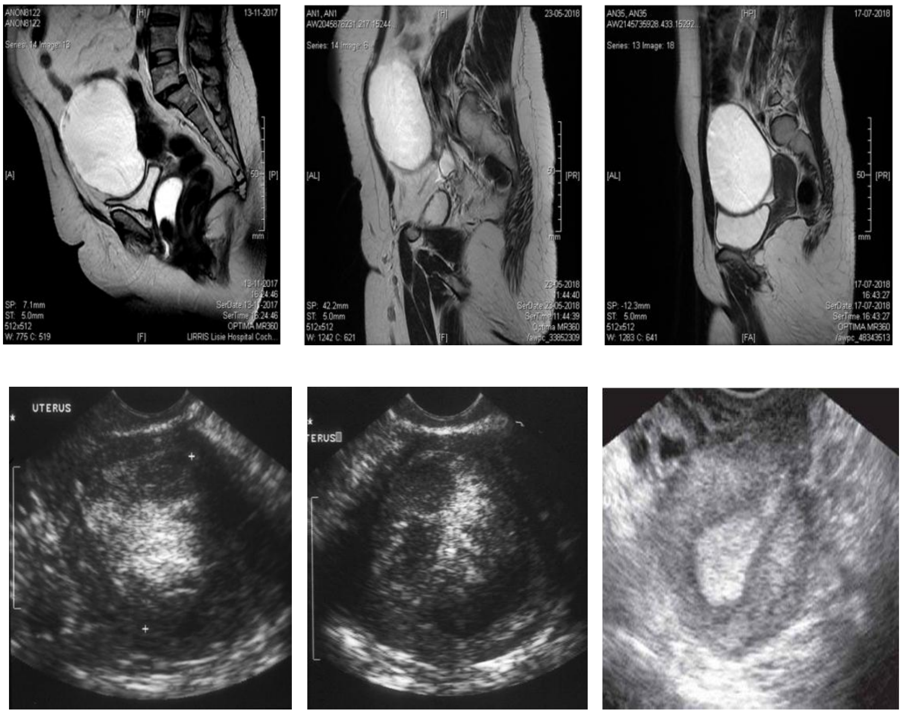

Fig. 5.5. Sample test images
Top row - Female Pelvic MRI (PMRI) input images
Bottom row - Female Pelvic Ultrasound (PUS) input images

The image under consideration is of the size of 512 x 512. By using the segmentation method given in Chapter 4 the important diagnostic region or ROI is obtained from the input medical image. On this region lower rate of compression is applied. The challenges when segmenting ROI in the case of both imaging modalities is that the lesion should not be missed out and at the same time the image area identified as ROI should not be large. Then the background is separated from the original image using the method of subtraction. On this region higher rate of compression is applied. The original image is multiplied with ROI (which is obtained in binary form after segmentation) to get the intensity image. Input image and the compressed input image using ROI based compression technique is shown in Figure 5.6.

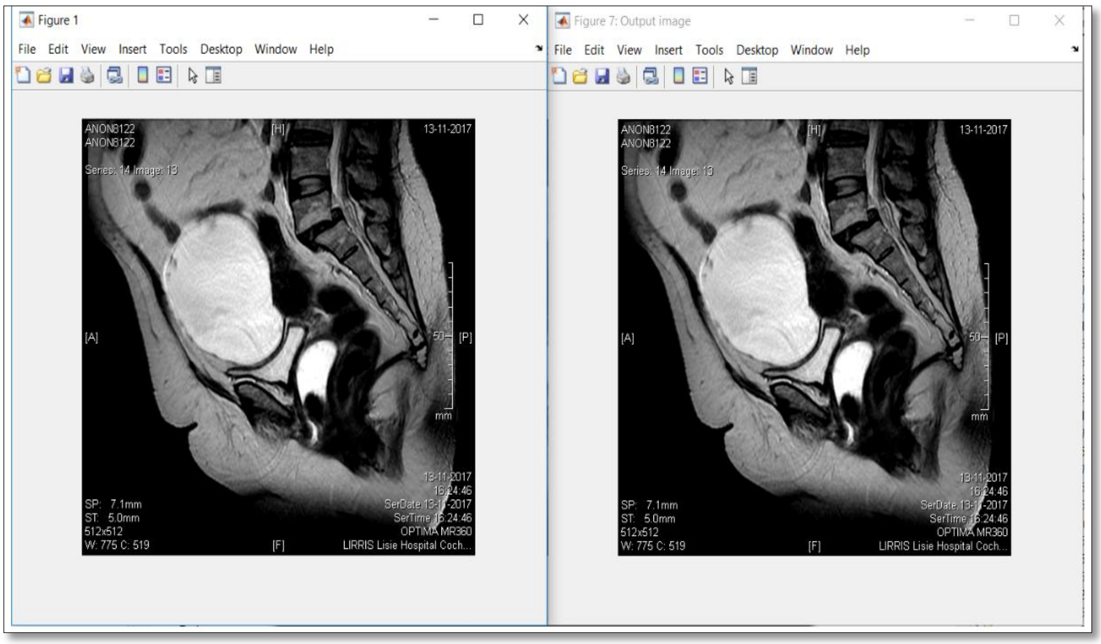

Fig. 5.6. Input image and ROI based compressed image output

In lossless type of compression methods, JPEG-LS (Jpeg lossless), FELICS (Fast efficient and lossless image compression) and CALICS (Context based adaptive lossless image) are considered whereas in lossy JPEG, DCT (Discrete cosine transform), BTCODE (Block truncation coding), SVD (Singular value decomposition) are considered. The plot of compression ratio and psnr using these methods (M1 to M8) is shown in Figure 5.7. Out of that the combination of JPEG-LS and JPEG yields good compression ratio with better image quality.

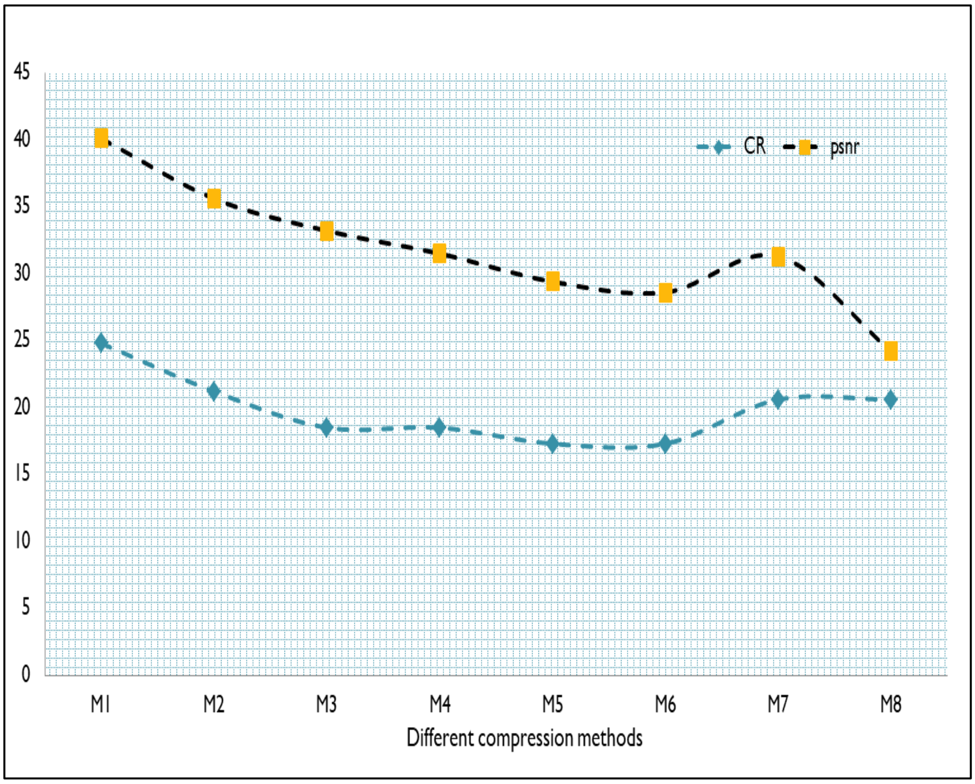

M1	JPEGLS - JPEG	M3	JPEGLS - SVD	M5	JPEGLS - BTCODE	M7	JPEGLS - DCT
M2	FELICS - JPEG	M4	FELICS - SVD	M6	FELICS - BTCODE	M8	FELICS - DCT

Fig. 5.7. Plot of CR and PSNR

5.4 SUMMARY

Image compression in medical field is unavoidable due to its large amount of storage space or increasing bandwidth. Transferring or communication of images to other side in its original form is difficult and time consuming. So here developed a region of interest based medical image compression to maximize the entire compression ratio at the same time maintains the quality of the image. Experimental results illustrate that the developed compression method produces high compression ratio and has a good fine detail.

Chapter -6

RESULTS AND DISCUSSION

Contents

6.1 INTRODUCTION

India the second most populous country in the world presently has 1.34 billion populations and is predicted to have more than 1.53 billion people by the end of 2030. Out of that, 432.2 million women aged 15 years and older are at risk of developing cancer. The risk of developing cancer is also expanding with the increase in population growth and most of the cases occur between the ages of 50 and 60 years. In order to ensure that these patients receive treatment on time yearly pelvic examination is advised by physicians. However growing incidents of pelvic disorders increase the number of patients in hospitals and as a result the number of images that need to be reviewed by expert radiologists. In addition, the high cost of examinations and the lack of expert radiologists prevent many patients from receiving effective treatment in right time.

Nowadays many hospitals make use of teleradiology applications in which the technicians can control the patients without the need of an expert. They take the image from the corresponding scanners and send via a network where the experts on the other side can read those images and send back a diagnosis. If a good quality compressed image reaches the other side radiologists then he can easily diagnose and at the same time waiting timing of patients can also reduce. An expert system for automatic detection of anomalies in images can also aid the radiologists for better outputs in limited time.

In our research work, two algorithms are developed for finding the important diagnostic region in female pelvic images: one for Ultrasound imaging modality and other for MRI imaging modality. Then an improved ROI based medical image compression is also developed for these imaging modalities. This chapter deals with comparison analysis of the developed algorithm with the existing or conventional systems. The developed algorithm was implemented using MATLAB R2016a and R2018b and all the results which are given in this chapter and the previous chapters are tested in 4 GB RAM, 500 GB HDD with an Intel (R) core (TM) i3-7020U (7^{th} Gen), x64 based processor system.

6.2 DATASET DESCRIPTION

The datasets available in public are not well suited for evaluating algorithms. So we have used real medical images to complete our entre research work. Our research is based on the finding of important diagnostic region from female pelvic MRI and Ultrasound imaging modalities. We collected 20 ultrasound images and 320 MRI images to carry out this research work. All exams in MRI images were acquired using OPTIMA 360 – INSPIRE GE Healthcare MRI machine and ultrasound images are obtained from Logic s7 Expert ultrasound machine. All the images for this research work are provided by radiology department in LIRRIS - Lisie Institute of Radiology Research and Imaging Sciences.

The ground truth data provides the gold standard against which the algorithms can be evaluated. The image cases we selected were already reviewed by a senior radiologist. The ground truth images are collected and marked with the presence of radiographers. The images can have 3 views in MRI: axial, sagittal and coronal. As the radiologists mostly prefer sagittal plane for diagnosing the abdomen part of women, we also took the images in that plane for algorithm development or method evaluation. An MRI contrast media or Gadolinium contrast media is injected into patient's body before doing the MRI scan. The amount of contrast is determined from BMI (body mass index) of each patient.

6.3 ALGORITHM EVALUATION IN FEMALE PELVIC ULTRASOUND IMAGING MODALITY

A preprocessing step is initialised before the segmentation to remove noise in medical ultrasound images. The different types of evaluation are performed as follows.

6.3.1 Evaluation of the Preprocessing Stage

The input ultrasound image shown in figure 6.1 is subjected to SRAD filtering as a preprocessing stage. For performance evaluation the SRAD filtered image shown in Figure 6.2 is compared to other adaptive mean filters like Lee and Kuan. The performance comparison of above filter with other filters is shown in Figure 6.3. It is seen that the SRAD filter performs well.

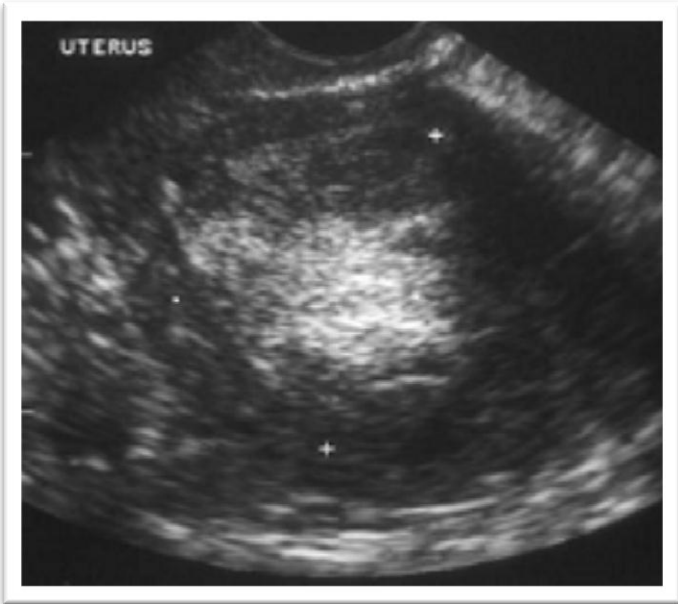

Fig. 6.1. Input Ultrasound Image-Endometrium Cancer

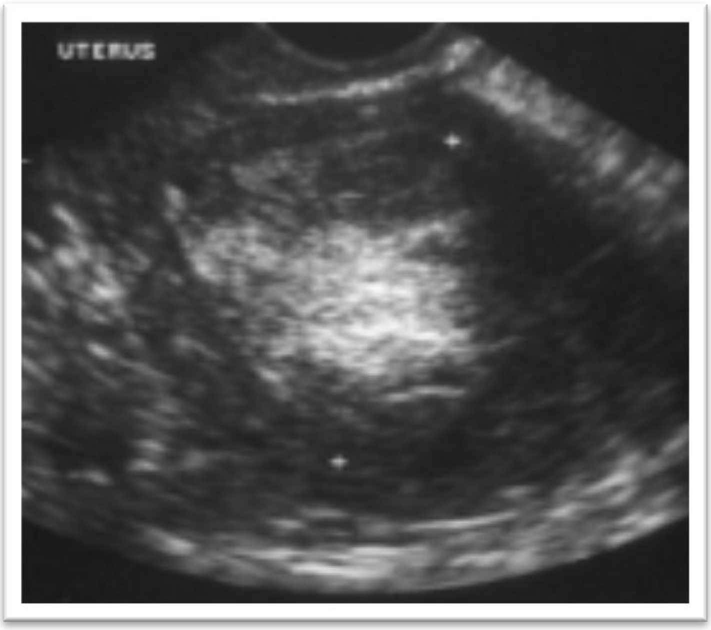

Fig. 6.2. SRAD Filtered Input Ultrasound Image

Certain quality metrics measurements like peak signal to noise ratio (PSNR), root mean squared error (RMSE), signal to noise ratio (SNR) and Coefficients of correlation (CoC) are used **(Finn, 2011)** Peak Signal to Noise Ratio is the ratio between possible power of a signal and the power of corrupting noise and it is also used as a measure to quantify enhancement or quality of an image. It's given by,

$$PSNR = 10\log_{10}\frac{(N-1)^2}{MSE} \tag{6.1}$$

$$\text{MSE} = \frac{1}{MN}\sum_{j=1}^{M}\sum_{k=1}^{N}(x_{j,k} - x'_{j,k})^2 \tag{6.2}$$

Root Mean Square Error or RMSE is the measure of the square root of the squared error averaged over a pixel window and is given by,

$$\text{RMSE} = \sqrt{\frac{1}{MN}\sum_{j=1}^{M}\sum_{k=1}^{N}(x_{j,k} - x'_{j,k})^2} \tag{6.3}$$

Where $X_{j,k}$ is the original image of size M x N, $X_{j,k}'$ is the enhanced image and N-1 is the maximum possible value in $X_{j,k}$.

Coefficient of Correlation or CoC [103] indicates the strength and direction of linear relationship between the original and denoised images and is widely used in pattern recognition and image processing. It is defined by,

$$\text{CoC} = \frac{\sum_j (x_j - x_k)(y_j - y_k)}{\sqrt{\sum_j (x_j - x_k)^2}\sqrt{\sum_j (y_j - y_k)^2}} \tag{6.4}$$

Where X_j is the intensity of the jth pixel in first image, Y_j is the intensity of the jth pixel in second image, X_k is the mean intensity of first image, and Y_k is the mean intensity of second image.

6.3.2 Extraction of multiple features from selected ROI

Multiple features are extracted from the female pelvic ultrasound images after the segmentation of region of interest (ROI). The optimal features can be selected from these multiple ROI features for proper classification of tumor part (considering only in future work). In this study, two categories of PUS image features are presented which includes shape and texture features.

Shape is one of the important observing criteria used for classifying the lesions in ultrasound images [40]. In this work the most frequently used 8 shape parameters like area (FE_1), perimeter (FE_2), major axis and minor axis length (FE_3), centroid (FE_4), equidiameter (FE_5), solidity (FE_6), circularity ratio (FE_7) & eccentricity (FE_8) are included. Area specifies the number of (non zero) pixels in the tumor region whereas perimeter specifies the distance around the boundary of that region.

In addition to this structure based features, texture features are also presented for discriminating the tumor from normal tissues. The obtained range of values for diverse ultrasound images is illustrated in Table 6.1.

Similarity of the required region to a circle is described by its circularity ratio and to a convex or concave is given by solidity.

$$CircularityRatio = \frac{4\pi \times Area}{Perimeter^{2}} \tag{6.5}$$

$$Solidity = \frac{Area}{ConvexhullArea} \tag{6.6}$$

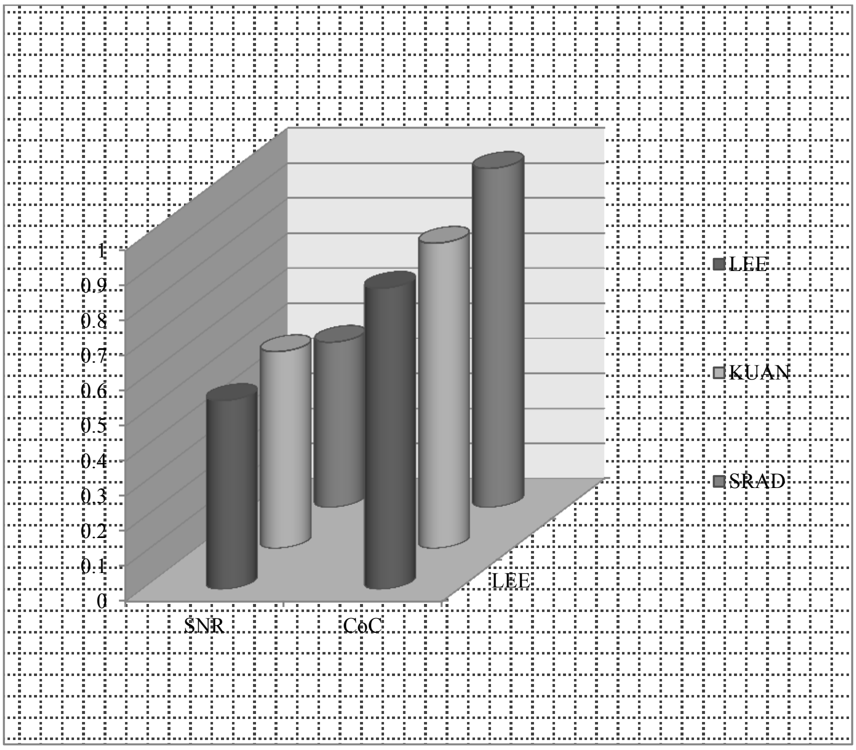

(a)

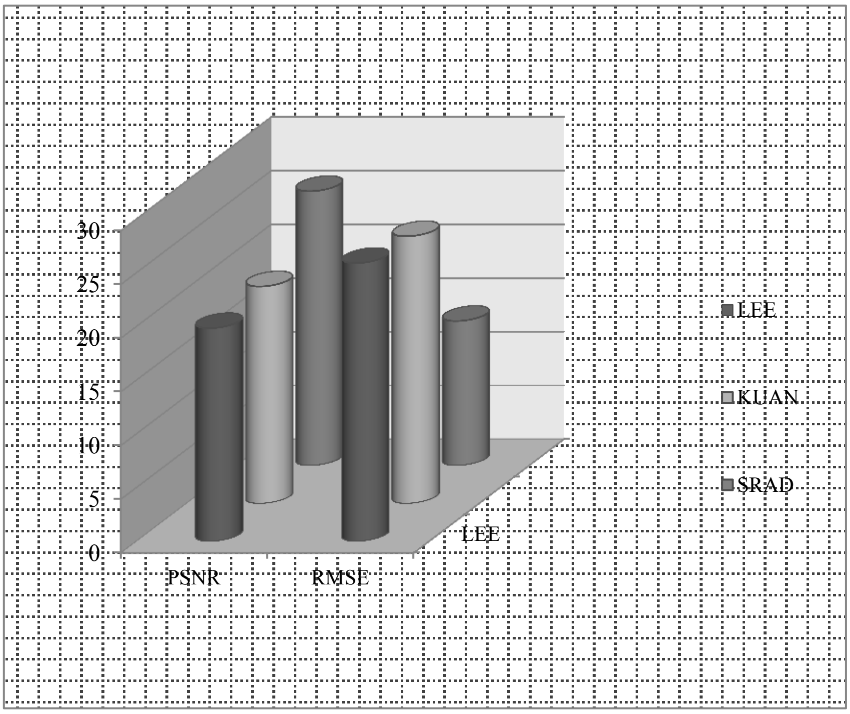

(b)

Fig. 6.3. Filter Comparisons for Lee, Kuan and SRAD.

(a) SNR and CoC

(b) PSNR and RMSE

Table 6.1. Details of extracted shape and textural features from the ROI of input ultrasound image

Feature Category	**Feature Description**	**Range of Values**
Shape Features	FE_1: Area	2755 – 4917
	FE_2: Perimeter	546 -1073
	FE_3: Major axis and Minor axis length	64 - 118.11; 76.2 –119.5
	FE_4: Centroid	130,137 – 243, 170
	FE_5: Equidiameter	59.23 – 79.12
	FE_6: Solidity	0.732 – 0.923
	FE_7: Circularity	0.054 – 0.17
	FE_8: Eccentricity	0.32 – 0.672
Textural Features **(Haralick 1973)**	FE_9: Angular second moment	0.901 – 0.972
	FE_10: Correlation	882.08 – 3.26e+03
	FE_11: Sum of Squares: Variance	903.2 – 3.33e+03
	FE_12: Inverse Difference	0.93 – 0.998
	FE_13: Entropy	0.08 – 0.2153
	FE_14: Contrast	42.24 – 179.52
	FE_15: Difference variance	0.0019 – 0.002
	FE_16: Difference entropy	-0.006 - -0.0192
	FE_17: Information measure of correlation 1	-0.915 - – 0.94
	FE_18: Information measure of correlation 1	0.36 – 0.56

Equidiameter is given by,

$$Equidiameter = sqrt(4\pi \times \frac{Area}{pi}) \tag{6.7}$$

The eccentricity characterizes to the un-circularity of ROI. It is given by,

$$Eccentricity = \frac{distance\ between\ the\ foci}{majoraxis\ length} \tag{6.8}$$

$$= \frac{\sqrt{a^2 - b^2}}{a}$$

Where *a* and *b* represents the semi-major and semi-minor axis length.

Total ten textural features (FE_9 to FE_18) are measured from the grey level co-occurrence matrix c(x). In that angular second moment, correlation, sum of squares: variance, entropy, inverse difference, contrast, difference variance, difference entropy, information measure of correlation 1, and information measure of correlation 2 are considered for diagnosis of data which is defined by Haralick **(Haralick, 1973).**

Figure 6.4 represents the segmentation results of 3 PUS images. Also, over-segmentation problem of three images can be seen clearly in Figure 6.4.c. The introduction of internal and external markers forms a distinction in effortless tumor identification. From the results it can be clearly observed that the proposed segmentation method can able to segment the tumor with different sizes and shapes.T1 and T3 are irregular shape contours whereas T2 is nearly an oval shape tumor. Due to the intensity difference of T2 from T1 and T3, algorithm wrongly segments two contours (Figure 6.4.d.) is one of the limitations of the proposed approach. The final contour outlined by green colour label as shown in Figure 6.4.d.

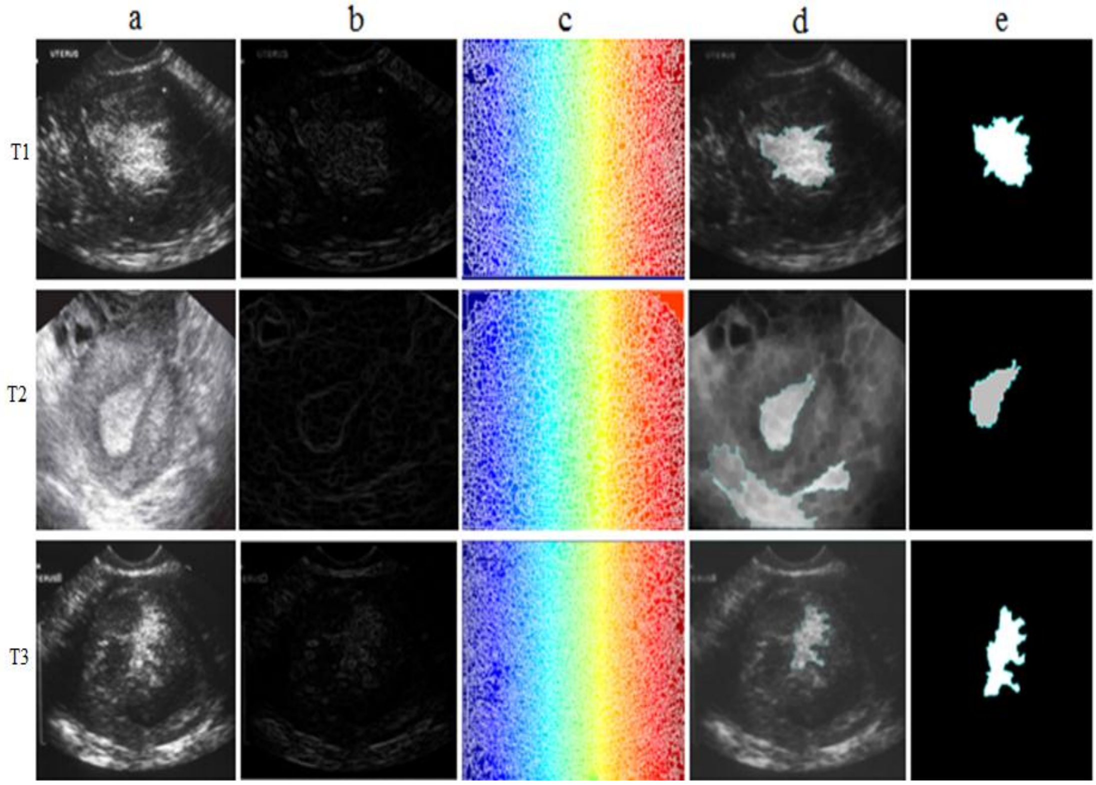

Fig. 6.4. Segmentation Results of Three Female PUS Tumor Image Samples.
Column ‘a’ Shows the Three Input Images T1, T2, T3,
Column ‘b’ Shows its Gradient Image Outputs.
Column ‘c’ Over-Segmentation Problem,
Column‘d’ Final Contour.
Column ‘e’ Separated ROI Part.

6.3.3 Similarity Metrics

The similarity check process involves in verification of manual segmented region with the contour of extracted region. The manual segmentation process would involve in segmenting the cancer region in the ultrasound images manually over the images. The manual segmented data would be stored separately and later compared with the achieved segmentation results for computing the similarity metrics.

For brevity the similarity measures was carried out on six ultrasound images which is reviewed and validated with the aid of radiologists. Similarity index refers to ratio of true positive pixel element number to the sum of automated and manual pixel element numbers. Jaccard similarity index and Dice similarity coefficient or (Zijdenbos similarity index) are used to calculate the similarity and diversity of manually *versus* automated segmentations. Both are equivalent but ZSI is commonly used in image segmentations.

$$SI = \frac{2 * Truepositive_{PixelNumber}}{Manual_{PixelNumber} + Automated_{PixelNumber}} \tag{6.9}$$

$$JSI = \frac{Manual_{segmentation} \cap Automated_{segmentation}}{Manual_{Segmentation} \cup Automated_{Segmentation}} \tag{6.10}$$

$$DSC = \frac{2 * (Manual \cap Automated)_{segmentation}}{Manual_{PixelNumber} + Automated_{PixelNumber}} \tag{6.11}$$

The results of three shape similarity indices between manual and automated segmentations can be seen in Table 6.2. The comparison result gives an average similarity index of 82.65% and JSI of 76.5% and a DSC of 83.8%. The proposed method achieved a good similarity result and JSI value when compared to 74.5% obtained in (**Gu, 2016).**

The values of true positive (TP), false positive (FP), true negative (TN) and false negative (FN) are also noted to calculate the False positive rate or fall-out and False negative rate or FNR. In addition, the system also got an average false positive rate which is less than 0.05 and an average false negative rate of 0.18 which is acceptable when compared with a *FPR and FNR* value of radiologists assessment (0.35 *and* 0.11) and the proposed method (0.04 *and* 0.08) in **(Shi, 2010).**

False positive rate or FPR = FP/ (FP+TN) (6.12)

False negative rate (FNR) = FN/ (FN+TP) (6.13)

Table 6.2. Comparison of manual segmentation and automated segmentation using similar metrics

Test Image	I1	I2	I3	I4	I5	I6	Average
SI (%)	87.8	92.5	80.5	78.3	75.6	81.2	82.7
JSI (%)	78.1	86.2	67.7	71.5	73.9	82.1	76.5
DSC (%)	87.2	92.5	80.6	83.4	79.2	80.4	83.8

6.4 ALGORITHM EVALUATION IN FEMALE PELVIC MRI IMAGING MODALITY

The MRI image obtained from the radiology department is in RGB form. As a preprocessing step, the obtained color image is first converted into YCbCr color space before doing the other image processing operations.

6.4.1 Evaluation in Color Space Transformation

Several color space transforms such as RGB, YCbCr, HSV, YIQ, and XYZ are studied and found that YCbCr color space are giving more accurate results. Histogram plot of different color spaces are given in Figure. 6.5. The conversion of RGB color space to YCbCr is already explained 4.2.2. Inorder to reduce the correlation among RGB color space the image is converted into YCbCr color space as a preprocessing step for certain compression applications **(Kumar, 2016).**

From the histogram plot of input image shown in Figure. 6.5 It is clearly seen that YCbCr color space having the values lying in constant range rather than the distributed values in other color spaces. The threshold values used for luminance and chrominance in our algorithm is x(i,j)>=147 && x(i,j)<=237) && (q(i,j)==128) && (z(i,j)==128 (6.14)

Where x(i,j) is luminance and q(i,j) is chrominance red and z(i,j) is chrominance blue.

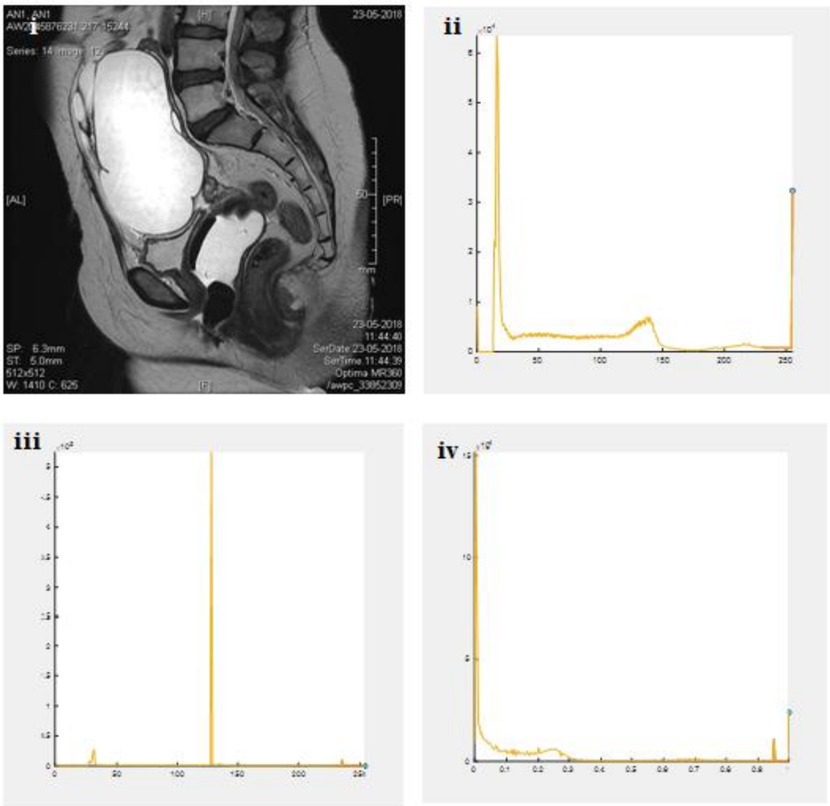

Fig. 6.5. Histogram Plot of Different Color Spaces of an MRI Image
(i) Input MRI Image (ii) RGB Color Space
(iii) YCbCr Color Space (iv) HSV Color Space.

Cyst type of lesions appeared as bright regions in T2 weighted MRI images (Figure 6.5 (i)), which need to be separated from the structured background. Inorder to focus on these bright objects, thresholding technique has been used. For that, a method of binarization can be done based on pixel intensity values and is given by:

$$bin(x,y) = \begin{cases} 1 \; if I(x,y) >= Th \\ 0 \; if I(x,y) < Th \end{cases} \qquad (6.14)$$

Where, bin(x,y)is the resultant binary image based on the threshold value *Th.* Here the luminance threshold value can be estimated based on the region of interest of mask image and input image *I(x, y)*. We set 0.68 as the level value for doing the binarization process. The value we set will be compared with the luminance of the pixel and if it is greater it will be set as 1and become white pixel and if it is less it is set as 0and will be black pixel.

6.4.2 Evaluation in Filtering Method

Median filtering approach is introduced to remove the unwanted pixels in an image. Each output pixel contains the median value in a specified neighbourhood around the corresponding pixel in the input image. The selection of window size has a greater impact on median filter outputs. The window size can be 3X3, 5X5, 7X7, 13X13 etc. Before applying the gradient operation, we perform median filtering with a mask size of 5X5 pixels on the binary image. The median filter output obtained using different window size is given in figure 6.6. From the figure it is clearly seen that a window size of 5X5 is giving smooth curvature on contours when compared with 3X3 and 5x5.

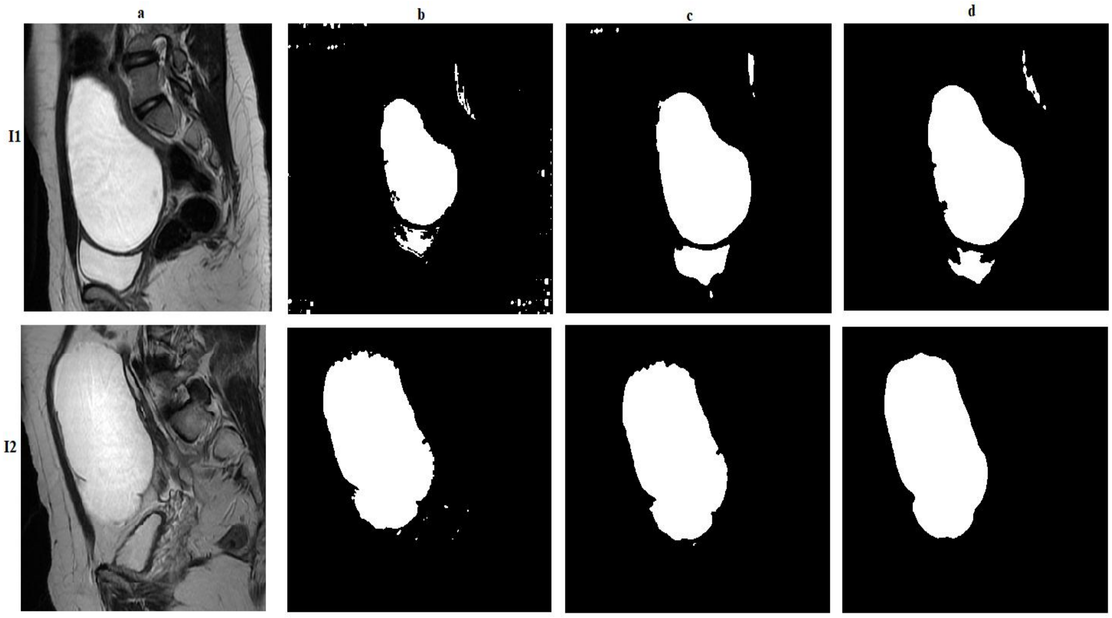

Fig. 6.6. Median Filter output using different window size. Column 'a' shows the input images. Using Window Size 3X3 (column 'b'), 5X5 (column 'c'), 7X7 (Column 'd').

6.4.3 Evaluation in Gradient Method

Gradient magnitude of the MRI image using different methods like prewitt, sobel robert's and intermediate is shown in figure 6.7. X axis shows the different input images and Y axis shows the number of detected objects which is obtained as a result of different gradient magnitude methods. For brevity 20 MRI input images are considered.

Here robert's operator is giving better results than prewitt, sobel and intermediate. Gradient method using intermediate operator also detects same number of objects as like robert's but failed in cases of input image 7 and 13. Thus the maximum number of detected objects is given by robert's method and hence it is chosen for doing gradient operation

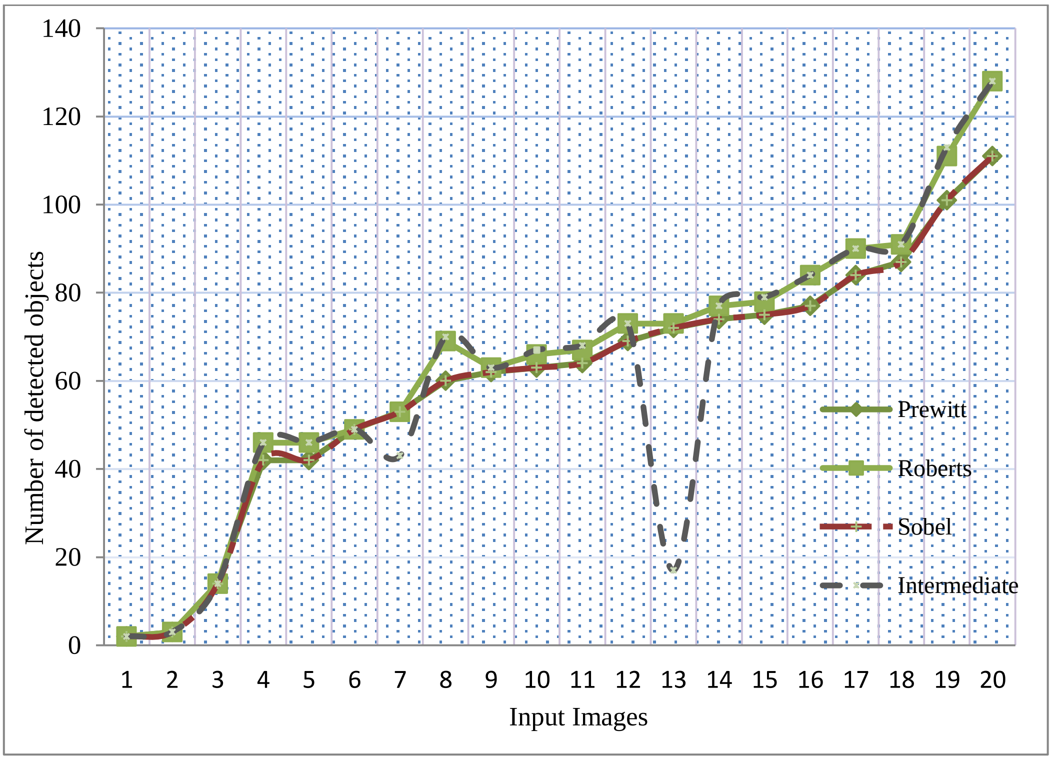

Fig. 6.7. Gradient Operator With Number of Detected Objects in an Image

Table 6.3. Details of extracted features from the ROI of input MRI image

Features / Images	FE_1	FE_2	FE_3	FE_4	FE_5:	FE_6	FE_7
I1	21648	0.0024	14.13035	26.2475	-0.03857	0.002373	0.004813
I2	18860	0.0032	12.47677	24.9117	-0.05647	0.003227	-0.00652
I3	23865	0.0044	11.70527	23.57087	-0.06747	0.004395	0.00842
I4	21150	0.0089	8.455791	20.53052	-0.14264	0.00885	-0.02993
I5	25270	0.0028	13.83474	25.45801	-0.0413	0.002846	0.004429
I6	26384	0.0026	14.35758	25.85393	-0.03661	0.002598	0.001909
I7	24420	0.0118	7.63042	19.26478	-0.17251	0.011845	-0.02502
I8	26325	0.003372	13.14596	24.72088	-0.04841	0.003372	-0.0026
I9	22608	0.014996	6.501946	18.24037	-0.22371	0.014996	-0.05478
I10	24444	0.003357	12.97462	24.74057	-0.05036	0.003357	-0.0076
I11	26004	0.002388	14.60888	26.21966	-0.03455	0.002388	2.86E-05
I12	26832	0.004807	11.98832	23.18169	-0.06322	0.004807	-0.00522
I13	27825	0.004425	12.39472	23.54082	-0.05756	0.004425	-0.00467
I14	28640	0.005936	11.03865	22.2653	-0.07868	0.005936	0.003083
I15	33567	0.056385	2.332965	12.48836	-0.58435	0.056385	0.106542
I16	36540	0.054005	2.661017	12.67569	-0.54184	0.054005	0.102879
I17	31395	0.060738	1.615768	12.16542	-0.68928	0.060738	0.145222

Table 6.4. Features: Area and Entropy

Images	Area	Entropy	Images	Area	Entropy
I1	27492	3557.8	I18	32012	3864.8
I2	25654	3435.8	I19	55902	5875.2
I3	30084	3841.3	I20	54165	5464.4
I4	29808	3938.9	I21	54931	5400.9
I5	38779	4573.2	I22	53138	5252.4
I6	38957	5229.2	I23	51660	5109.4
I7	38779	4802.7	I24	49856	4935.3
I8	46001	4920.6	I25	46240	4751.5
I9	49896	5000.9	I26	43018	4554.3
I10	54432	5312.8	I27	38656	4291.4
I11	56112	5327.7	I28	33696	3989.9
I12	58480	5490.2	I29	25576	3420.4
I13	60180	5645.4	I30	37600	4808.6
I14	61009	5733.9	I31	38160	4552.4
I15	61500	5837.7	I32	41583	5028.6
I16	60697	6225.3	I33	36640	4476.4
I17	61341	6446.4	I34	23552	3289.9

6.4.4 Feature Extraction

Multiple features are extracted from the female pelvic MRI images after the segmentation of important diagnostic part. Since our work is not extended to classification part we are considering only optimal features capable of extracting the ROI. Inorder to analyse the structure of obtained ROI certain features are extracted and the details are shown in Table 6.3.

The features include area (FE_1), average absolute difference (FE_2), signal to noise ratio (FE_3), peaksnr (FE_4), image fidelity (FE_5), mean square error (FE_6), and difference entropy (FE_7). Features like Area and entropy (Table 6.4) are giving better results in segmentation of ROI. So a threshold value is set for both area and entropy to find out the final part.

An average of both entropy (A_e) and area (A_a) are taken for setting a threshold value. A tolerance of 15 % and 20 % is chosen according to the characteristics of image. Table 6.4 shows the entropy and area features of 36 MRI images with cyst type of region of interest. A tolerance for entropy is $2937 <= A_e <= 4221$ and that of area is $25450 <= A_a <= 45174$. We considered 320 MRI input images with cyst type of lesion to carry out this work. Different input images having different texture and shape. Our algorithm can able to segment 286 input images with this threshold range. Our fast and reliable segmentation approach can detect the lesion with a segmentation time of 1.25 seconds.

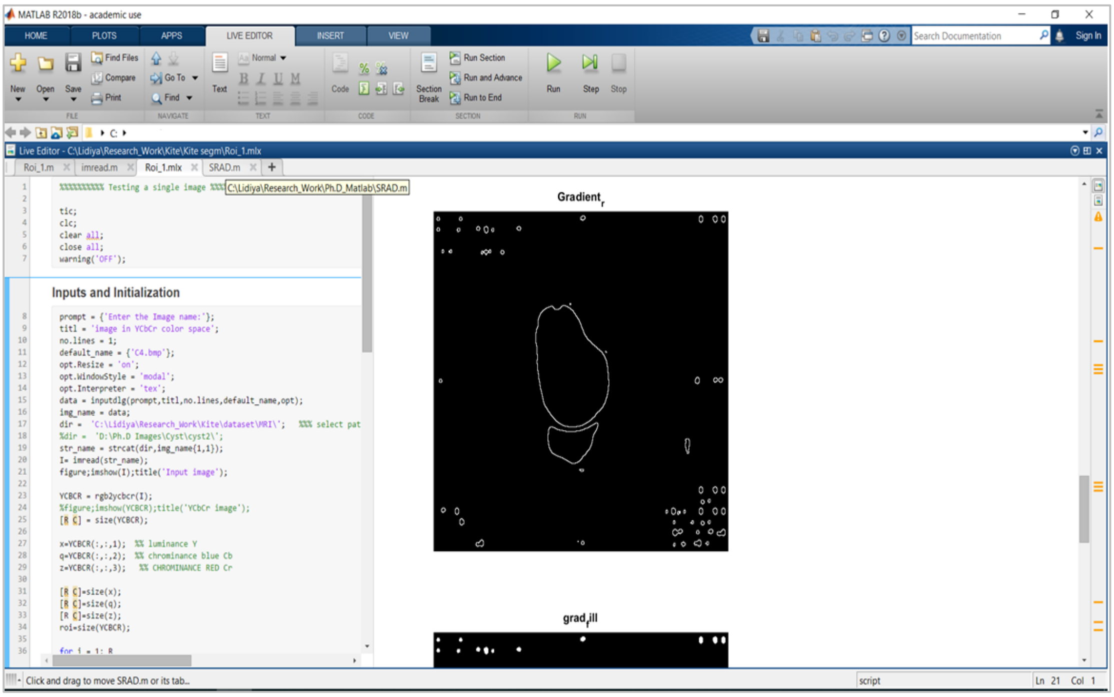

Fig. 6.8. Implementation in MATLAB Live Script

6.5 PERFORMANCE ANALYSIS OF ROI BASED MEDICAL IMAGE COMPRESSION

The whole image is divided into two parts after the process of image segmentation. The important diagnostic part or ROI is compressed in lossless manner and the other region is considered in lossy way. The performance measures like PSNR (peak signal to noise ratio) and CR (compression ratio) are used for evaluating the performance of lossless and lossy compression methods. PSNR discussed in section 6.3.1. gives the measure of quality of image. Compression ratio gives the ratio of original size of the image to the size of compressed image ie, uncompressed size/ compressed size. Figure 6.9 shows the graphical representation of compression methods like DWT (Discrete wavelet transform), Gamma and LoG on medical ultrasound images. In that DWT gives better CR.

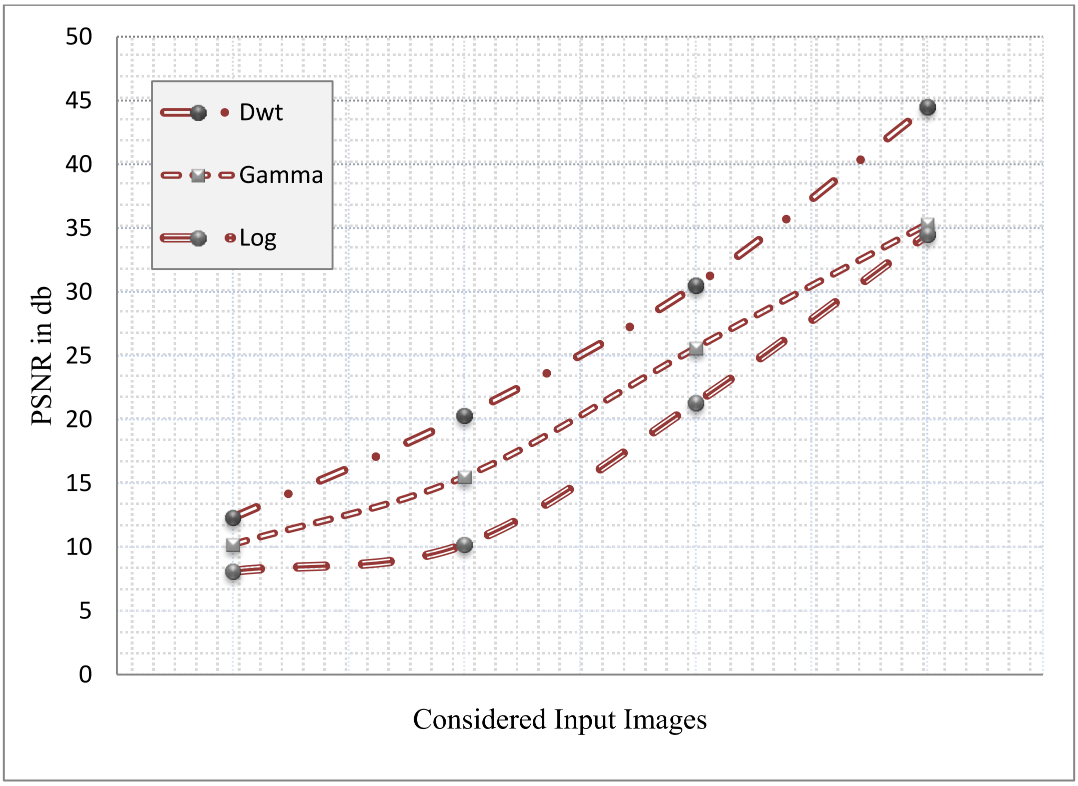

Fig. 6.9. Graphical Representation of Different Compression Methods.

6.5.1 Evaluation in Lossless Methods

The different lossless compression methods discussed in section 5.2.2 were used for compressing the important diagnostic part of input medical images. Inorder to get a good reconstruction quality, ROI is compressed with a high bit rate ie, low compression ratio. So we choose lossless methods to compress the ROI part. Our research work is mainly for teleradiology applications, so the radiologists on the other side needs a good quality image to provide a better diagnosis. When the lossless methods are directly applied on input medical images, compression ratio achieved is very low. The part of the image which is more important than the others is considered and the lossless methods like JPEG-LS, FELICS and CALICS is applied.

6.5.2 Evaluation in Lossy Methods

The different lossy compression methods discussed in section 5.2.1 were used for compressing the background region of input images. The unimportant region or background part is compressed with a low bit rate ie, high compression ratio. The PSNR and CR values of different lossy compression methods are shown in Table 6.5 and 6.6. For brevity five input images are shown. A graphical representation of three input images was also shown in Figure 6.10 and 6.11.

The background region is not very important when compared with the important part of the image. But with the help of background region only the experts can came to the conclusion whether the tumor part is invade to other organs or not. So we can't neglect the background region for this reason and proceed with the lossy type of compression methods. From the Table 6.5 and 6.6 it is clear that JPEG having good compression ratio and low PSNR values when compared with other lossy methods.

Table 6.5. PSNR of different lossy compression methods

Images	JPEG	DCT	SVD	BT_CODE
I1	25.69	19.36	56.3	29.91
I2	23.245	19.602	88.2	31.201
I3	21.23	18.5	76.2	31.114
I4	22.34	18.65	80.54	30.21
I5	24.56	17.23	67.56	28.945

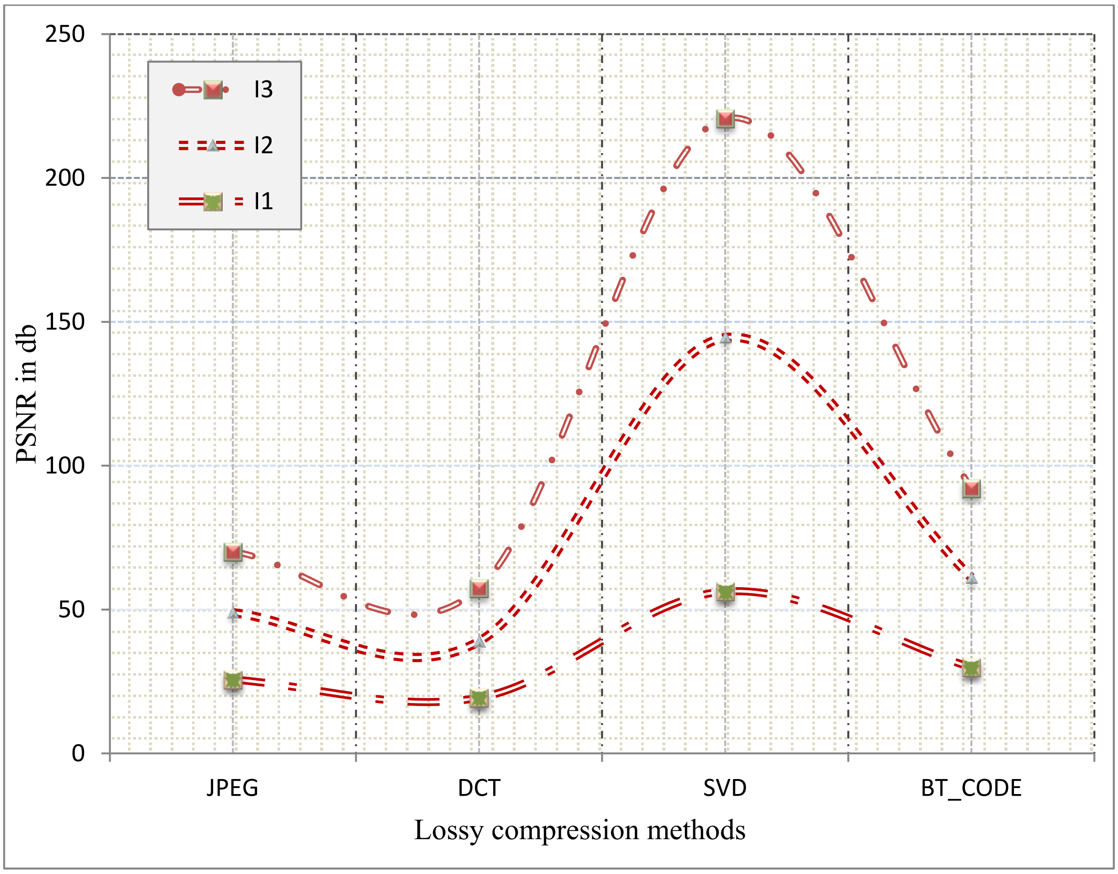

Fig. 6.10. PSNR Plot of Different Lossy Compression Methods on Input Images

Table 6.6 CR of different lossy compression methods

Images	JPEG	DCT	SVD	BT_CODE
I1	45.12	27.47	25.68	22.15
I2	39.27	31.12	23.73	23.0326
I3	43.35	28.25	25.23	23.12
I4	41.58	29.224	24.313	24.023
I5	42.23	29.036	24.97	24.434

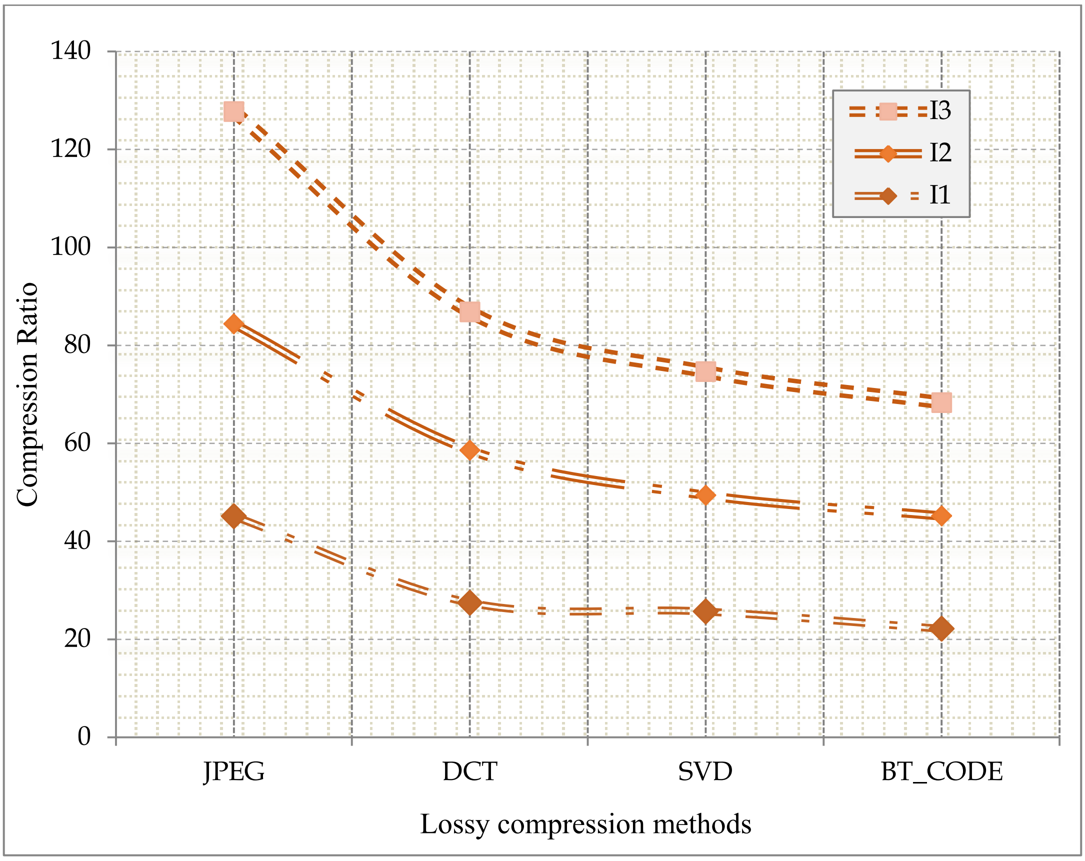

Fig. 6.11. CR plot of different lossy compression methods on input images

Graphical representations of different combination of lossy and lossless methods are given in Figure 6.12 and 6.13. In that Figure 6.12 shows the PSNR and CR plot of ROI obtained as manually whereas Figure 6.13 shows the PSNR and CR plot of automatic ROI. Manual ROI was drawn with the help of radiologists and automatic ROI was obtained using the segmentation method. The different combinations of lossy and lossless methods are shown below,

Method 1 or M1 – JPEG - LS in ROI and JPEG in background region

Method 2 or M2 - FELICS in ROI and JPEG in background region

Method 3 or M3 – JPEG - LS in ROI and SVD in background region

Method 4 or M4 – FELICS in ROI and SVD in background region

Method 5 or M5 – JPEG - LS in ROI and BT-CODE in background region

Method 6 or M6 – JPEG - LS in ROI and BT-CODE in background region

Method 7 or M7 – JPEG - LS in ROI and DCT in background region

Method 8 or M8 – JPEG - LS in ROI and DCT in background region

Out of the above eight combinations, method 1 gives better compression ratio and good image quality in both automatic and manual cases. Different input images having ROI with different size and shapes. Since the background region obtained also depends on the size of ROI, the range of CR obtained will vary.

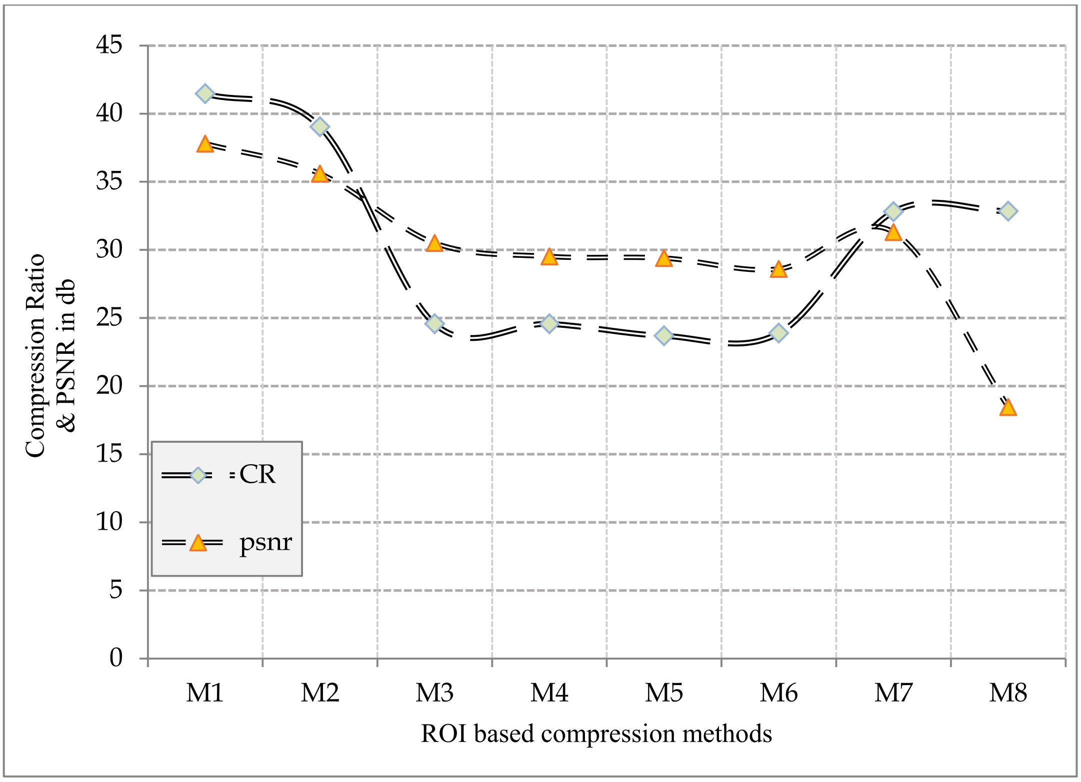

Fig. 6.12. PSNR and CR Plot of Manual ROI Based Compression Methods

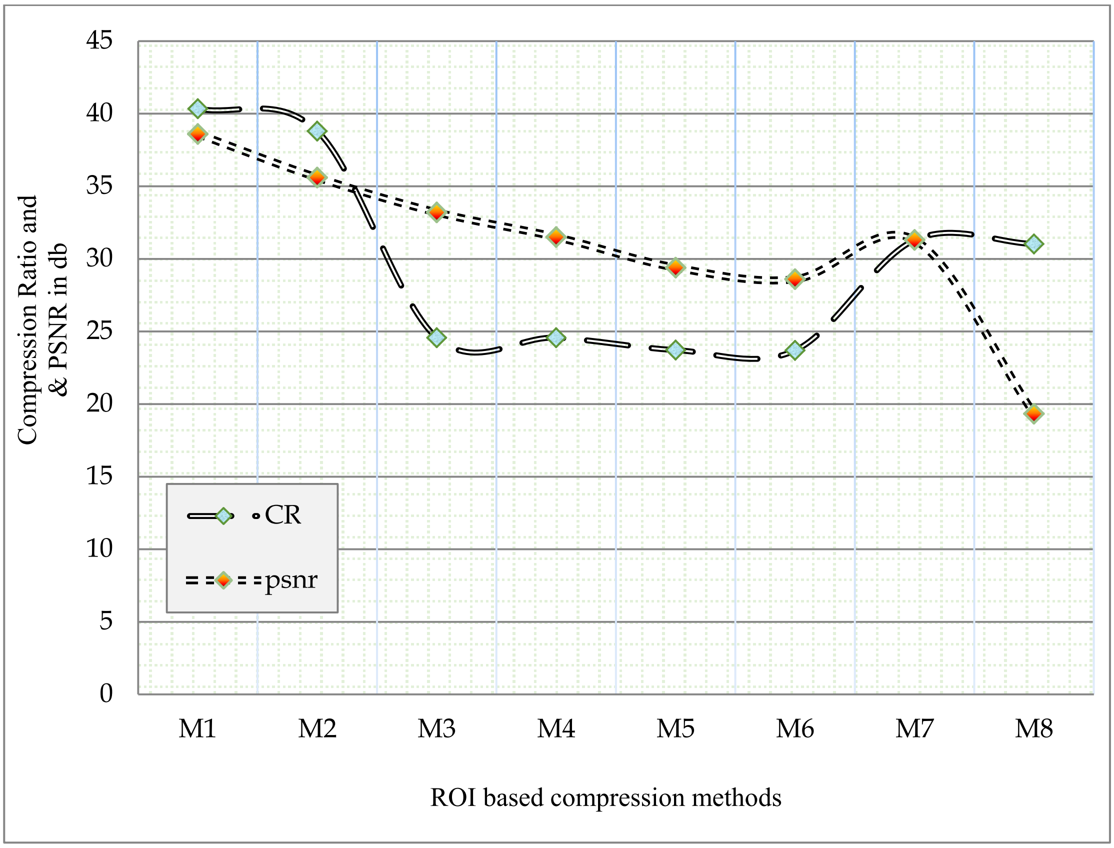

Fig. 6.13. PSNR and CR Plot of Automatic ROI Based Compression Methods

Table 6.7 Comparison of CR and PSNR with proposed and existing methods

Performance Parameters	**Proposed Method**	**Existing Method by Zuo et.al**	**Existing Method Kaur et.al**
Compression Ratio	40.1	15.7	30.1
Peak Signal to Noise Ratio	38.65	38.5	39.4

6.6 GRAPHICAL USER INTERFACE

A GUI or graphical user interface was developed for interactive marking of ROI's. ROI can be selected either manually or automatically. Many of the researchers had used some traditional methods for automatic selection of ROI. It includes region based methods (**Zuo, 2015**), active contour based methods (**Cyriac, 2016**), feature based methods **(Moorthi, 2015)** and threshold methods etc. An interactive marking of arbitrary shaped ROI's is possible by developing a graphical user interface (**Bruckmann, 2000**).

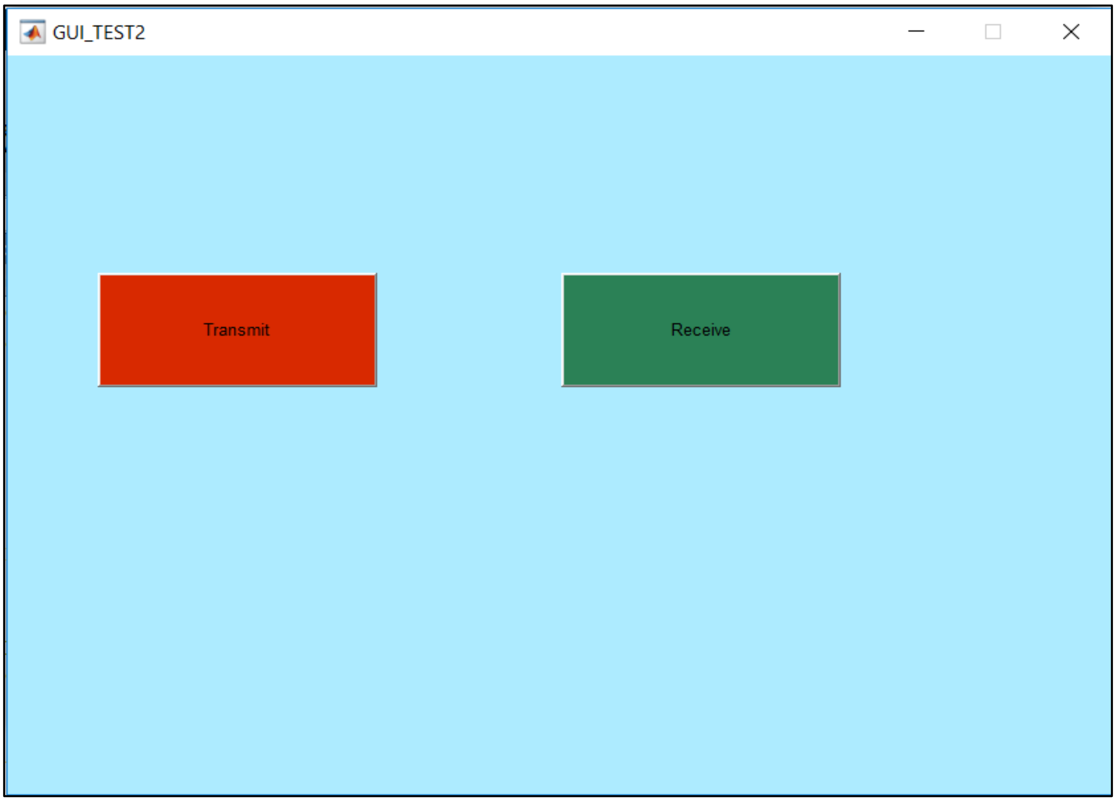

Fig. 6.14. Graphical User Interface

In our research work, ROI was developed automatically both in the case of female PUS imaging and in female PMRI imaging. Automatic method is preferred in the absence of radiologists or experts. Manual selection can be done in the presence of experts or with the help of experienced technicians. Here, in our research work two mode of ROI selection is possible both automatically and manually. The inputs can be selected according to the need of situation. If we have the experts available then we could do the manual selection else does the automatic mode of selection.

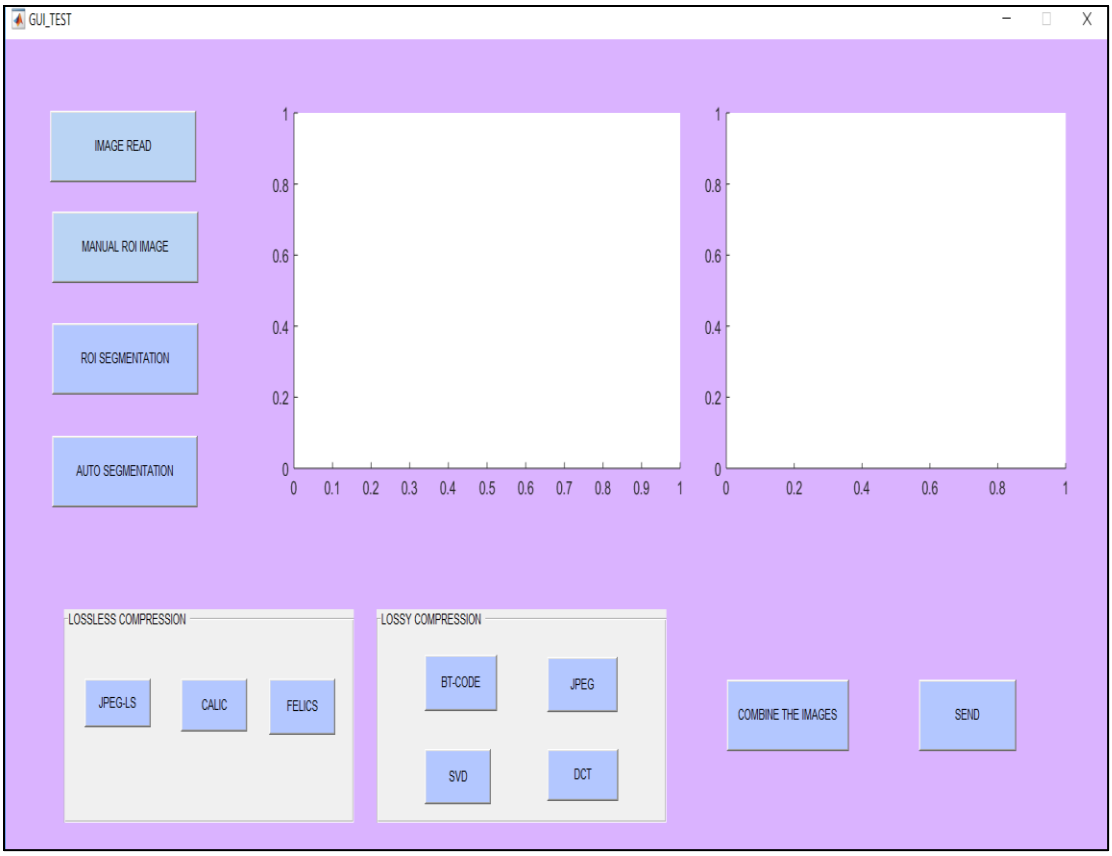

Fig. 6.15. Graphical User Interface – Transmitter Side

The image getting after the ROI based compression is sending in mat format through the transmitter button. On the other side, the original image is formed by pressing the receiver button where the different performance measures can be seen. A graphical user interface with transmitter and receiver button is shown in Figure 6.10. The details regarding the transmitter side and receiver side is shown in Figure 6.11 and 6.12.

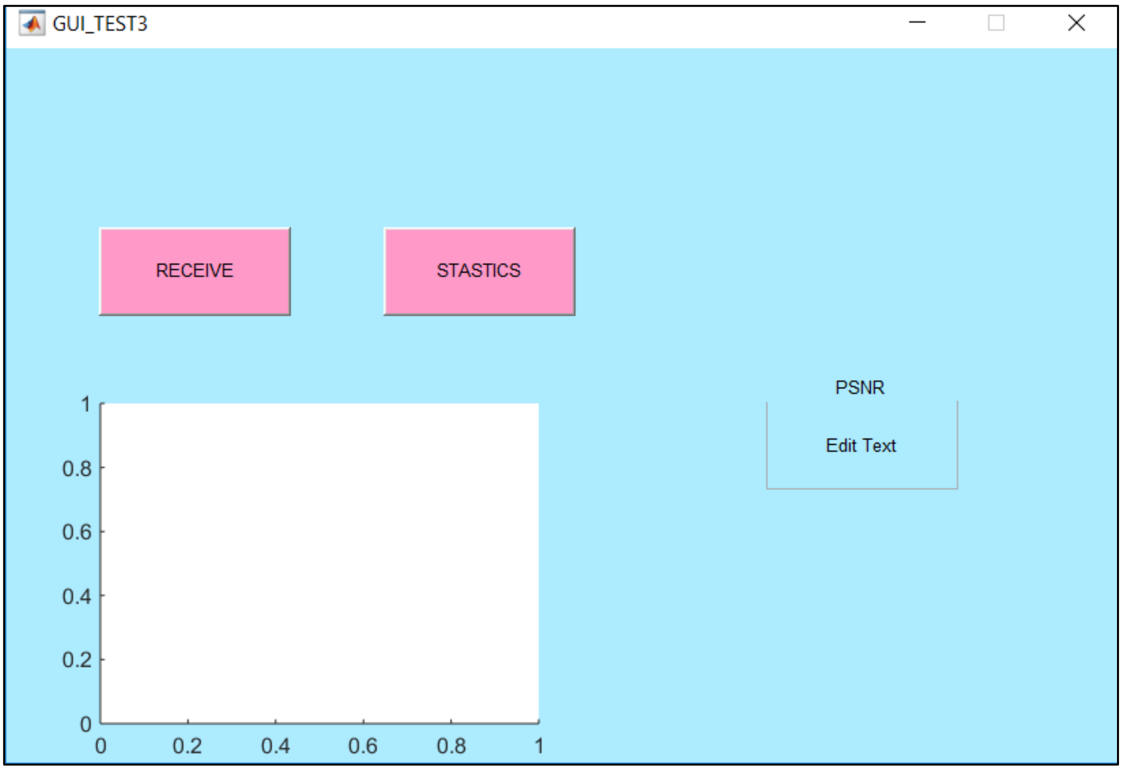

Fig. 6.16. Graphical User Interface – Receiver side

6.7 SUMMARY

In this Chapter we discuss the different result analysis in each stage of work. Our work was carried out in two imaging modalities of female pelvis. One is in female pelvic Ultrasound (PUS) imaging and other is in female pelvic MRI (PMRI) imaging. Algorithm evaluation in each modality is conducted separately. The chapter ends with the performance analysis ROI based medical image compression. The simulation result analysis of female PUS imaging was carried out in MATLAB R2016a and female PMRI imaging was carried out in MATLAB R2018a.

Chapter -7

CONCLUSION AND SCOPE FOR FUTURE WORK

A completely automated segmentation of female pelvic images can greatly help in the proper management of abnormalities like cyst, fibroid, endometrial tumor which require the screening of large populations. But the development of an automated system for this purpose needs a robust system capable of doing fast segmentation which is not an easy task. Due to the complexities arising from the low contrast, high speckle ratio and low SNR, computer aided diagnosis systems are absolutely necessary for analysing the lesions in different imaging modalities.

A typical image presented in our research work having a size of 512 X 512 and occupies a size of I MB. Our research work is based on the finding of important diagnostic region, real medical images are utilized. All the images collected for this research work are provided by radiology department in LIRRIS - Lisie Institute of Radiology Research and Imaging Sciences.

In this research work, we proposed an automatic segmentation scheme which will aid the radiologists for better outputs in limited time. Segmentation in two imaging modalities is considered one in Ultrasound and the other in MRI imaging modality. Since the quality of the images vary due to the difficult imaging conditions, a preprocessing step is initialized before doing the segmentation. A speckle reduced anisotropic diffusion filter is used as a preprocessing approach in female PUS imaging modality whereas a median type of filtering was performed in MRI imaging modality. Furthermore, morphological marker controlled watershed segmentation is applied to identify the lesion region in ultrasound imaging. A total of 18 features are extracted including shape and textural. Finally the method is compared with manual drawing in order to evaluate the performance. Important diagnostic region in MRI imaging modality is identified using gradient method and was also compared with the ground truth images. An improved medical image compression based on region of interest on different imaging modalities was performed. The compression ratio is validated with compression standards defined by a group of radiologists.

Because of the high dynamic range of received sound waves in ultrasound imaging various global and local compression techniques were studied as a replacement for logarithmic one **(Akkala, 2014)** This will help to transmit the scanned images from the patients to cloud so that the doctors can access the data and carry out the diagnosis in limited time duration. An FPGA (Xilinx Kintex 7) based CAD algorithm is implemented for discriminating cysts and stones in kidney ultrasound images **(Krishna, 2016)**. A look up table based approach used here is helpful in differentiating normal and abnormal images. A bicluster score optimal feature selection is employed in **(Huang, 2015)** to select 25 features from a total of 73 features.

The proposed method can be extended to classification part by extracting maximum number of features. Classification based on types of abnormalities and different stages of tumor can also be done. For achieving this stage, images in different type of abnormalities (like cyst, cervix tumor, ovarian cancer) and images in different stages of abnormalities (benign and malignant) is needed. Stage by stage prediction (cysts, fibroids, PCOS- Polycystic ovarian syndrome) (**Sahadev, 2008)** of tumor is possible by supervised classification output. Stage by stage prediction also helps to identify benign and malignant stage of tumor. In the case of cyst type of abnormality neoplasmic stage and granulosa type cell is there. It is important to train the algorithm with maximum number of input images for achieving a finer result. The initial staging diagnosis may be suggested for better verification and any suspected problems.

REFERENCES

1. **A. Bruckmann and A. Uhl** (2000) Selective medical image compression techniques for telemedical and archiving applications. *Computers in biology and medicine*, ***30*(3)**, 153-169.

2. **Ahmed, M. N., S.M.Yamany, N.Mohamed, A.A Farag and T. Moriarty** (2002) A modified fuzzy c-means algorithm for bias field estimation and segmentation of MRI data. *IEEE transactions on medical imaging*, ***21*(3)**, 193-199.

3. **Akkala, V., R. Bharath,P. Rajalakshmi and P. Kumar** (2014) Compression techniques for IoT enabled handheld ultrasound imaging system. In *2014 IEEE Conference on Biomedical Engineering and Sciences (IECBES)*, December, 648-652.

4. **Alcázar, J. L.,S. Arribas, J.A.Mínguez, and M. Jurado** (2014) The role of ultrasound in the assessment of uterine cervical cancer. *The Journal of Obstetrics and Gynecology of India*, ***64*(5)**, 311-316.

5. **Aldosari, H., B. Saddik, and K. A. Kadi** (2017) Impact of picture archiving and communication system (PACS) on radiology staff. *Informatics in Medicine Unlocked,* **10**, 1-6.

6. **Antunes, S. G., J.S.Silva, J.B. Santos,P. Martins, and E. Castela** (2011) Phase symmetry approach applied to children heart chambers segmentation: a comparative study. *IEEE transactions on biomedical engineering*, ***58*(8)**, 2264-2271.

7. **Anusuya, V., V.S.Raghavan and G. Kavitha** (2014). Lossless compression on MRI images using SWT. *Journal of digital imaging*, ***27*(5)**, 594-600.

8. **Avramović, A. and S. Savić** (2011) Lossless predictive compression of medical images. *Serbian Journal of Electrical Engineering*, ***8*(1)**, 27-36.

9. **Balakrishnan, B., S.H.Darsana, J. Mathews and M.S.Nair** (2018) Satellite /aerial image compression using adaptive block truncation coding technique ,*Journal of Indian Society of Remote Sensing* ,**46(11)**, 1761-1771.

10. **Balasubramaniam, G., S. Sushama,B.Rasika and Mahantshetty, U** (2013) Hospital-based study of endometrial cancer survival in Mumbai, India. *Asian Pacific Journal of Cancer Prevention*, ***14*(2),** 977-980.

11. **Barad, D. H.** (2018) Pelvic Mass. *Gynecology and Obstetrics, MSD Manual Professional Version*.

12. **Behra, M. and T. Gest** (2015) Uterus Anatomy, https://emedicine.medscape.com/article/1949215-overview.

13. **Belaid, A., D.Boukerroui, , Y.Maingourd, and J.F.Lerallut** (2010) Phase-based level set segmentation of ultrasound images. *IEEE transactions on information technology in biomedicine*, ***15*(1)**, 138-147.

14. **Benacerraf, B. R.,A.Z. Abuhamad, B. Bromley,S.R. Goldstein, Y.Groszmann,T.D Shipp and I.E.Timor-Tritsch** (2015) Consider ultrasound first for imaging the female pelvis. *American journal of obstetrics and gynecology*, ***212*(4)**, 450-455.

15. **Brocker, K. A., C.D.Alt, M.Eichbaum, C. Sohn, H.U. Kauczor, and P. Hallscheidt** (2011) Imaging of female pelvic malignancies regarding MRI, CT, and PET/CT. *Strahlentherapie und Onkologie*, ***187*(10),** 611.

16. **Bruni, L., G. Albero, B. Serrano, M. Mena, D. Gómez, J. Muñoz, F. X. Bosh, S. Sanjosé** (2017) Human Papillomavirus and Related Diseases in India, *ICO/IARC Information Centre on HPV and Cancer (HPV Information Centre) July Summary Report.*

17. **Bruni**, L., L.Barrionuevo-Rosas,B.Serrano, M. Brostons, G. Albergo, R. Osano, and Castellsague, X. (2014) Human papillomavirus and related diseases in

India. *Information Centre on HPV and Cancer (HPV information cancer), Summary Report*.

18. **Burt, P., and E. Adelson** (1983) The Laplacian pyramid as a compact image code. *IEEE Transactions on communications*, ***31*(4)**, 532-540.

19. **Butler, H.,P.J. Bryan, J.P. LiPuma, A.M. Cohen, S. El Yousef, J.G.Andriole, and J. Lieberman** (1984) Magnetic resonance imaging of the abnormal female pelvis. *American journal of roentgenology*, ***143*(6)**, 1259-1266.

20. **Calóope, P. B., F.N.Medeiros, R.C.Marques, and R.C.Costa** (2004) A comparison of filters for ultrasound images. In *International Conference on Telecommunications* ,Springer, Berlin, Heidelberg, August, 1035-1040.

21. **Canadian Association of Radiologists** (2011). CAR Standards for Irreversible Compression in Digital Diagnostic Imaging within Radiology, Canada, 1-12.

22. **Chaabouni, I., W.Fourati and M.S. Bouhlel** (2016) Using ROI with ISOM compression to medical image. *International Journal of Computational Vision and Robotics*, ***6*(1-2)**, 65-76.

23. **Chang, R. F., W.J. Wu, W.K. Moon, W.M.Chen, W. Lee and D.R. Chen** (2003) Segmentation of breast tumor in three-dimensional ultrasound images using three-dimensional discrete active contour model. *Ultrasound in medicine & biology*, ***29*(11)**, 1571-1581.

24. **Chen, Z.** (2018) Singular Value Decomposition and its Applications in Image Processing. *Proceedings of the 2018 International Conference on Mathematics and Statistics, October,* 16-22.

25. **Cheng, H. D., J.Shan, W. Ju, Y. Guo, and L. Zhang** (2010) Automated breast cancer detection and classification using ultrasound images: A survey. *Pattern recognition*, ***43*(1)**, 299-317.

26. **Chou, C. Y., K.F. Hsu, S.T. Wang, S.C. Huang, C.C. Tzeng, and K.E. Huang** (1997) Accuracy of three-dimensional ultrasonography in volume estimation of cervical carcinoma. *Gynecologic oncology*, ***66*(1)**, 89-93.

27. **Chuang, K. S., H.L.Tzeng,S. Chen, J.Wu and T.J Chen** (2006) Fuzzy c-means clustering with spatial information for image segmentation. *Computerized medical imaging and graphics*, ***30*(1)**, 9-15.

28. **Cyriac, M., and C. Chellamuthu (**2016) An object-based lossless compression approach for medical images using DPCM. *International Journal of Bioinformatics Research and Applications*, ***12*(1)**, 59-71.

29. **David, G., M. Mutch and W.B. Scott** (2014**)** Fibroids, *Gynecology and Obstetrics,* MSD Manual Professional Edition.

30. **Delp, E., and O. Mitchell** (1979) Image compression using block truncation coding. *IEEE transactions on Communications*, ***27*(9),** 1335-1342.

31. **Doukas, C. and I. Maglogiannis** (2007) Region of Interest Coding Techniques for Medical Image Compression. *IEEE Engineering in Medicine and Biology Magazine*, **26(5)**, 29–35.

32. **El Allaoui, A.** (2012) Medical image segmentation by marker-controlled watershed and mathematical morphology. *The International Journal of Multimedia & Its Applications*, ***4*(3)**, 1.

33. **El-Dahshan, E. S. A., H. M. Mohsen, K. Revett and A. B. M. Salem** (2014) Computer-aided diagnosis of human brain tumor through MRI: A survey and a new algorithm. *Expert systems with Applications*, ***41*(11)**, 5526-5545.

34. **Faria, S. C, T. Sagebiel, A. Balachandran, C. Devine, C. Lal, P. R. Bhosale** (2015) Imaging in endometrial carcinoma, Indian Journal Radiology Imaging, **25(2)**, pp.137-47.

35. **Fayed, L** (2019) Differences Between a Malignant and Benign Tumor. www.verywellhealth.com.

36. **Fenster, A., G. Parraga and J. Bax** (2011) Three-dimensional ultrasound scanning. *Interface focus*, ***1*(4)**, 503-519.

37. **Finn, S., M. Glavin, and E. Jones** (2011) Echocardiographic speckle reduction comparison. *IEEE Transactions on Ultrasonics, Ferroelectrics, and Frequency Control*, ***58*(1)**, 82-101.

38. **Frost, V. S., J. A. Stiles, K. S. Shanmugan and J. C. Holtzman** (1982) A model for radar images and its application to adaptive digital filtering of multiplicative noise. *IEEE Transactions on pattern analysis and machine intelligence*, **2**, 157-166.

39. **Gokturk, S. B., C. Tomasi, B. Girod and C. Beaulieu (**2001) Medical image compression based on region of interest, with application to colon CT images. *Conference Proceedings of the 23rd Annual International Conference of the IEEE Engineering in Medicine and Biology Society*, **3**, 2453-2456.

40. **Gonzalez, R. C. and R. E. Woods** *Digital image processing* (3rd ed., pp. 526–527). Upper Saddle River: Prentice Hall. 2008.

41. **Gu, P., W. M. Lee, M. A. Roubidoux, J. Yuan, X. Wang, and P. L Carson** (2016). Automated 3D ultrasound image segmentation to aid breast cancer image interpretation. *Ultrasonics*, ***65***, 51-58.

42. **Gupta, D., and R. S Anand** (2017) A hybrid edge-based segmentation approach for ultrasound medical images. *Biomedical Signal Processing and Control*, ***31***, 116-126.

43. **Gupta, M., H. Taneja, L. Chand and V. Goyal** (2018) Enhancement and analysis in MRI image denoising for different filtering techniques. *Journal of Statistics and Management Systems*, ***21*(4)**, 561-568.

44. **Haralick, R. M., and K. Shanmugam** (1973) Textural features for image classification. *IEEE Transactions on systems, man, and cybernetics*, **6**, 610-621.

45. **Howard, P. G., and J.S. Vitter** (1993) Fast and efficient lossless image compression. In *[Proceedings] DCC93: Data Compression Conference*, 351-360.

46. **Huang, Q., F.Yang, L. Liu, and X. Li** (2015) Automatic segmentation of breast lesions for interaction in ultrasonic computer-aided diagnosis. *Information Sciences*, ***314***, 293-310.

47. **Huang, Q., F.Yang, L. Liu, and X. Li** (2015) Automatic segmentation of breast lesions for interaction in ultrasonic computer-aided diagnosis. *Information Sciences*, ***314***, 293-310.

48. **Huffman, D. A.** (1952) A method for the construction of minimum-redundancy codes. *Proceedings of the IRE*, ***40*(9)**, 1098-1101.

49. **Joseph, R. P., C.S. Singh and M. Manikandan** (2014) Brain tumor MRI image segmentation and detection in image processing. *International Journal of Research in Engineering and Technology*, ***3*(1)**, 1-5.

50. **Kass, M., , A. Witkin and D. Terzopoulos** (1988) Snakes: Active Contour Models‖ International Journals of Computer Vision, **1(4)**, 321-331.

51. **Kaur, M., and V. Wasson** (2015) ROI based medical image compression for telemedicine application. *Procedia Computer Science*, ***70***, 579-585.

52. **Khalid, S**. Introduction to data compression (3rd ed.). Oxfod: Butterworth-Heineman, 2005.

53. **Klema, V., and A. Laub** (1980) The singular value decomposition: Its computation and some applications. *IEEE Transactions on automatic control*, ***25*(2)**, 164-176.

54. **Krishna, K. D., Akkala, V., Bharath, R., Rajalakshmi, P., Mohammed, A. M., Merchant, S. N., & Desai, U. B.** (2016) Computer aided abnormality detection for kidney on FPGA based IoT enabled portable ultrasound imaging system. *Irbm*, ***37*(4)**, 189-197.

55. **Kuan, D. T., A.A. Sawchuk, T.C. Strand, and P. Chavel** (1985) Adaptive noise smoothing filter for images with signal-dependent noise. *IEEE Transactions on Pattern Analysis & Machine Intelligence*, **2**, 165-177.

56. **Kumar, M., and A. Vaish** (2016) Prediction error based compression of color images using WDR coding. *AEU-International Journal of Electronics and Communications*, ***70*(9),** 1164-1171.

57. **LaPolla, J. P., J. B. Schlaerth, O. Gaddis, and C. P. Morrow** (1986) The influence of surgical staging on the evaluation and treatment of patients with cervical carcinoma. *Gynecologic Oncology*, ***24*(2)**, 194-206.

58. **Lee, J. S** (1980) Digital image enhancement and noise filtering by use of local statistics. *IEEE Transactions on Pattern Analysis & Machine Intelligence*, **2,** 165-168.

59. **Lee, J. S** (1981) Speckle analysis and smoothing of synthetic aperture radar images. *Computer graphics and image processing,* **17**, 24-32.

60. **Lema, M., and O.Mitchell** (1984) Absolute moment block truncation coding and its application to color images. *IEEE Transactions on communications*, ***32*(10)**, 1148-1157.

61. **Li, C., R. Huang, Z. Ding, J. C. Gatenby, D. N. Metaxas and J. C. Gore** (2011) A level set method for image segmentation in the presence of intensity inhomogeneities with application to MRI. *IEEE transactions on image processing*, ***20*(7)**, 2007-2016.

62. **Li, L., P. Ross, M. Kruusmaa and X. Zheng** (2011) A comparative study of ultrasound image segmentation algorithms for segmenting kidney tumors. *Proceedings of the 4th International Symposium on Applied Sciences in Biomedical and Communication Technologies, Spain, October* ,126.

63. **Liu, B., H.D.Cheng, J. Huang, J. Tian,X. Tang and J. Liu** (2010) Fully automatic and segmentation-robust classification of breast tumors based on local texture analysis of ultrasound images. *Pattern Recognition*, ***43*(1)**, 280-298.

64. **Loose, R., R. Braunschweig, E. Kotter, P. Mildenberger, R. Simmler and M. Wucherer** (2009) Compression of digital images in radiology-results of a consensus conference. *RoFo: Fortschritte auf dem Gebiete der Rontgenstrahlen und der Nuklearmedizin*, ***181*(1)**, 32-37.

65. **Loupas, T., W.N.McDicken, and P.L. Allan** (1989) An adaptive weighted median filter for speckle suppression in medical ultrasonic images. *IEEE transactions on Circuits and Systems*, ***36*(1)**, 129-135.

66. **Lucas, L. F., N.M.Rodrigues, L. A da Silva Cruz, and S.M. de** Faria (2017) Lossless compression of medical images using 3-d predictors. *IEEE transactions on medical imaging*, ***36*(11)**, 2250-2260.

67. **Maheshwari, A., N.Kumar and U.Mahantshetty** (2016) Gynecological cancers: a summary of published Indian data. *South Asian journal of cancer*, ***5*(3)**, 112.

68. **Manjón, J. V., P. Coupé, L. Martí- Bonmatí, D.L. Collins and M. Robles** (2010) Adaptive non-local means denoising of MR images with spatially varying noise levels. *Journal of Magnetic Resonance Imaging*, ***31*(1)**, 192-203.

69. **Manjón, J. V., P.Coupé, A.Buades, D.L Collins and M. Robles** (2012) New methods for MRI denoising based on sparseness and self-similarity. *Medical image analysis*, ***16*(1)**, 18-27.

70. **Mohamed, N. A., M.N.Ahmed and A. Farag** (1999) Modified fuzzy c-mean in medical image segmentation. In *1999 IEEE International Conference on Acoustics, Speech, and Signal Processing. Proceedings.* **6**, 3429-3432.

71. **Mohan, J., V.Krishnaveni and Y. Guo** (2014) A survey on the magnetic resonance image denoising methods. *Biomedical signal processing and control*, ***9***, 56-69.

72. **Moorthi, M., and R. Amutha** (2015) Region-based medical image compression in teleradiology. *International Journal of Telemedicine and Clinical Practices*, ***1*(1)**, 47-63.

73. **Mounika, K., D. S. N. Lakshmi, K. Alekya** (2015) SVD Based Image Compression. *International Journal of Engineering Research and General Science,* **3(2)**, 1271-1278.

74. **Neto, A. M.,A.C. Victorino, I. Fantoni, D.E. Zampieri, J.V. Ferreira, and D.A. Lima** (2013, April). Image processing using Pearson's correlation coefficient: Applications on autonomous robotics. In *2013 13th International Conference on Autonomous Robot Systems*, Lisbon, Portugal, Apr 2013.

75. **Otsu, N.,** (1979) A threshold selection method from gray-level Histograms. *IEEE Transactions on Systems, Man, and Cybernetics,* **9(1)**, 62-66

76. **Parvati, K., P.Rao, and M. Mariya Das** (2008) Image segmentation using gray-scale morphology & marker controlled watershed transformation. *Discrete Dynamics in Nature and Society*.

77. **Pati, N., A. Pradhan, L.K. Kanoje, and T.K .Das** (2015) An approach to image compression by using sparse approximation technique. *Procedia Computer Science*, ***48***, 769-775.

78. **Perona, P and J. Malik** (1990) Scale-space and edge detection using anisotropic diffusion. *IEEE Transactions on pattern analysis and machine intelligence*, ***12*(7)**, 629-639.

79. **Ramesh, N., J.H. Yoo and I.K. Sethi** (1995) Thresholding based on histogram approximation. *IEE Proceedings-Vision, Image and Signal Processing*, ***142*(5)**, 271-279.

80. **Reddy, M. P., Pradesh, A., B. V. R. Reddy, A., C. S. Bindu** (2014) The Lossless Medical Image Compression for Telemedicine Applications with Delimiter", *Journal of Advanced Research in Dynamical & Control Systems*, ***10*(3),** 74–79.

81. **Rissanen, J., and G.G Langdon** (1979) Arithmetic coding. *IBM Journal of research and development*, ***23*(2)**, 149-162.

82. **Rosenfeld, A., and A. Kak**, *Digital Picture Processing.* New York: Academic, 1976.

83. **Rudin, L. I., S. Osher and E. Fatemi** (1992) Nonlinear total variation based noise removal algorithms. *Physica D: nonlinear phenomena*, ***60*(1-4)**, 259-268.

84. **Said, A., and W.A Pearlman** (1996) A new, fast, and efficient image codec based on set partitioning in hierarchical trees. *IEEE Transactions on circuits and systems for video technology*, ***6*(3)**, 243-250.

85. **Sahdev, A., & Reznek, R. H.** (2008) Magnetic resonance imaging of endometrial and cervical cancer. *Annals of the New York Academy of Sciences*, ***1138*(1),** 214-232.

86. **Sankaranarayanan, R., B. M.Nene, S. S. Shastri, K. Jayant, R. Muwonge,A. M. Budukh, R. Chinoy** (2009) HPV screening for cervical cancer in rural India. *New England Journal of Medicine*, ***360*****(14)**, 1385-1394.

87. **Sapkal, A. M. and V. K. Bairagi** (2011) Telemedicine in India: a review challenges and role of image compression. *Journal of Medical Imaging and Health Informatics*, ***1*****(4)**, 300-306.

88. **Selvathi, D., and Bama, S.** (2017) Phase based distance regularized level set for the segmentation of ultrasound kidney images. *Pattern Recognition Letters*, ***86***, 9-17.

89. **Setiawan, V. W., H. P Yang, M. C. Pike, S.E. McCann, H. Yu,Y. B. Xiang and P.A. van den Brandt** (2013) Type I and II endometrial cancers: have they different risk factors?. *Journal of Clinical Oncology*, ***31*****(20)**, 2607-2618.

90. **Shapiro, J. M**. (1993) Embedded Image Coding Using Zerotrees of Wavelet Coefficients," *IEEE Trans. on Signal Processing,* **41(12)**, 3445 – 3462.

91. **Shi, X., H.D.Cheng, L. Hu, W. Ju and J. Tian** (2010) Detection and classification of masses in breast ultrasound images. *Digital signal processing*, ***20*****(3)**, 824-836.

92. **Skodras, A., C. Christopoulos and T. Ebrahimi** (2001) The JPEG 2000 still image compression standard. *IEEE Signal Processing Magazine*, 36–58.

93. **Sreedevi, A., R. Javed and A. Dinesh** (2015) Epidemiology of cervical cancer with special focus on India. *International journal of women's health*, **7**, 405.

94. **Ström, J., and P.C. Cosman** (1997) Medical image compression with lossless regions of interest. *Signal processing*, ***59*****(2)**, 155-171.

95. **Suhas, S., and C.R. Venugopal** (2017) MRI image preprocessing and noise removal technique using linear and nonlinear filters. *2017 International*

Conference on Electrical, Electronics, Communication, Computer, and Optimization Techniques (ICEECCOT), December, 1-4.

96. **Tang, H., E.X.Wu, Q.Y. Ma, D. Gallagher, G.M. Perera and T. Zhuang** (2000) MRI brain image segmentation by multi-resolution edge detection and region selection. *Computerized Medical Imaging and Graphics*, ***24*(6)**, 349-357.

97. **The Royal College of Radiologists** (2008) The adoption of lossy image data compression for the purpose of clinical interpretation, Board of the Faculty of Clinical Radiology, UK, 1-19.

98. **Torbati, N.,A. Ayatollahi and A. Kermani** (2014) An efficient neural network based method for medical image segmentation. *Computers in biology and medicine*, ***44***, 76-87.

99. **U. Rajyalakshmi, R. S. Koteswara and P. K. Sathya** (2017) Integrated variable marker controlled watershed method with level sets for semisupervised classification, *International Journal of advanced science and technology* **(98)**, 1–12.

100. **Wallace, G. K.** (1992) The JPEG still picture compression standard. *IEEE Transactions on Consumer Electronics*, **38(1)**, 29-35.

101. **Wang, R., J.Lin, D.Li, and T. Wang** (2007) Edge enhancement and filtering of medical ultrasonic images using a hybrid method. In *2007 1st International Conference on Bioinformatics and Biomedical Engineering* , 876-879.

102. **Wang, X., S.Wan, and T. Lei** (2014) Brain Tumor Segmentation Based on Structuring Element Map Modification and Marker-controlled Watershed Transform. *JSW*, **9(11)**, 2925-2932.

103. **Weinberger, M. J., G. Seroussi, and G. Sapiro** (2000) The LOCO-I lossless image compression algorithm: Principles and standardization into JPEG-LS. *IEEE Transactions on Image Processing*, **9(8)**, 1309– 1324.

104. **Witten, I. H.,R.M Neal and J.G.Cleary** (1987) Arithmetic coding for data compression. *Communications of the ACM*, ***30*(6)**, 520-540.

105. **Wu, B. F. and C. F. Lin** (2005) A high-performance and memory-efficient pipeline architecture for the 5/3 and 9/7 discrete wavelet transform of JPEG2000 codec. *IEEE Transactions on Circuits and Systems for Video Technology*, ***15*(12),** 1615-1628.

106. **Wu, X. and N. Memon** (1997) Context-based adaptive lossless image coding. *IEEE Transactions on Communications*, **45(4)**, 437–444.

107. **Yousuf, M. A., and M.N. Nobi** (2011) A new method to remove noise in magnetic resonance and ultrasound images. *Journal of scientific research*, ***3*(1)**, 81-81.

108. **Yu, Y and S.T .Acton** (2002) Speckle reducing anisotropic diffusion. *IEEE Transactions on image processing*, ***11*(11)**, 1260-1270.

109. **Zuo, Z., X. Lan, L. Deng, S. Yao and X. Wang** (2015) An improved medical image compression technique with lossless region of interest. *Optik*, ***126*(21)**, 2825-2831.

LIST OF PAPERS SUBMITTED ON THE BASIS OF THIS THESIS

I. REFEREED JOURNALS

1. **Thampi. L and V. Paul** (2018). Abnormality recognition and feature extraction in female pelvic ultrasound imaging. *Informatics in Medicine Unlocked*, 13, 133–138.
2. **Thampi. L and V. Paul**. (2018). Automatic Segmentation and Classification in Cervical Cancer Images: Evaluation and Challenges. *International Journal of Pure and Applied Mathematics,* 119, No. 12, 12549-12560.
3. **Thampi. L and V. Paul**. (2017) Different compression techniques on ultrasound imaging *International Journal of Advanced Research,* 5, 1782-1786.

II. PRESENTATION IN CONFERENCES

1. **Thampi, L. L., and Paul, V.** (2017, April). Application of compression after the detection of endometrial carcinoma imaging: Future scopes. *In Electronics, Communication and Aerospace Technology (ICECA), 2017 International conference of* IEEE, Vol. 1. 28-32.

2. **Thampi, L. L., and Paul, V.** (2016) An Endometrial cancer Lossless Image Compression with Lossless ROI" *Proceedings of 65th IRF International Conference*, 20th November Pune, India, ISBN: 978-93-86291-38-7.

CURRICULUM VITAE

NAME : Lidiya Lilly Thampi

DATE OF BIRTH : 6th August 1988

EDUCATIONAL QUALIFICATIONS

2010 Bachelor of Technology

Institution : Mar Athanasius College of Engineering, Kothamangalam, Kerala

Specialization : Electronics & Communication

University : M G University

2013 Master of Engineering

Institution : K S Rangasamy College Technology, Erode, Tamilnadu

Specialization : Electronics & Communication

University : Anna University, Chennai

2014 GATE Qualified

Specialization : Electronics & Communication

Doctor of Philosophy (Ph.D)

Department : School of Engineering

University : Cochin University of Science and Technology

Registration Date : 23-01-2015